Fall 2018

Development of fluorescent sensors based on molecularly imprinted biomimetic polymers

Rongfang Yang
University of New Hampshire, Durham

Development of fluorescent sensors based on molecularly imprinted biomimetic polymers

BY

Rongfang Yang

B.S. Chemistry, Lanzhou University. 2011

DISSERTATION

Submitted to the University of New Hampshire
in Partial Fulfillment of
the Requirements for the Degree of

Doctor of Philosophy
in
Chemistry

September, 2018

This dissertation has been examined and approved in partial fulfillment of the requirements for the degree of Doctor of Philosophy in Chemistry by:

Dissertation Director, Dr. W. Rudolf Seitz, Professor of Chemistry
University of New Hampshire

Dr. Roy P. Planalp, Associate Professor of Chemistry
University of New Hampshire

Dr. Gonghu Li, Associate Professor of Chemistry
University of New Hampshire

Dr. Anyin Li, Assistant Professor of Chemistry
University of New Hampshire

Dr. Jeffrey Halpern, Assistant professor of Chemical Engineering
University of New Hampshire

On 08/08/2018

Original approval signatures are on file with the University of New Hampshire Graduate School.

ACKNOWLEDGEMENTS

Much appreciation to my advisor, Professor W. Rudolf Seitz, who leads me to the chemical sensor world, who guides me to solve every conundrum, who supports me to finish the Ph.D. study, and who sets the best example for me to follow. Without his encouragement and patience, I would be forwarded to another route.

I would like to appreciate Professor Roy P. Planalp for all his assistance, guidance, and support of my research. Also I would like to express thanks to Professor Gonghu Li, Professor Anyin Li, and Professor Jeffery Harlpen, I learned many exciting pieces of knowledge from them.

I would also like to express my appreciation for professor Sterling A. Tomellini and John Tsavalas, who spent much time working with me and instructing me. I gratefully acknowledge all contributions they made to my development

Countless thanks and appreciation to Cindi Rohwer, Stephanie Labadie, and Katharine Winans who spent much time helping me during these years.

A huge thanks Nancy Cherim, UNH Instrumentation Center, for her help with the Scanning Electron Microscope and Transmission Electron Microscope.

I would also like to thank Peggy Torch, Kristin Blackwell, Laura Bicknell, and Bob Constantine for their continued help, encouragement, and friendship.

TABLE OF CONTENTS

LIST OF TABLES

LIST OF FIGURES

ABSTRACT

Fluorescent sensors based on molecular imprinting technology using novel biomimetic polymers

Rongfang Yang

Department of Chemistry, University of New Hampshire, Durham NH 03824

Molecular recognition can be thought as the process in which two or more molecules bind to one another in specific geometry through noncovalent bonding. Bioreceptors, such as antibodies, enzymes, and DNAs can specifically bind to its target with high binding affinity and selectivity. However, the bio receptors are suffering from low stability and tolerance to extreme pH, temperature and organic solvents.

To overcome the disadvantages of the bioreceptors, novel biomimetic molecularly imprinted polymers (MIPs) were developed by Seitz group. Different from the conventional MIPs with high percentage of covalent crosslinking, the biomimetic MIPs contain less than 5% mole percent covalent crosslinking. A second kind of non-covalent crosslinking was incorporated into the MIPs to keep the configuration of the binding sites. With the combination of covalent crosslinking and noncovalent crosslinking, the MIPs can bind to the template with high affinity and fast kinetics, just like bioreceptors.

The novel material was based on the Poly(*N*-isopropylacrylamide) (PNIPAm) which is a well known thermally responsive material. PNIPAms exist as well solvated coils at low

temperature but aggregate out of solution when temperature is elevated above the critical temperature. This is similar to the denaturation of protein upon elevation of temperature.

The MIPs were prepared in the presence of the template molecules by Reversible Addition-Fragmentation Transfer (RAFT) polymerization. After removal of the template, binding cavities with a three-dimensional structure complementary to the template were left inside the polymer scaffold. RAFT polymerization is compatible with different kinds of monomers. This makes it convenient to make MIPs for various target molecules.

The MIPs with high physical stability, straight forward preparation, predictable binding affinity and low cost have been proved to be excellent receptors in fluorescent sensors. Sensors based on fluorescence resonance energy transfer (FRET) and “on/off” sensors with internal standard were developed in this dissertation.

LIST OF ABBREVIATIONS

MIPs	Molecularly Imprinted Polymers
NIPs	Non-Imprinted Polymers
RAFT	Reversible Addition –Fragmentation Transfer polymerization
FRET	Fluorescence Resonance Energy Transfer
PNIPAm	Poly(N-isopropylacrylamide)
PNnPAm	Poly(N-n-propylacrylamide)
LCST	Lower Critical Solution Temperature
DLS	Dynamic Light Scattering
NMR	Nuclear Magnetic Resonance Spectra
SEM	Scanning Electron Microscopy
TEM	Transmission Electron Microscopy
FTIR	Fourier-transform infrared spectra
DMNSE	2-(Dodecylthiocarbonothioylthio)2-methylpropanoic acid N-hydroxylsuccinimide ester
MPTT	*S*-methoxycarbonylphenylmethyl *S*¢-trimethoxysilylpropyltrithiocarbonate
MAA	Methacrylic acid
MBAm	N,N'-Methylenebisacrylamide
4VP	4-Vinylpyridine

3VA	3-Vinylaniline
7CM	7-Hydroxycoumarin
4NP	4-Nitrophenol
3NP	3-Nitrophenol
BMA	Benzyl methacrylate
NBD-Cl	4-Chloro-7-Nitrobenzofurazan

CHAPTER 1 INTRODUCTION

1.1 Molecular recognition process in nature

Molecular recognition can be thought of as the process by which two or more molecules bind to one another in specific geometry through noncovalent bonding such as van der Waals forces, π-π interactions, hydrogen bonding,[1] metal coordination,[2] hydrophobic forces, [3] and electrostatic effects[4].

The principle of Molecular recognition can be explained with a "lock-and-key" mechanism, involving interactions between host (the "lock") and the structural complementary guest (the " key"). [5,6,7] The functional groups on the "key" compound are unique, like grooves on keys, and are complementary to binding sites on the "lock" compound.[8,9,10] Therefore, the "lock" compound will only bind to its "key" while ignoring other structural analogues as illustrated in figure 1.[11]

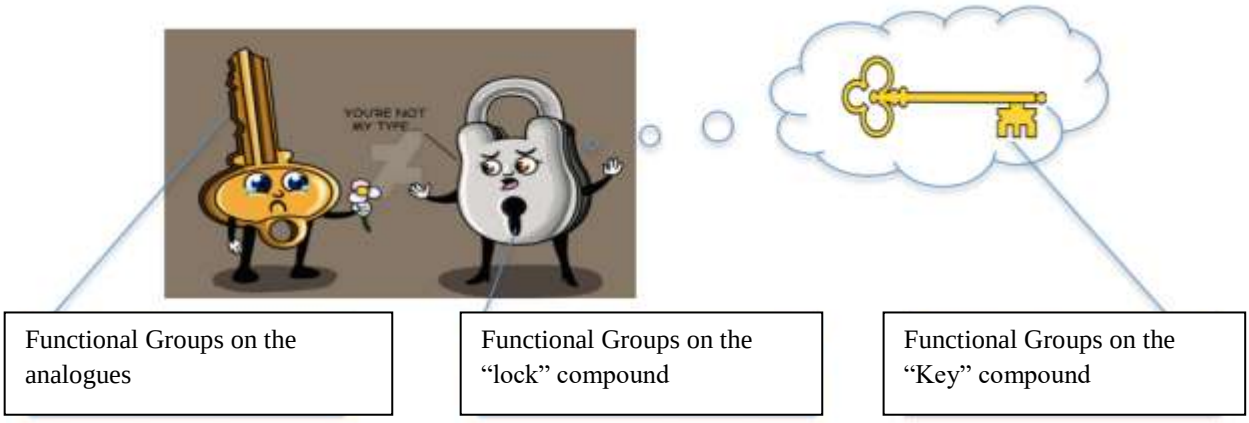

Figure 1.1 " Lock " and " Key "analogy for molecular recognition process[11]

Molecular recognition forms the basis for virtually all biological processes.[12] It is the driving force in many biological systems including the interactions between enzyme and substrate[13], antibody and antigen[14], DNA and protein[15], sugar and lectin[16], RNA and Ribosome[17], etc.

Enzymes are macromolecular biological catalyst that can catalyze more than 5,000 biochemical reaction.[18] They are generally globular proteins with a specific binding pocket. This pocket has a complementary shape, charge and hydrophilic/hydrophobic characteristics to the substrate. [19, 20] Enzymes can therefore distinguish between very similar substrate molecules to be chemoslective, regioselective and stereospecfic.[21] For example, lactase can specifically bind to lactose and break it down to glucose as shown in figure 1.2. [22] Lacking lactase, a person may experience the symptoms of lactose intolerance when consuming dairy products. [23]

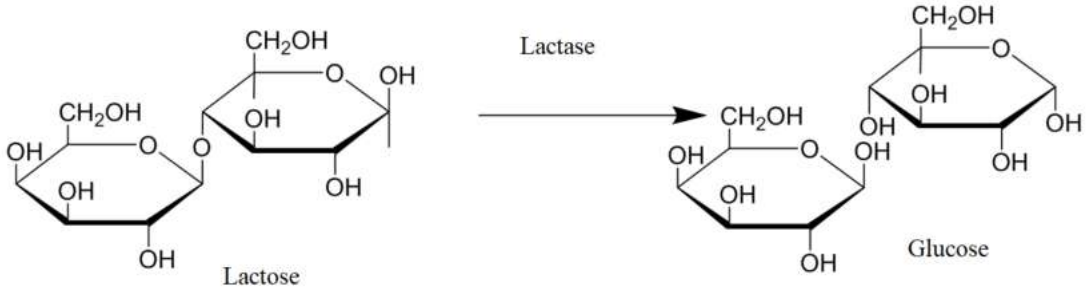

Figure 1.2 Lactase break lactose into glucose

Another example of the molecular recognition is the interaction between antibody and antigen after the introduction of vaccination. Every year millions of people have been protected against potentially fatal diseases by vaccination program.[24] Each vaccine contains different type of antigen, usually a weaken form of virus or bacterium that can cause a particular disease.[25] When the vaccine was injected into human body, the B lymphocytes cells from the body immune

system could detect the antigen, and evolved into memory B cells that could produce antibodies.[26] These Y- or T-shaped molecules contained binding sites that are specifically tailored for the antigen. Therefore, the antibody could recognize the antigen, selectively bind to it, and prevent it from attacking healthy cells.[27, 28] Over time, the antibodies will gradually disappear, but the memory B cells will remain dormant in human body for many years.[25]

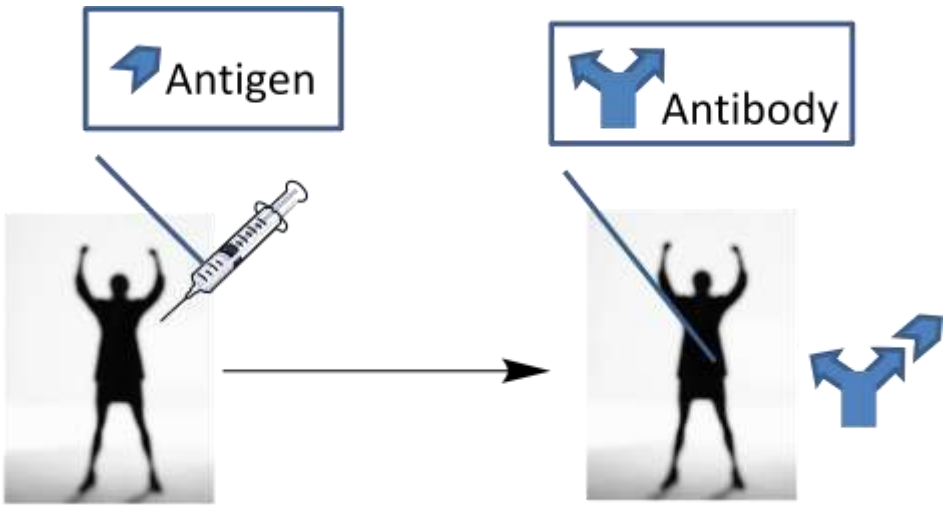

Figure 1.3 The interaction between antibody and antigen after the introduction of vaccination

Due to the astonishing capacity for specifically recognizing target molecules, bioreceptors have been widely used in affinity technology, in applications such as biosensors,[29] immunosorbent assay,[30] bio separation,[31] medical treatment,[32] and targeted drug deliver[33].

However, the synthesis and separation of these bio-macromolecules are time and labor consuming. They have low stability and tolerance to extreme pH, temperature and organic solvents, and often require labeling or indirect assay formats for the generation of a measurable signal.[34, 35]

1.2 Molecularly Imprinted Polymers (MIPs)

In order to mimic the molecular recognition in natural and synthesis artificial receptors, the molecularly imprinted polymers (MIPs) were developed. [36] The first MIP was made by M.V. Polyakov in 1931. He synthesized inorganic polysilicate in the presence of small template molecules such as benzene. It was noticed that the formed polysilicate can uptake higher amount of the additive template. [37] Once developed, the MIPs have attracted broad interests and are continually advanced. [38]

A typical MIPs synthesis protocol contains template, functional monomers cross-linker, initiator and solvent (porogen) as shown in figure 1.4. [39] The process starts with dissolution of template, functional monomer, cross-linking agent and initiator in a porogenic solvent. The functional monomers self-assemble around the template molecules through noncovalent crosslinking. After initiation, polymer scaffold grows around the template to form a robust shell which is complementary in size, shape, and functional groups of the template. The MIPs obtained had a porous matrix possessing binding cavities with a three-dimensional structure complementary to the template. After the removal of the template molecules, these binding cavities were left inside the polymer and could recognize the template molecules. [40]

Template molecules are the target for MIPs. The template molecules could be ions, [41] organic molecules [42] or biomacromolecules [43]. An ideal template molecule should satisfy three requirements: 1) It does not inhibit the polymerization; [40]

2) It contains functional groups that can interact with the functional monomer;

3) It is stable under the polymerization condition.

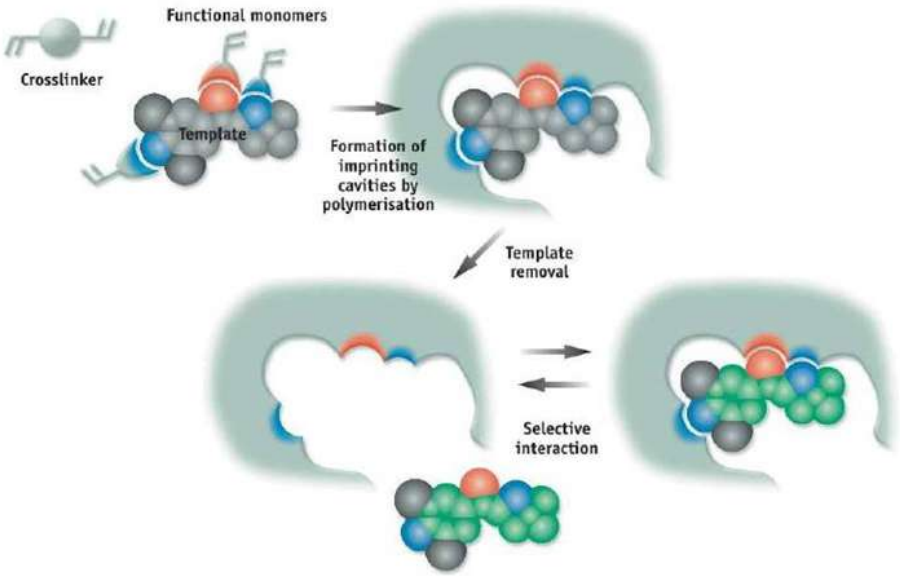

Figure 1.4 Scheme for molecularly imprinted polymers (Biotage)[39]

The functional monomers interact with the template molecules by its functional groups. Some typical functional monomers are shown in figure 1.5. Among them, methacrylic acid (MAA) has been used as a "universal" functional monomer. The explanation for this is that the MAA is hydrogen donor as well as acceptor, so it can form dimer during polymerization. This dimerization could enhance the effect of imprinting. [44, 45] Furthermore, higher fraction of MAA would increase the pore size of the MIPs, which increases the rate of mass transfer during the binding process. [46]

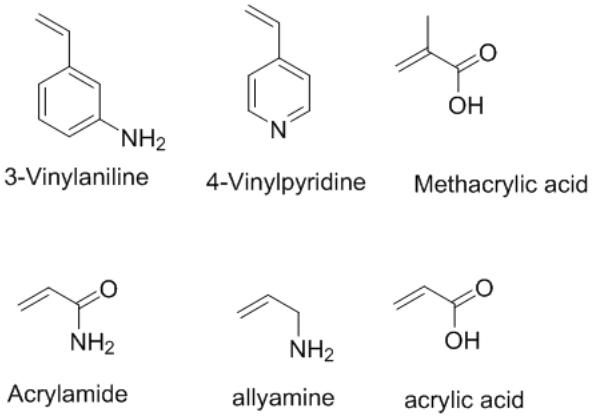

Figure 1.5 Typical functional monomers used in molecular imprinting

The cross-linker is used to hold the configuration of the binding sites. The crosslinked polymer is less able to collapse into a "random coil" state in the absence of the template. [47, 48] A higher percentage of cross-linker usually forms more selective and stronger binding sites. [49] Compared to the bioreceptors, MIPs have many advantages:

1) High physical stability. The MIPs can tolerate a wide range of different conditions.

2) Straightforward preparation. The synthesis method can be easily up scaled for industrial production.

3) Predictable recognition specificity. The binding sites can be tailored for various target molecules by using different functional monomers and cross-linkers.

4) Low cost.

Owing to these unique features, MIPs have found a wide range of applications in various fields such as solid phase extraction[50], enatiomer separation[51], water quality control[52], and biology and chemical sensing[53].

1.3 Existing Problems and Challenges

Conventional MIPs can be prepared by sol–gel processes, [54] bulk polymerization, [55] suspension polymerization[56] and emulsion polymerization[57]. All these methods involve addition of high percentages of cross-linkers and yield structure rigid particles. There are several intrinsic disadvantages that limit the applicability of MIPs.

1) The retention of the template molecules inside the MIPs. Due to the highly cross linked structure of MIPs, the template molecules buried deep inside cannot be removed. They not only occupy the binding sites and but also interfere with the recognization process.
2) Slow mass transfer inside MIPs. The highly cross linked structure hindered the diffusion of the template molecule into the binding sites. As a result the binding process usually takes hours.
3) Low solubility. MIPs are not soluble due to their mechanical rigid structure. This imposes tedious processes for their inclusion in devices.

The challenge is to develop polymeric scaffold with selective binding sites and soluble polymer chains, reduce the hindrance for diffusion of the template and increase the rate of response.

1.4 Biomimetic MIPs proposed by Seitz group

To overcome the disadvantages of the conventional MIPs, novel biomimetic MIPs have been developed by Seitz group. The covalent crosslinking in these materials was reduced to less

than 5% mole percent. This level of covalent crosslinking works like the disulfide bonds in proteins to maintain the topology of the MIPs. To keep the configuration of the binding sites, a second kind of noncovalent crosslinking was incorporated into the MIPs. This non-covalent crosslinking includes acid-base crosslinking, π–π interaction**,** and electronic interactions. It was observed that the combination of low percentage of covalent crosslinking and noncovalent crosslinking could increase the binding affinity.

The novel material was based on the Poly(*N*-isopropylacrylamide) (PNIPAm) which is a well known thermal responsive material. At high temperature, the PNIPAm can fold into specific tertiary structure; which can be used to build the binding sites. When the temperature decreases, the flexibility of the polymer increases. This accelerates the mass transfer inside the polymer so the template molecules can be conveniently removed.

With the combination of covalent crosslinking and non-covalent crosslinking, the binding sites can be restored after the phase transition. This increased the stability of the MIPs under extreme condition.

The structure of the new material is shown in figure 1.6.

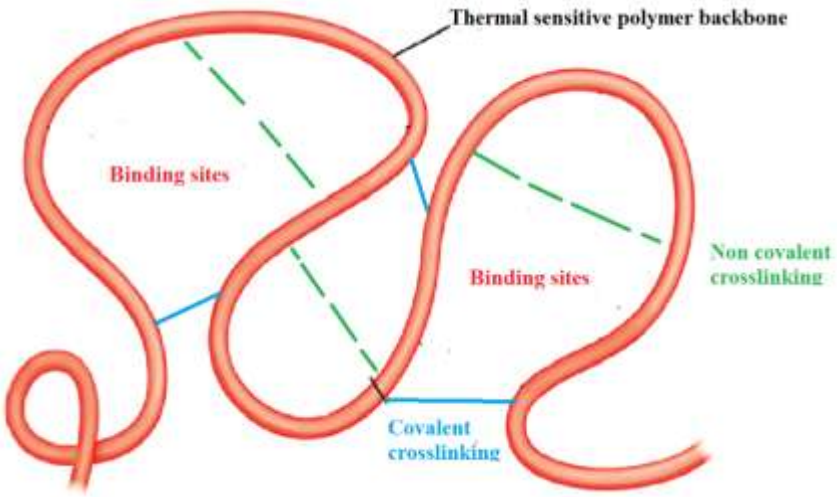

Figure 1.6 Scheme of the biomimetic molecularly imprinted polymer (The MIPs were made of a thermal sensitive backbone. The binding sites were maintained by low percentage of covalent crosslink and noncovalent crosslinking.)

1.5 MIPs based on poly(NIPAm)

Poly(N-iso-propylacrylamide) (PNIPAm) is poly-vinyl polymer well known for its thermal sensitivity. PNIPAm is a chemical isomer of poly-leucine, but has the polar peptide group in the side-chain rather than in the backbone. [58]

PNIPAm exists as well solvated coils at low temperature but aggregates out of solution when the temperature is elevated above the critical temperature. This is similar to the denaturation of protein upon elevation of temperature. [59] The conformation of each state is established and maintained by the balance between hydrophobic interaction between monomers and hydrophilic interaction between monomers and solvents. At low temperature, PNIPAm is soluble because the hydrophilic interaction is dominant. At high temperature the hydrogen bonding is not strong enough to overcome hydrophobic interactions between the vinyl backbones

and alkyl segments. Thus, the polymer forms a tight packed globule with hydrophobic interactions dominating the center and hydrophilic interactions on the surface of the polymer. With continuous elevation of the temperature, the globules will collapse and aggregate out of solution due to the intermolecular interactions between the hydrophobic groups on the surface of the resulting globules. [60] The temperature at which the hydrophilic-hydrophobic transition occurs is known as the Lower Critical Solution Temperature (LCST). The LCST temperature of PNIPAM is 32°C and this temperature can be driven up or down depending on the co-monomers used and their abundance in the polymer. [61,62]

The phase transition process and similarities of PNIAMs with protein make PNIPAm an excellent candidate for the development biomimetic material.

1.6 Reversible Addition –Fragmentation Transfer (RAFT) polymerization

Reversible addition-fragmentation transfer polymerization (RAFT) is a sequential "living" polymerization method in the presence of a Chain Transfer Agent (CTA), which contains a thiocarbonylthio moiety. [63] General structures of CTA are showed in Figure 1.7.

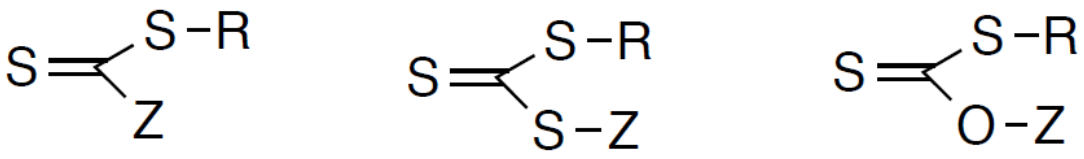

Figure 1.7 General structures of RAFT agents

Due to the presence of a CTA, a RAFT equilibrium stage sets off between the dormant and growing chains. In a successful RAFT polymerization, group R and Z in the CTA should be chosen carefully. The R group should be a better leaving group than the propagating chain and must efficiently reinitiate monomer as an expelled radical. The Z group is important in the pre-equilibrium stage to stabilize the radicals. [64] So the radical and CTA group can be transferred from chain to chain through this equilibrium allowing continued growth of the dormant chain. The generally accepted mechanism is shown in Figure 1.8.

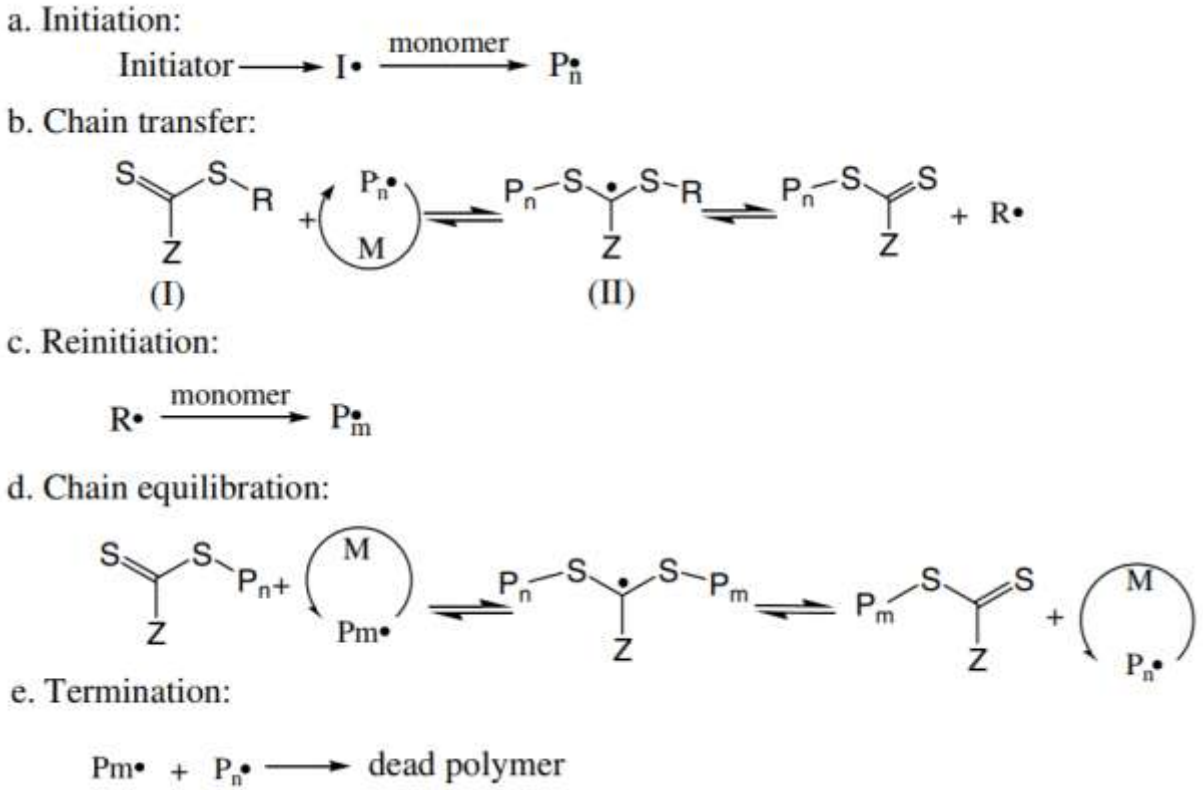

Figure 1.8 Mechanism of RAFT polymerization [64] (Copyright © 2003 Elsevier Ltd.)

Initiation of the polymerization is accomplished through thermal degradation of Azobisisobutyronitrile (at 70 °C). The resulting primary radicals proceed like a normal free-radical process until the growing chain (PA1) interacts with the CTA. Ideally, all RAFT agents should be consumed in this step before any further propagation begins. The radical then is transferred to the thiocarbonylthio group on the CTA, resulting in a radical intermediate. As the R group is a good leaving group, this intermediate radical can fragment to a chain with CTA end-group (Dormant chain) and a reinitiating R radical. Then this R radical can re-initiate monomer polymerization forming a polymer chain (PA2). Finally, rapid equilibrium between existing growing radicals and the dormant chain sets off. The RAFT equilibrium step reduces the concentration of propagating chain, slowing down the reaction time and allowing for highly uncrosslinked polymers of NIPAm to form.

RAFT polymerization is compatible with different kind of monomers, and allows control of polymer architecture. The R and Z end group can be modified for a particular application. Therefore, RAFT provides a convenient platform for the design of biomemetic polymers. [65, 66]

1.7 Application of MIP as receptor in chemical sensor

Chemical sensors are devices that can transfer information like, composition presence of a particular ion or molecule, concentration change, and partial pressure into an analytical signal. [67] There are two basic functional units in an ideal sensor: receptor and transducer. The receptor detects the chemical or biological information. The transducer transforms the information into a form of detectable signal. [68] The working process can be depicted by figure 1.9

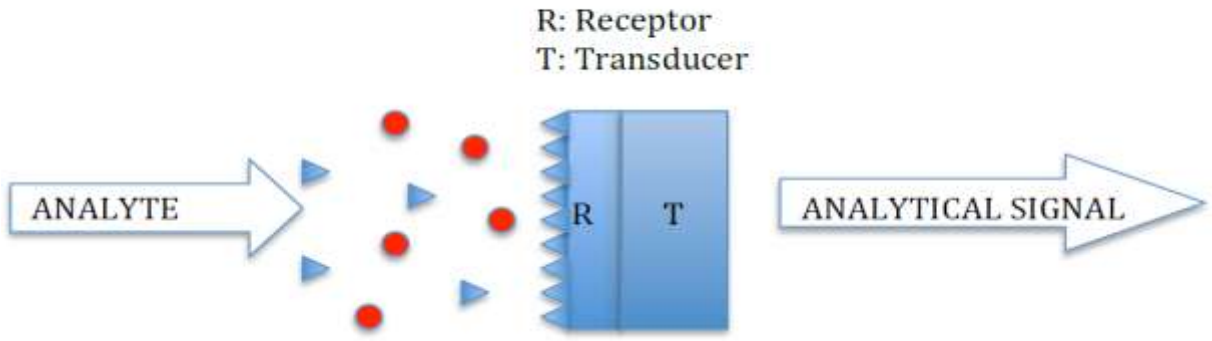

Figure 1.9 Scheme for chemical sensor (The receptor can only bind to the triangles while immune to the circles. The transducer can convert the chemical signal to a analytical signal.)

In figure 1.9, only the target molecules, the triangles, can fit into the receptor and trigger the transducer. The selectivity of the sensor is determined by the receptor, which has high specificity to target analyte. Chemical sensors are normally designed to operate under well defined conditions for specific analysis in certain samples. Therefore, the intrinsic requirement for a sensor is highly selective receptor. [69,70]

Sensors can be classified based on its signal, such as optical sensor[71], elecetrochemical sensor[72], mass sensors[73] and magnetic sensors[74]. Among all the sensors, fluorescent sensors attracted wide interests due to the ease of operational process, simple setup, high sensitivity, online throughput readouts, and most importantly the well understood principles behind fluorescence spectroscopy. [75]

Fluorescent sensors with MIPs as receptors can be developed by incorporating fluorescent monomers during polymerization, labeling the fluorophores onto the MIPs after polymerization or immobilizing the MIPs onto fluorescent nonparties.

Fluorescent intensity can be easily affected by the changing measurement conditions, such as temperature, pH, and ionic intensity. [76] To eliminate these environmental interferences , ratiometric sensors are developed. These sensors give more precise measurement owing to their self-referencing capability by calculation of two emission intensity ratio instead of the absolute intensity of one peak. [77.]

1.8 Thesis goal

The ultimate goal for this dissertation is to develop ratiometric fluorescent sensors with the novel biomimetic MIPs as receptors. Fluorescent ratiometric sensors can be designed based on following two mechanisms: fluorescence resonance energy transfer (FRET) and "on/off" sensor with internal standard.

A FRET sensor was developed in chapter 3, a pair of donor fluorophore and acceptor fluorophore was labeled on the MIPs. The emission spectrum of the donor fluorophore overlaps with the excitation spectrum of the acceptor fluorophore. [78,79] So the donor can transfer energy to the acceptor through non-radiation dipole-dipole coupling. The efficiency of the energy transfer is controlled by the distance between those two fluorophores. In the event of binding on the MIPs, the distance between donor and acceptor fluorophores increased. Accordingly, the efficiency of the energy transfer decreased. Therefore, the intensity of the donor peak increased while the intensity of the acceptor peak decreased as shown in figure 1.10.

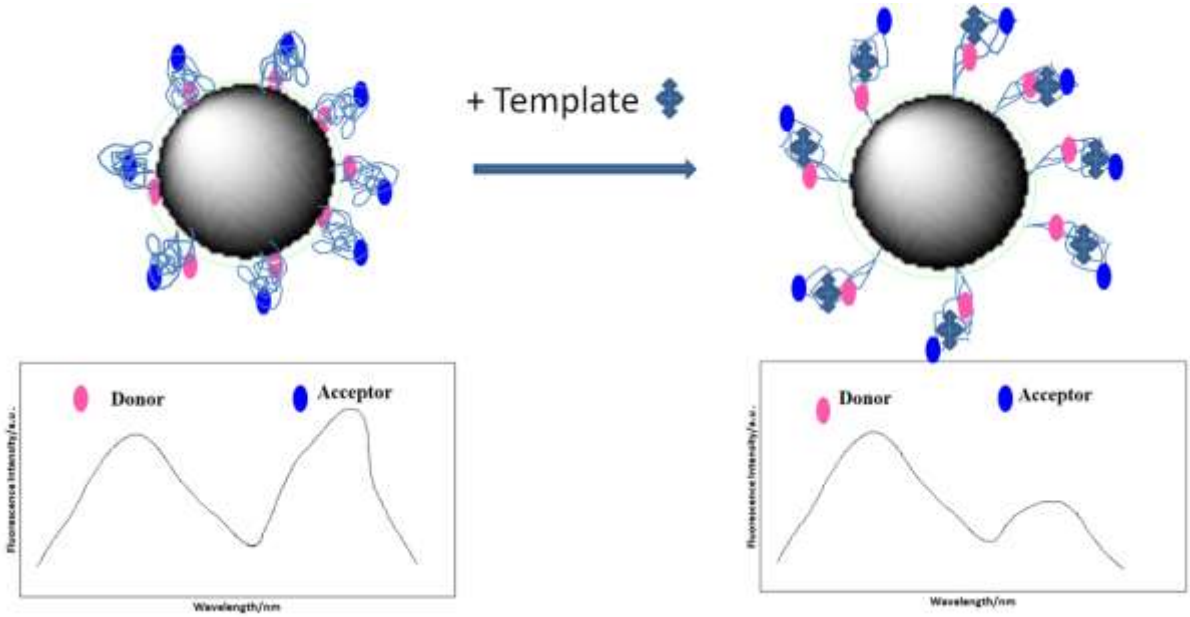

Figure 1.10 Scheme of FRET ratiometric fluorescent sensor

In on/ off sensor with internal standard, two individual fluorophores with different fluorescence emission wavelengths are built into same ratiometric sensors. [80,81] As the two different emissions have different responses to analytes, one emission peak can be used as specific recognition signal for the target analyte, while the other one is constant as reference signal. [82,83] In chapter 6, red quantum dots with emission at 610 nm were embedded into silica nanoparticles as internal standard. A fluorescein based trifunctional monomer (F-lysine) was used as functional monomer in the MIPs coated on the nanoparticles surface. When the templates bond to the MIPs, the fluorescent signal of F-lysine was quenched while the signal of quantum dots stayed constant as shown in figure 1.11.

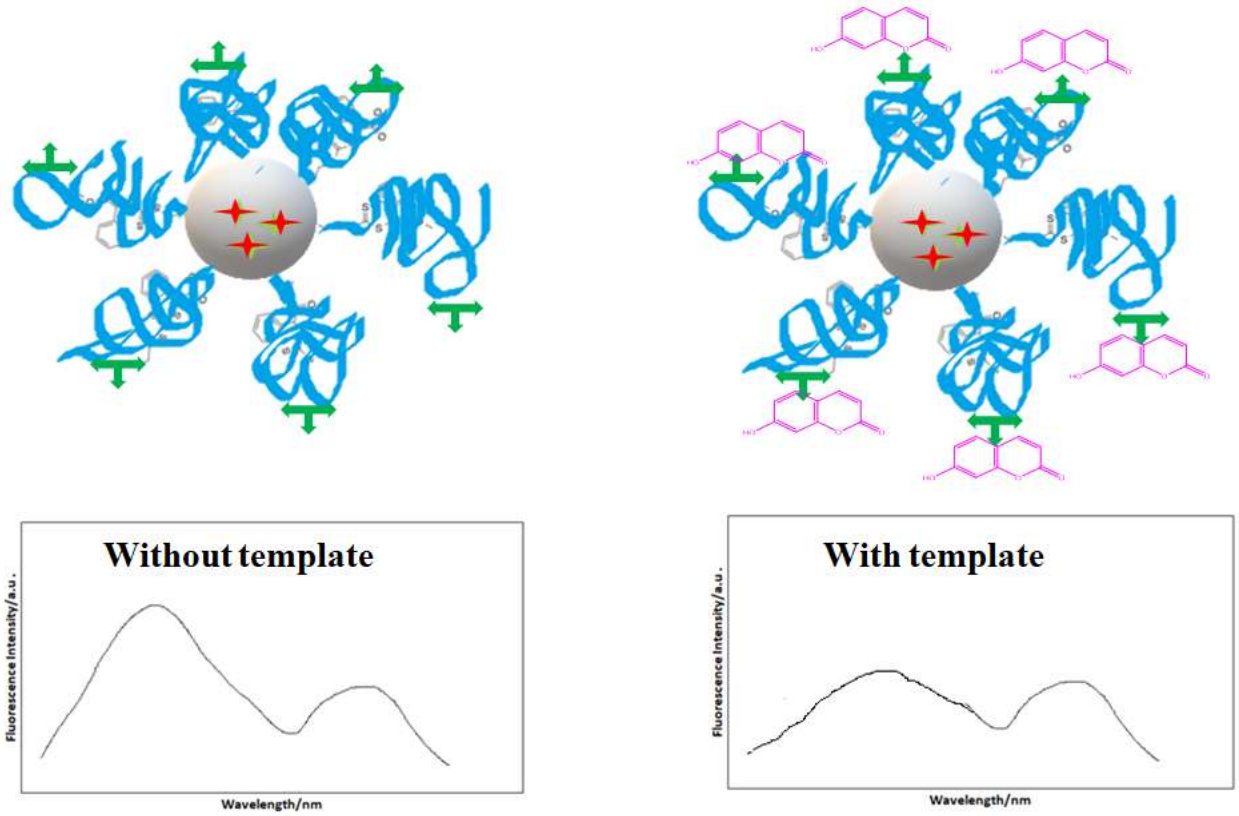

Figure 1.11 Scheme of on/off ratiometric fluorescent sensor

CHAPTER 2 EXPERIMENTAL METHOD

2.1 Reagents

Reagents are listed by their sources. Abbreviations are in parentheses in bold. The following list of materials and chemicals were used in these experiments:

Sigma Aldrich

- Methacrylic acid 99% purity (**MAA**). Passed through a column of basic alumina and inhibitor remover column to remove inhibitor.
- 4-Vinylpyridine 95% purity (**4VP**). Passed through a column of basic alumina and inhibitor remover column to remove inhibitor.
- N,N'-Methylenebisacrylamide 99% purity (**MBAm**). Recrystallized from methanol (3 times) to remove inhibitor.
- Benzyl Methacrylate 96% purity (**BMA**). Vacuum distilled then passed through a column of basic alumina and inhibitor remover column to remove inhibitor.
- 2-Acrylamido-2-Methyl-1-Propanesulfonic Acid Sodium Salt Solution 50% (w/w) in H_2O (**AMPS**). Passed through a column of basic alumina to remove inhibitor.
- [3-(Methacryloylamino) propyl] Trimethylammonium Chloride Solution 50% (w/w) in H_2O (**MPTA**). Passed through a column of basic alumina to remove inhibitor.
- 2-(Dodecylthiocarbonothioylthio)2-methylpropanoic acid N-hydroxylsuccinimide ester 98% purity (**DMNSE**). Used as received.
- Fluorescein *O*-acrylate, 97% purity (F). Used as received.
- (3-Aminopropyl)triethoxysilane, 99% purity (APTES). Used as received.

- 2,2’ Azobisisobutyronitrile 98% (**AIBN**). Recrystallized from methanol (3 times) to remove inhibitor.
- Inhibitor remover beads. Used as received.
- 2-Nitrophenol 99% purity (**2NP**).
- 3-Nitrophenol 99% purity (**3NP**).
- 4-Nitrophenol 99% purity (**4NP**). Recrystallized from methanol (3 times) to remove inhibitor.
- 7-hydroxycoumarin 99% purity (**7CM**). Recrystallized from methanol (3 times) to remove inhibitor.
- 4-Hydroxycoumarin, 98% purity (**4CM**). Used as received.
- 7-methoxylcoumarin, 99% purity (**7MC**). Used as received.
- 4-Chloro-7-Nitrobenzofurazan 98% purity (**NBD-Cl**). Used as received
- 8-Hydroxyquinoline, ACS reagent, ≥99%. Used as received
- Sodium Hydroxide, ACS reagent, ≥97% pellets (**NaOH**). Used as received.
- 1,4-Dioxane, 99.8% anhydrous. Used as received
- Acryloyl chloride, 97% purity. Used as received
- Dimethyl Sulfoxide, ACS Grade (**DMSO**). Used as received.
- Methanol, ACS Grade.
- Ethanol, ACS Grade.
- Acetone, ACS Grade.
- Chloroform, ACS Grade.
- Hexane, ACS Grade.
- Dichloromethane, ACS Grade.

- Acetonitrile, ACS Grade.
- Ethyl Acetate, ACS Grade.

Spectrum Labs

- Flat Dialysis Sheet Spectra/Por 3, MWCO 3.5 kD
- Dialysis Tubing Spectra/Por 2, MCWO 12-14 kD
- Dialysis Clips 78 millimeters, weighted and unweighted.

EMD Millipore

- Acetic Acid
- Hydrochloric Acid

Tokyo Chemical Industry

- N-isopropylacrylamide 99% purity (**NIPAm**). Recrystallized from hexane (3 times) to remove inhibitor.

Alfa Aesar

- Basic Alumina Activated. Used as received.

Invitrogen

- Alexa Fluor 647 carboxylic acid (A647), succinimidyl ester. Used as received.

Polysciences

- *N*-(3-aminopropyl) methacrylamide hydrochloride, 98+% purity (APMA). Used as received.
- **N**-n-propylacrylamide, 97% purity((NnPAM). Passed through a column of basic alumina and inhibitor remover column to remove inhibitor.

- PolyFluor 570: Methacryloxyethyl thiocarbamoyl rhodamine B (R). Used as received.

Wako Chemicals

- Methanol, ACS Grade.
- Ethanol, ACS Grade.
- Acetone, ACS Grade.
- Chloroform, ACS Grade.
- Hexane, ACS Grade.
- Dichloromethane, ACS Grade.
- Acetonitrile, ACS Grade.
- Ethyl Acetate, ACS Grade.
- Acetic Acid, ACS Grade
- Hydrochloric Acid, ACS Grade
- Nitric Acid, ACS Grade

2.2 Apparatus

The fluorescent emission and excitation spectra (**FS**) were measured on a Cary Eclipse Fluorescence Spectrophotometer with a Peltier thermostatted single cell holder.

Ultra-violet/Visible absorption spectra (**UV-Vis**) were measured on a Varian Cary 60 UV-Vis spectrophotometer. The concentration of the analyte is directly proportional to the absorption and can be quantified using Beer's law: $A=\varepsilon bc$, where A= absorbance, ε= molar absorptivity, b= cell path length, and c= concentration of template molecule.

Nuclear Magnetic Resonance Spectra (**NMR**) were measured on a Varian 400 MHz Mercury Liquid State NMR to determine the structure of the analyte.

Scanning Electron Microscopy (**SEM**) was performed on a Tescan Lyra3 GMU FIB SEM. By scanning a beam of electron across the surface of the sample and detecting the reflected electrons, the morphology, size and surface information of the sample can be determined.

Transmission Electron Microscopy (**TEM**) was performed on Zeiss/LEO 922 Omega TEM. A beam of electrons is transmitted through an ultra-thin specimen, interacting with the specimen as it passes through it. The size and morphology of the sample can be measured.

Dynamic Light Scattering (**DLS**) were performed on Malvern Zetasizer Nano ZS90. The LCST of the polymer were determined by measuring the size of the polymer particle with temperature.

Fourier-transform infrared spectra (**FTIR**) were measured on a Thermo Nicolet iS10 FTIR. The transmission spectra were collected for MIP coated nanoparticles to confirm the immobilization of MIPs on the nanoparticle surface.

A Branson model 1210 sonicator was used for reagent dissolution and sonication. A Buchi RE111 Rotavapor was used to evaporate solvents. Separation of precipitated polymer from the solution and nanoparticle from supernatant was performed with an Eppendorf Centrifuge 5415 D (13,200 rpm) Microcentrifuge 26 Tube Holder. A Labconco FreeZone 1 Liter Bench Top Freeze Dry System to remove water from samples. Dialysis tubing, Sigma Aldrich MWCO of 12,000 to 14,000, was used to purify MIPs. Sigma Dialysis Sheets with MWCO of 3,500 was used in the equilibrium dialysis cell by Bel-Art, 1.4 mL volume.

2.3 Monomer purification

To increase the yield and efficiency of the polymerization, all monomers have to be purified before use.

The solid monomers were recrystallized in one of the solvent listed in the 2.1. A saturated solution of monomer in a solvent was prepared at high temperature. Then, the solution was cooled. During the cooling process, the monomer will recrystallized out of solution due to the reduced solubility. This solvent mixture was vacuum filtered to separate the crystal from the solvent. [84,85] The impurity was removed with the solvent. The recrystallization was repeated three times to completely remove the impurity.

All liquid monomers (except AMPS and MPTA) were purified by passing through a column packed with inhibitor remover and basic alumina to fully remove the inhibitor. [86]

The AMPS and MPTA, which are used as cation and anion for electron static interaction, were mixed together first with 1:1 mole ratio. After stirring at room temperature for one day, the mixture was extracted with chloroform. The anion-cation complex formed during stirring had higher solubility in chloroform. So it can partition into the organic layer. After rotovaping the chloroform, the anion and cation complex can be used for polymerization.

2.4 Freeze-pump-thaw degassing

Before polymerization, the monomer mixture was degassed to remove oxygen. Molecular oxygen has a high reactivity towards radical species due to its ground state "biradical"

nature.[87] The reaction yields peroxy radicals which are less reactive as initiator. In other words, the oxygen can scavenge effective propagating radicals and reduce the yield of polymerization. [88]

To remove the oxygen, the monomer mixture was degassed by going through 4 cycles of the Freeze-Pump-Thaw process as shown in figure 2.1. The mixture was placed in a Schlenk flask and sealed well. After freezing the mixture in acetone dry ice bath, the flask was hooked up to a Schlenk line to pump off the atmosphere for 10 min. Afterwards the flask was sealed again and placed at room temperature to thaw the mixture. Bubbles were released from the solution. After 4 cycles of Freeze-Pump-Thaw process, the flask then was filled with nitrogen gas and ready for polymerization.

This method takes advantages of pressure dependence of gas solubility in liquid. The pressure of the gas inside the Schlenk flask is reduced during the pumping process. During the thawing process, a new liquid- gas phase equilibrium were established. As a result the dissolved gas was released from the liquid as bubbles.

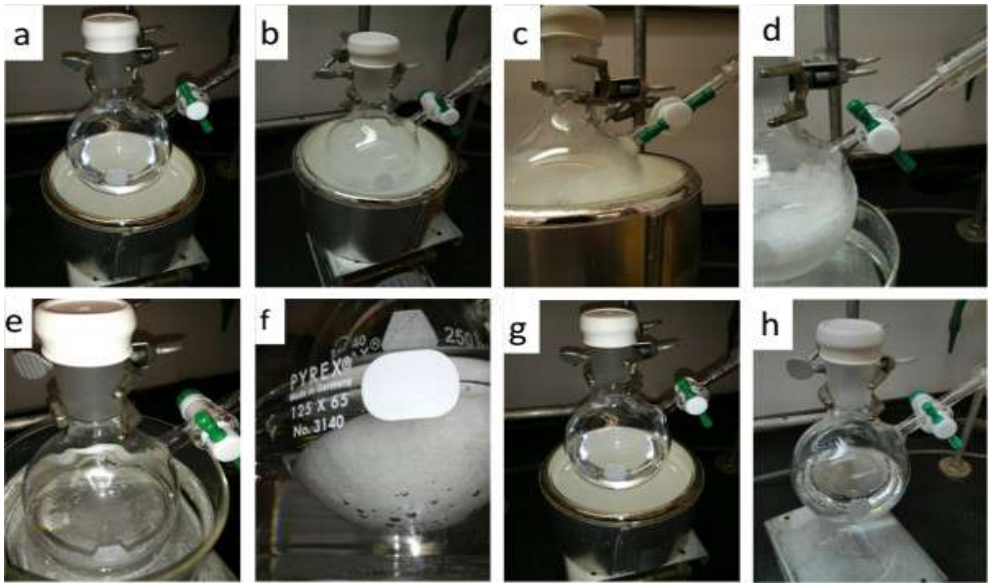

Figure 2.1 Detail photos of the free-pump-thaw steps [89]: (a) place solvent in flask; (b) freeze the solvent in dry ice; (c) introduce vacuum; (d) seal the flask under vacuum; (e), (f) thaw the solvent and observe evolution of gas bubbles; (g) repeat freeze thaw process (Four cycles recommended); (h) seal the solvent under nitrogen.

2.5 Template removal process

After polymerization, the template molecules need to be removed from the MIPs scaffold. The removing processes were adjusted based on MIP the properties.

For free floating MIPs, the polymer was precipitated out of the solution by adding hexane. The solubility of the monomer in hexane is higher than polymer. So the unreacted monomer and most of template molecules were left in the hexane. The polymer was separated by centrifugation. It was observed that after 4 rounds of precipitation over 90% template molecules can be removed. Then, the MIPs were dissolved in a good solvent for the template molecules and dialyzed against

acid and base alternately. For 7-hydroxyl imprinted polymers, the very last 1 percent of the template need to be removed by refluxing in methanol and sodium hydroxide solution for over 2 days.

For MIPs grown from the silica nanoparticles, the template molecules were removed by washing the nanoparticles with THF 3 times, methanol and acetic acid (90:10, v/v). For MIPs coated magnetic nanoparticles, the template was removed by soxhlet extraction. The magnetic nanoparticles were attached onto a magnetic bar and placed inside the soxhlet extractor as shown in figure 2.2. The function of the stir bar is to hold the nanoparticles inside the extractor. The sample was extracted for 1 week.

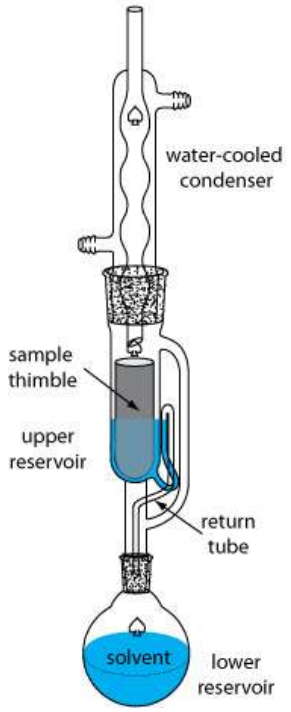

Figure 2.2 Soxhlet extraction [90] (This is for the template removal of MIP coated magnetic nanoparticles. The magnetic nanoparticles were first attracted onto a magnet sir bar. Then this stir bar was place inside the extractor.)

2.6 Coating MIPs onto nanoparticle

For the design of different fluorescent sensors, The MIPs were coated onto nanoparticles surfaces by different method. Typically, the methods can be classified as “grown from” and “graft onto” by how the polymer was prepared. [91]

2.6.1 “Grown from” method“

The “grown from” method was applied for coating MIPs onto arosil 200 silica nanoparticles, silica coated magnetic nanoparticles, dye doped silica nanoparticles and quantum dots embedded silica nanoparticles. A RAFT agent was first grafted onto the silica surface to form nanoparticles supported macro-RAFT agent. Two RAFT agent were used for this purpose: DMNSE and MPTT, structures shown in figure 2.3.

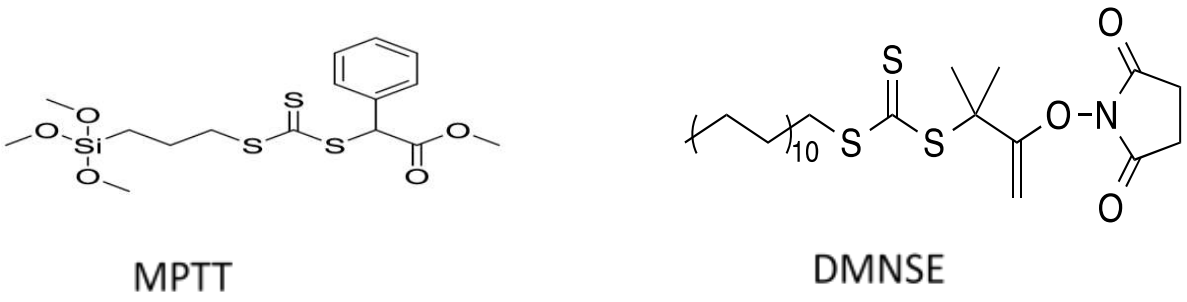

Figure 2.3 Structure of RAFT agent MPTT and DMNSE

The RAFT agent MPTT contains a trimethoxysilyl end group, which can react with the silanol groups on the silica surface. Due to the water sensitivity of the trimethoxysilyl group, the whole process was conducted under anhydrous environment.

The RAFT agent DMNSE contains a N-hydroxysuccinimide esters (NHS ester) group. It was attached to the silica surface by NHS ester conjugation with pre-aminated silica surface as shown figure2.4.

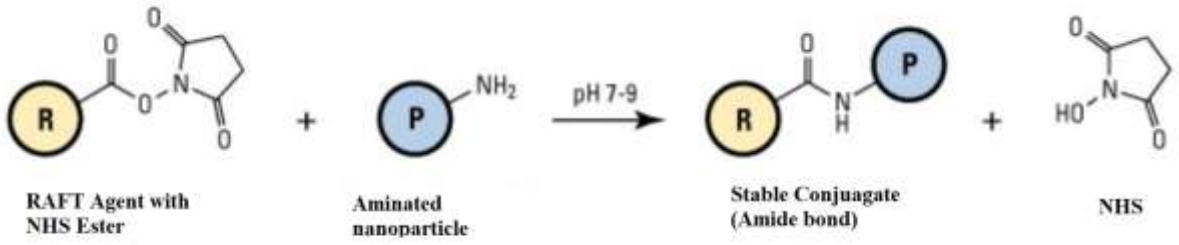

Figure 2.4 Scheme of NHS ester reaction[92] (This is the reaction between DMNSE and aminated silica surface.)

2.6.2 "Graft onto" method

The "Graft onto" method was utilized by attaching the MIPs on to gold nanoparticles. In this method, the free floating polymer was prepared by RAFT polymerization in dioxane with DMNSE as the RAFT agent. After polymerization and removal of the template, the polymer contained a dithioester group. Dithioester end groups were reduced by sodium borohydride to a thiol end group. In aqueous media at ambient temperature, the thiol reacted with gold nanoparticles as shown in figure 2.5.

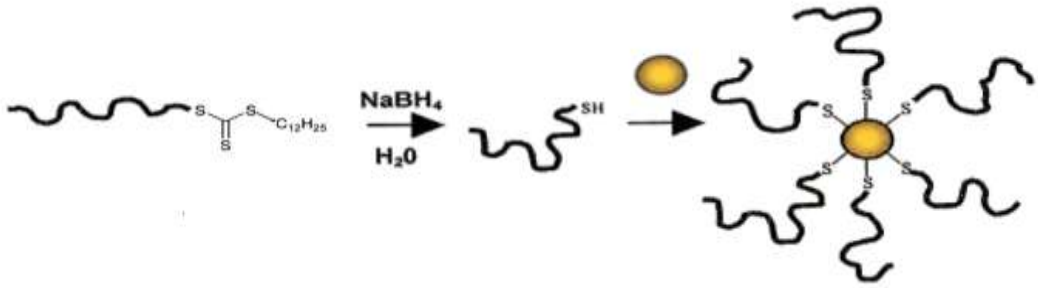

Figure 2.5 RAFT MIPs were reduced to a thiol and attached to gold nanoparticle surface.[93]

2. 7 Fluorescence experiments

The fluorescent emission and excitation spectra of the sensors were measured by a Cary Eclipse Fluorescence Spectrophotometer with a Peltier thermostatted single cell holder. It was equipped with intense Xenon flashlamp for highsenaitivity and a Red-sensitive Photomultipler tube detectors that can detect wave length from 200-900nm for both excitation and emission spectra. The detector is located at a 90-degree angle from the light source. This geometry is used instead of placing the detector at the 180-degree angle to avoid the interference of the transmitted excitation light and increase sensitivity.[94, 95] The 90-degree geometry is shown in figure 2.6.

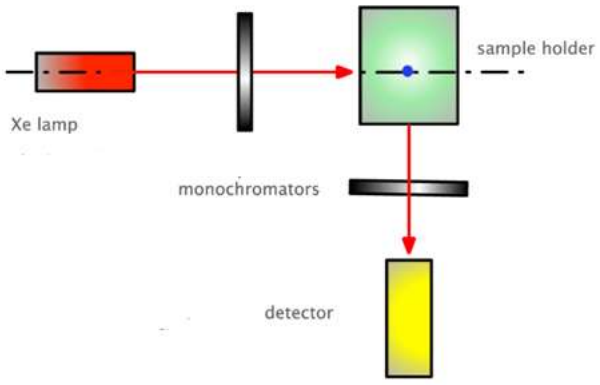

Figure 2.6 Optical configuration of Cary Eclipse Fluorescence Spectrophotometer. [95]

For the FS experiments, sensor samples were first dissolved in different solvents to form stock solution with known concentration. Then 1ml or 3ml of the sensor stock solution was transferred to a quartz cuvette. After measuring the initial spectra, template solutions of different concentrations were added to investigate the binding effect. The temperature of the samples was held at the LCST of the MIPs.

Fluorescent emission spectra were collected by fixing the excitation wavelength, and scanning fluorescent emission intensity at different wavelength. The excitation spectra were collected by fixing the emission wavelength and scanning the excitation wave length.

2.8 Dynamic light scattering

The size for the polymer particles are measured by Malvern Zetasizer Nano ZS 90 instrument based on dynamic light scattering. In a solution, particles are constantly moving due to the random collision with the molecules of the liquid surrounding the particles. This movement is known as Brownian motion. [96] The larger the particle, the slower the Brownian motion will be. The smaller particles were kicked further by the solvent molecules and move rapidly. [97]

When a Laser beam went through the solution with particles, most of the beam passed through the sample, but some were scattered by the particles within the sample at all angels. The scattered light at either 173 degree or 90 degree was detected for the size calculation as shown in figure 2.7. The attenuator controlled the intensity of the laser sourced to maintain intensity of the scattered light with a specific range of the detector.

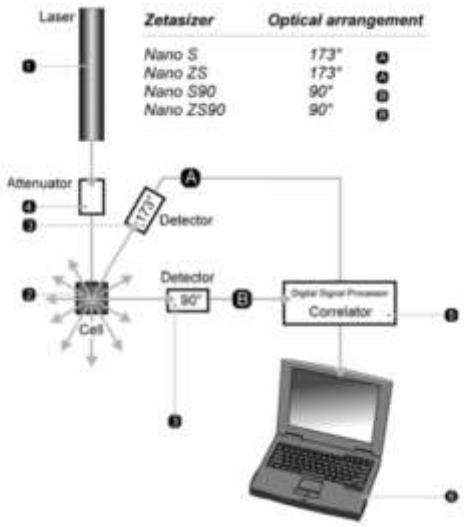

Figure 2.7 Optical configurations of the Zetasizer Nano series [98] (1. laser source; 2. sample cell; 3. detector ; 4. attenuator ; 5. digital signal processor; 6. computer)

The Brownian motion caused randomness to the phase of the scattered light. When the scattered light from two or more particles was added together, there will be a changing destructive or constructive interference. This leads to time-dependent fluctuation in the intensity of scattered light. The Zetasizer Nano instrument measures the rate of the intensity fluctuation and then used this data in an algorithm to calculate the hydrodynamic radius of the particles.[99]

The smaller particles caused the intensity to fluctuate more rapidly than the larger ones.

For the size measurement, the samples were dissolved in water first. Then this solution was filtered twice with a filter to remove the dust and filled into a cuvette. Then the temperature and other parameters of the measurement were set up. The viscosity of the sample was estimated based on the viscosity of water. The diffusion coefficient was estimated by using the "protein" setting available on the instrument.

2.9 Binding tests

Binding tests were conducted in equilibrium dialysis blocks. Two sides of the blocks with identical volume were separated by the dialysis membrane with a specific molecular weight cut off (MWCO) pore size. The polymer was contained on one side. The template can pass through the membrane and equilibrate with the other side. [100]

Typically, polymer was placed in one side of the polymer and template was placed in the other side of the polymer. There were two equilibria established within the block. The first one is the distribution equilibrium of the template molecules between two sides of the blocks across the membrane. The second one is the binding equilibrium between the template and the MIPs. If the binding occurs the concentration of the template on the polymer side would be higher than then the other side.[101]

However in the situation of binding between 7-hydroxycoumarin and the MIPs, it took too long for the template to cross the membrane and then bind with the MIPs even at the LCST. This is a serious problem when there are limited numbers of the blocks. To improve the efficiency, the MIPs were dissolved directly inside the template standard solution. Then this template and MIPs mixture was dialyzed against the blank solution as shown in figure 2.8.

The distribution ratio (K_d) would be larger than 1 in the event of binding. The K_d was calculated by:

$$K_d = \frac{T_{original} - T_{Free}}{T_{Free}}$$

The T_{Free} is the concentration of the template diffused to blank side after equilibrium dialysis. $T_{original}$ is the original concentration of template solution that dissolved MIPs.

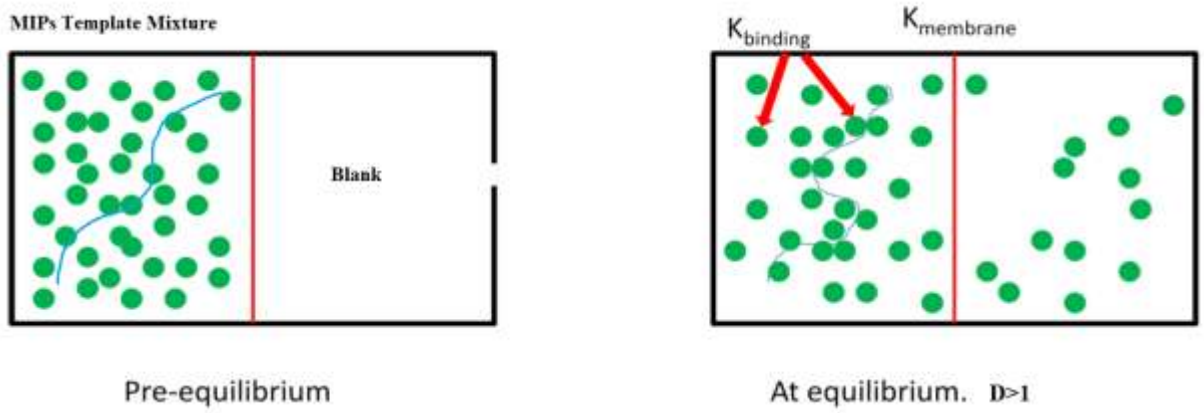

Figure 2.8 Equilibrium dialysis block (before equilibration(left), at equilibration(right))

2.10 Spin-down experiments

To determine the binding affinity of MIPs, the polymer coated nanoparticles were titrated with the template.

First the composite nanoparticles were equally distributed into 1.5 ml micro centrifuge tubes. Then 6 standard template solutions with different concentration were added into different tubes. After mixing well and equilibrating for 15 min at LCST, the MIPs on the nanoparticles interacted with the template. After centrifugation, the bound template molecules moved with the nanoparticles to the bottom of the tube as pellets, while the unbound template molecules stay in the supernatant as shown in figure 2.9.

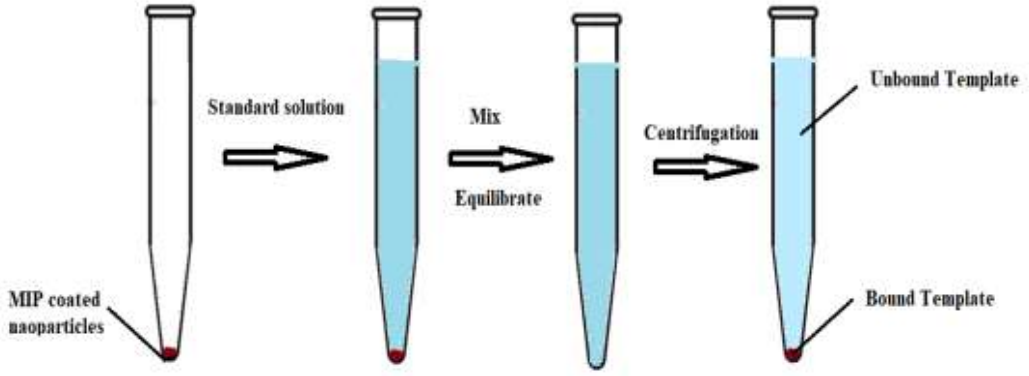

Figure 2.9 Scheme of spin-down experiments

After separation, the FS emission spectra of the supernatant were collected. The intensity of the emission was proportional to the concentration of the template. So moles of unbound templates molecules can be calculated. The concentration difference between the supernatant and the initial standard solution was the bound template molecule concentration.

CHAPTER 3

DEVELOPMENT OF SILICA NANOPARTICLE SUPPORTED RATIOMETRIC FLUORESCENT SENSOR

3.1 Introduction

In this project, a ratiometric fluorescent sensor that can sensitively detect 4-nitrophenol (4NP), a poison in ground water and food, is prepared by growing molecularly imprinted thermo responsive poly(N-n-propylacrylamide) (PNnPAM) brushes from the Aerosil 200 silica nanoparticle surface. The polymer brushes are grown via Reversible Addition-Fragmentation chain Transfer (RAFT) polymerization. This living polymerization process make it possible to copolymerize a Fluorescence Resonance Energy Transfer (FRET) donor, Polyfluor 570 Rhodamine B (Rhodamine), in one block of the polymer, and an acceptor, Alexa fluor 647 (A647), in another block, thereby generating poly(NnPAM-co-Rhodamine)-b-(NIPAM-co-A647).

Upon exposure to analytes, the binding sites developed by the molecular imprinting technique will specifically bind to the analyte molecules. It was hoped that binding would changes the distance between these two fluorophores as shown in figure 3.1, thereby affecting the FRET efficiency. Therefore, the chemical binding process is converted to detectable spectroscopic signal. The ratio of the emission intensities of these two fluorophores is measured to eliminate the interferences from the matrix and instrumental variations.

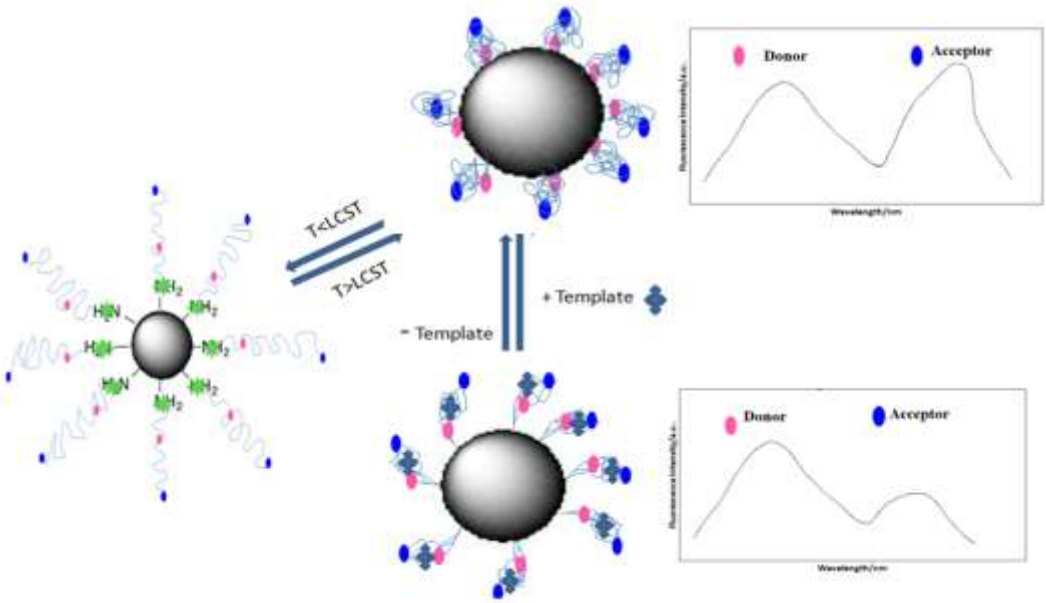

Figure 3.1 Sensing mechanisms for the ratiometric fluorescent sensor (The biding process between the template and the MIPs was expected to increase the distance between those two fluorophores. Due to the decreased FRET efficiency, the intensity of the acceptor fluorophore would increase; the intensity for the acceptor would decrease.)

It was expected that the addition of the template 4NP into the sensor might change the intensity ratio between the acceptor fluorophore and donor fluorophore (A/D ratio). The sensor will only respond to the template 4NP and should be immune to the structural isomers 3NP. The structures of the 4NP and 3NP are shown in figure 3.2.

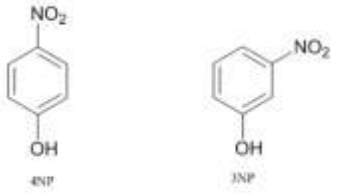

Figure 3.2 Structure of the template (4-Nitrophenol (**4NP**) and 3-Nitrophenol (**3NP**))

The binding sites on the indicator are built by imprinting template into the polymer chains at high temperature in aprotic organic solvent, followed by removing the template at low temperature in aqueous solution. Unlike the traditional molecular imprinting technology based on high percentage of covalent crosslinking, the binding site conformation in this project is maintained by non-covalent crosslinking such as acid-base interactions, π-π interactions and electrostatic effects to achieve faster binding/unbinding kinetics.

It is believed that the combination of 2 different kinds of different non-covalent crosslinking can increase the binding affinity. Sensors based on different non-covalent crosslinking are investigated in this project:

1) Sensor MQQ1324 and MQQ1325 based on the combination of acid-base crosslinking with , π-π interactions
2) Sensor MQQ1326 based the combination of π-π interactions with electrostatic effects
3) Sensor MQQ1327 based the combination of acid-base crosslinking with electrostatic effects

3.2 Preparation of sensor MQQ1324 based on acid-base interaction and π-π interaction

The sensor was developed by growing polymer form the silica surface using RAFT polymerization method. First, the RAFT agent was grafted onto silica nanoparticle surface. Then this silica supported RAFT agent was used to grow MIPs. Two fluorophores Alexa Fluor 647 and Rhodamine B were used to label the polymer.

3.2.1 Amination of silica nanoparticles

1.0036g Aerosil 200 silica and 528ul (2.26mmol) (3-Aminopropyl) triethoxysilane (APTES) were added to a 100 ml round bottom flask with 50 ml anhydrous toluene. The solution was stirred and reacted at room temperature for 8 hours. Then the particles were centrifuged and washed 3 times with ethanol and another 3 times with deionized. [102]The mechanism of this reaction is shown in figure 3.3.

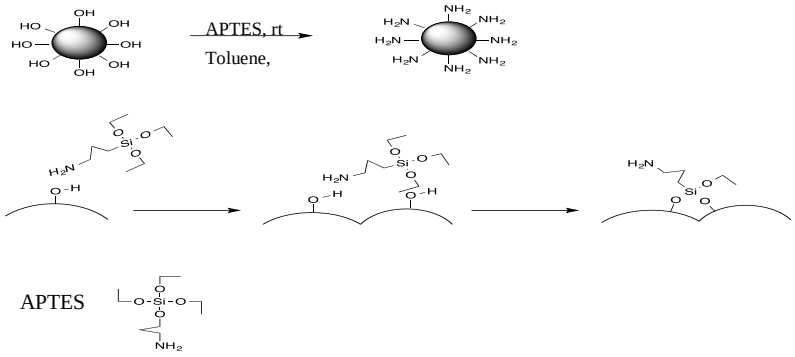

Figure 3.3 Mechanism of amination on silica nanoparticle surface

At the beginning of the reaction, the electron-rich nitrogen center of the amine group on APTES could interrupt the hydrogen bonds between silanol groups on the silica surface, thus resulting in fast physisorption of APTES onto silica nanoparticles. Then the amine group catalyzed the condensation between the silicon side of the APTES with silanol groups on the silica particle surface. As a result the amine group was attached on the surface of the silica nanoparticles and served as an active site to bind other molecules.

3.2.2 Attaching RAFT agent (DMNSE) onto silica nanoparticle surface

The aminated silica nanoparticles were suspended in 50 mL 0.1 M bicarbonate buffer in a round bottom flask. 0.2 mmol RAFT agent DMNSE was dissolved in a vial in 10 ml DMSO.

Then the dissolved raft agent was added into the silica suspension. The mixture was stirred at room temperature for 8 hours. The yellowish product was then collected by centrifuge and washed with ethyl alcohol three times and 1,4-dioxane three times.

The surface area of aerosol 200 nanoparticle was 200m^2 /g. On each square nanometer, there are 2.5 OH groups on the silica. So the total number of OH groups on the surface of 1.0 g silica was 8.3×10^{-4} moles. In the amination process APTES was 10 fold in excess. So theoretically after the amination, the coverage of amine group should be 100%. This meant about 0.2 mmoles amine groups were attached to the surface of the silica. As the ratio between the amine groups and DMNSE is 1:1, the theoretical amount of RAFT agent on the surface is about 0.2 mmoles.

3.2.3 Growing polymer from silica nanoparticle

The formulation of the polymer was shown in table 3.1. Tthe mole ratio of monomer, RAFT agent and initiator was 100 : 1 : 0.1. The feed mole percent of monomers were 75 mol% NnPAm, 10 mol% 4VP, 5 mole% MAA and 10 mole% BMA. The recognition monomer to template (R to T) ratio is 5: 1.

Sensor	NnPAM	4VP	MAA	BMA	RAFT agent	Initiator	R to T ratio
MQQ1324	75%	10%	5%	10%	1%	0.1%	3:1

Table 3.1 Formulation of polymer layer in sensor MQQ1324

One fourth of the product from previous reaction (0.05 mmoles CTA) was added into a round bottom flask with 50ml 1,4-dioxane. 0.125mmoles 4-nitrophenol, 3.75 mmoles NnPAM, 0.25 mmoles MAA, 0.5 m moles BMA and 0.5 m moles 4-VP were also dissolved in this flask. 0.05 mmoles AIBN were dissolved in 1.00 ml 1,4-dioxane in a vial. Then 100ul of this solution was added into the round bottom flask.

The round bottom flask was sealed with a rubber septum. Then the mixture was degassed with nitrogen for fifty minutes followed by heating to 70°C for ten hours with moderate stirring. Then 0.025 mmoles AEMA were dissolved in 1 ml alcohol, degassed for ten minutes, and added into the round bottom flask by syringe. Four hours after the addition of AEMA, the nanoparticles were separated by centrifugation and washed with ethyl alcohol three times and diethyl ether three times. Then the product was air dried over night.

The mechanism of RAFT polymerization is shown in figure 3.4. The 2-methylpropionic group in the RAFT agent DMNSE was the R group, the dodecyl group is the Z group.

The initiation step started with the decoposition of initiator Azobisisobutyronitrile (AIBN) into two free radicals. Then these free radicals proceeded to form the primary radical (PA1). In the pre-equilibrium step, the primary radical (PA1) attacked the RAFT agent (RA-silica) on the silica surface, resulting a intermediate radical. When the leaving group R (2-methylpropionic group) was eliminated, a domain chain with thiocarbonylthio moiety and a radical on the silica surface were formed (PA2). In the RAFT main equilibrium step, the propagation of PA2 is going on, all the monomers (including MAA, BMA, 4-NP and Nnpam) and Rhodamine in the solution are polymerized randomly. After 10 hours of polymerization, PA3 was formed which contained the donor fluorophore and functional monomers. Then AEMA was added and polymerized at the

end of the polymer chain, which is away from the silica surface.

The sensor MQQ1325 was made with the same formulation, except that the template was 3NP instead of 4NP.

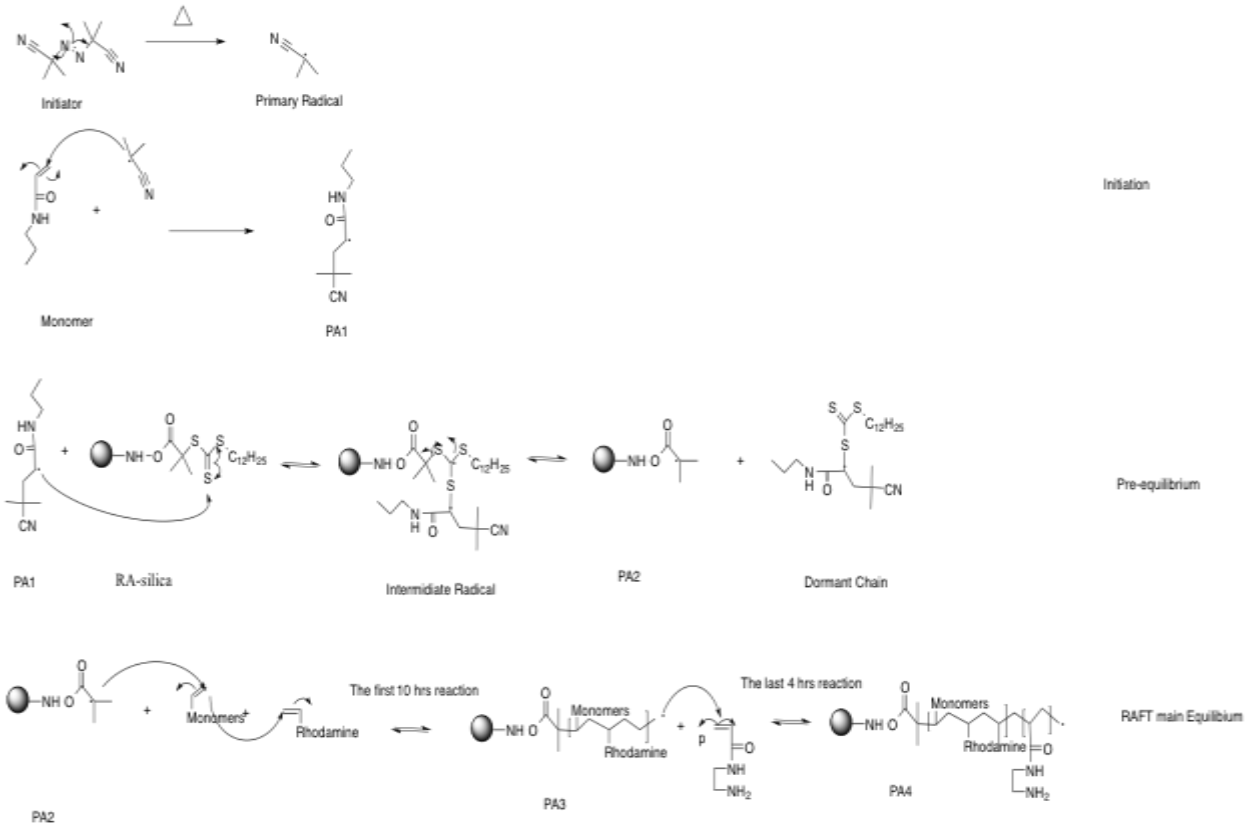

Figure 3.4 Mechanism of RAFT polymerization on silica surface

3.2.4 Labeling Alexa 647 to the polymer chain

0.0013g of the product from previous part was suspended in 1 ml deionized water and 100 ul of this solution was transferred into 1 ml 0.1 M bicarbonate buffer in a small vial. Then 100 µl A647 (1 mg/mL DMF) were added into the vial. Afterwards, this vial was placed on the stir plate at room temperature for 8 hours. The final structure of the sensor is depicted in figure 3.5.

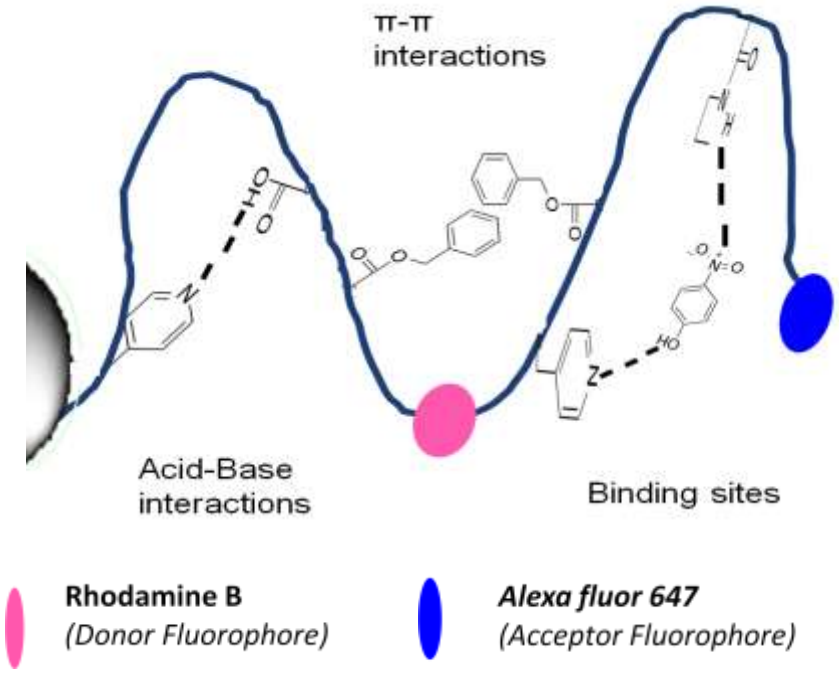

Figure 3.5 Schematic illustration of the fluorescent ratiometic sensor MQQ1324

The hydrogen bonds between the MAA and 4VP hold the configuration of binding sites on the polymer chain. So the memory of the template was imprinted inside the polymer layer. There were two blocks in these polymer chains. The first block is formed in the first 10 hours of polymerization, in which the donor fluorophore Rhodamine B was incorporated. The second

block was formed in the last 4 hours of polymerization after the addition of AEMA. The acceptor fluorophore Alexa 647 was attached to the amine groups in AEMA. The distance between the donor and acceptor can be controlled by the lengths of each block.

3.2.5 Template removal

The product from the previous reaction was transferred into a dialysis tube with a MWCO of 12,000-14,000 and dialyzed against 1000ml D.I. water. 1 ml of acetic acid was added into the first dialysis to remove the template molecules. The final product was collected by centrifugation and washed with DI water for three times.

3.3 Results and discussion

3.3.1 Thermal tests

PolyNnPAm is a well known thermal responsive material. The theoretical LCST for Poly NnPAm is 22°C, where the phase transition of the polymer chain happens. At the beginning of the phase transition the polymer chains will form globules from random coils. Then these globules will aggregate at the end of the phase transition. The phase transition process of the sensor MQQ1324 was investigated by dynamic light scattering. The diameter of the polymer at different temperatures are plotted in figure 3.6.

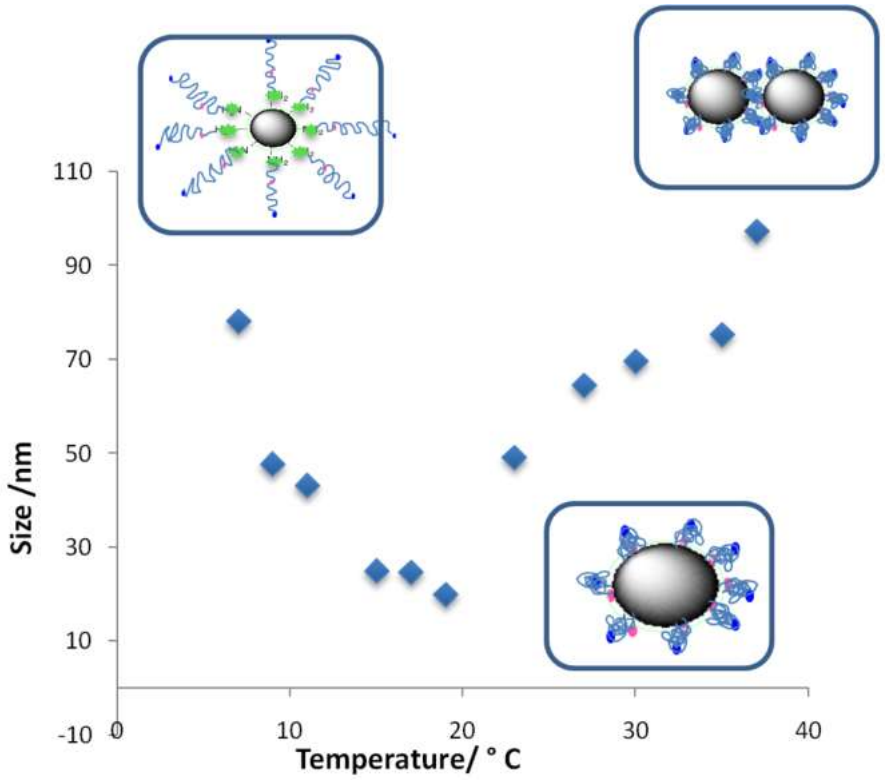

Figure 3.6 Size of MQQ1324 at different temperatures measured by DLS

The size of the sensor decreased from 6 °C to 20 °C, this is due to the transition from random chains to globule. Then the size increased after 20°C, this indicated the aggregation of nanoparticles. During the phase transition, the distance between the donor fluorophore and accepter fluorophore was decreasing. So the FRET energy transfer from donor to accepter should be more efficient. As a result, the peak of the donor should decrease and the peak of the accepter should increase. The fluorescence intensities of both fluorophores were measured at the three different temperatures. The spectra are showed in figure 3.7.

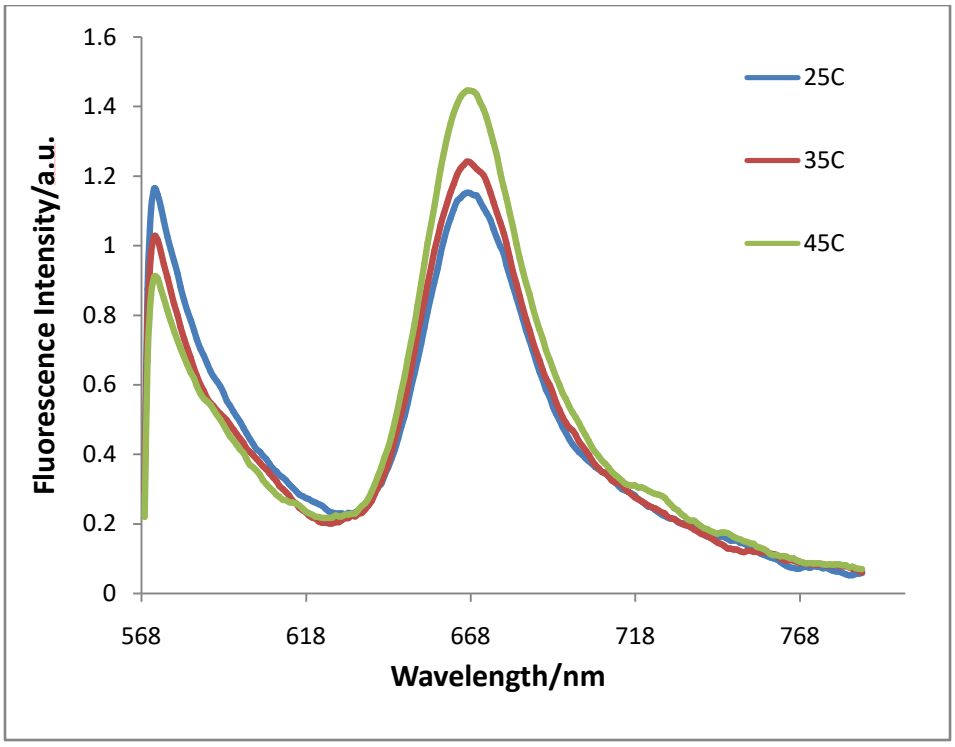

Figure 3.7 Thermal tests for the sensor MQQ1324 (The intensity of the donor peak decreased the intensity of the acceptor increased. This indicated the distance between the fluorophores are decreased, the polymer were shrinking.

3.3.2 Sensing experiments

In order to investigate the binding between nitrophenol and the sensor, fluorescence intensity of donor and acceptor fluorophores have been measured by the Varian Cary Eclipse fluorometer. The selectivity and binding affinity were measured by titrating the sensor with different concentrations of template molecules and its isomers.

The sensor MQQ1324 was imprinted by 4-Nitrophenol. It is expected that the template 4NP can interact with the binding sites in the polymer layer and decrease the distance between

the donor fluorophore and the accepter fluorophore. The emission intensities of the donor and accepter fluorophore would be changed. Therefore, the Acceptor to Donor ratio (A/D ratio) will be decreased. The emission spectra of the sensor at different template concentration were shown figure 3.8. These spectra were scanned from 545 nm to 800 nm, which covered both the emission of Rhodamine, at 570 nm, and Alexa 647, at 670 nm.

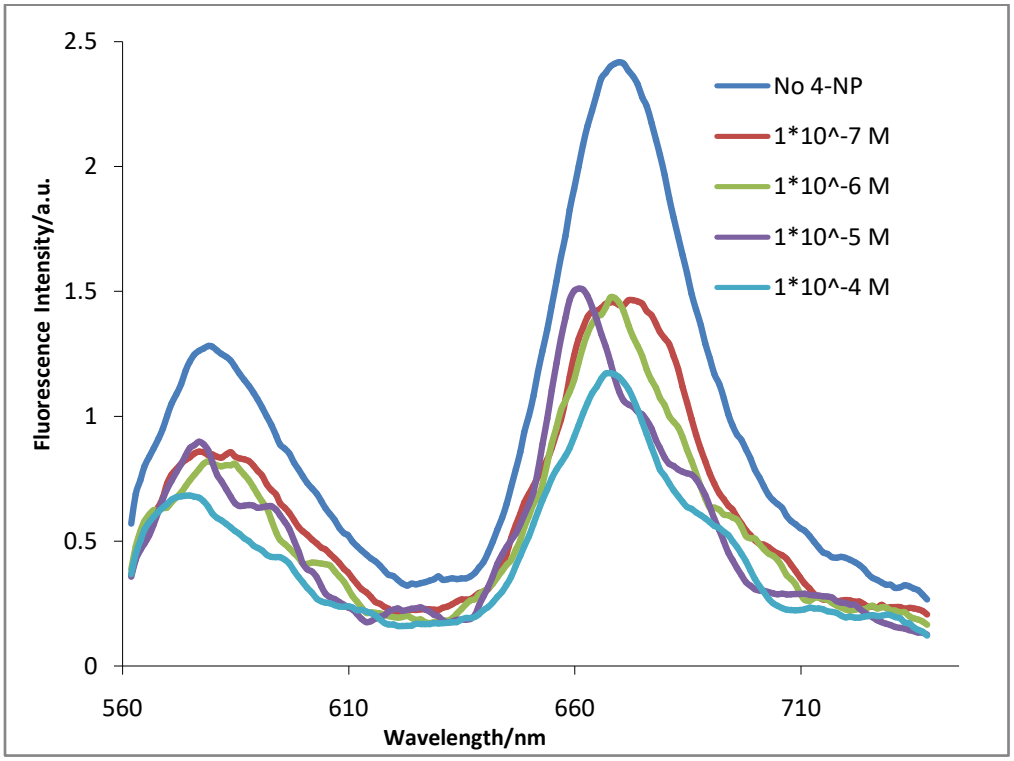

Figure 3.8 Fluorescence spectra for addition of 4NP into MQQ1324 (at 20°C, λex=545nm)

Upon addition of the template, intensity of both the donor and acceptor peak decreased significantly upon the addition of template 4NP. This is because the 4NP interact with the binding sites in the polymer and quench the fluorescent intensity of both donor and acceptor fluorophores. These results also indicated that the sensor MQQ1324 could bind to its template 4NP with high binding affinity at concentrations as low as 1×10^{-7}M.

3.3.3 Selectivity tests

Since the sensor MQQ 1324 was imprinted by 4NP, it is expected that this sensor would selectively bind to its template while ignoring isomer 3-nitrophenol (3NP). The data for addition of 3NP into MQQ 1324 are shown in figure 3.9.

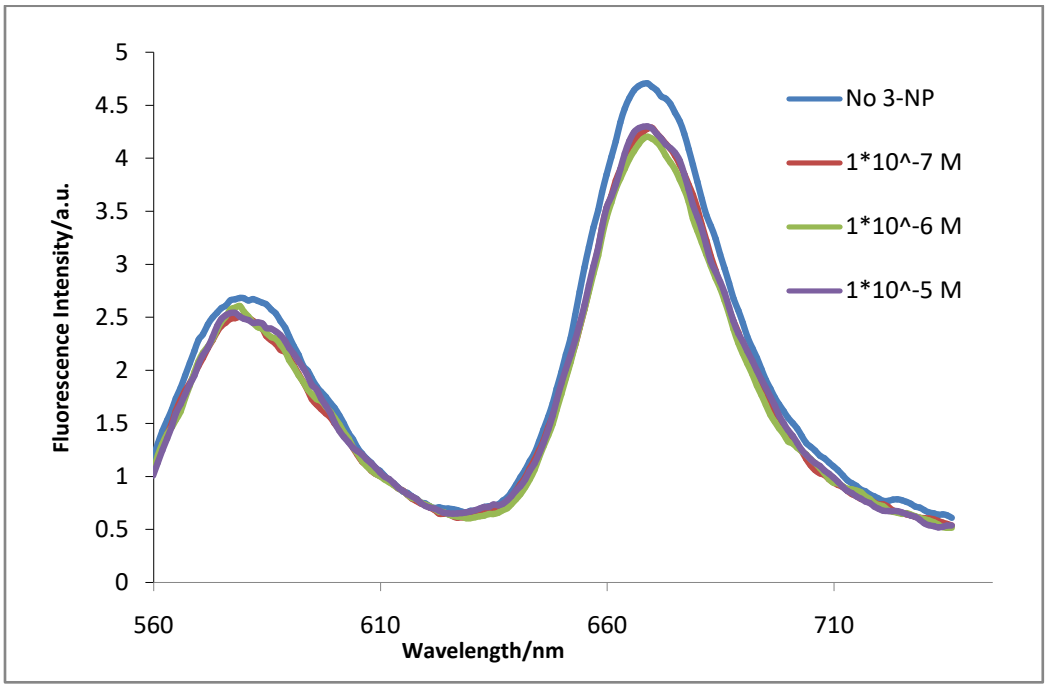

Figure 3.9 Fluorescence spectra for addition of 3NP into MQQ1324 (at 20°C, λex=545nm)

The addition of 3NP didn't cause significant change of fluorescent intensity of both acceptor and donor. This indicated that the biding sites built inside the polymer layer can distinguish the 3NP with 4NP.

3.3.4 Confirmation of selectivity

To confirm this selectivity results, another sensor MQQ1325 was made by the same method. This sensor was imprinted by 3NP. The fluorescence spectra for MQQ1325 with

addition of 3NP are shown in figure 3.10; with addition of 4NP in figure 3.11.

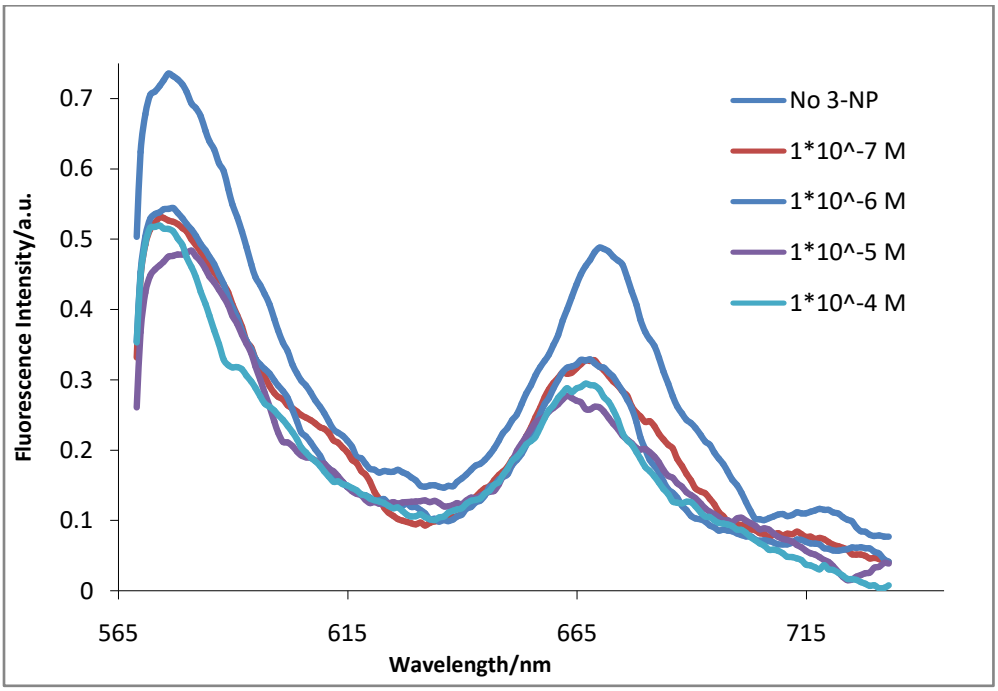

Figure 3.10 Fluorescence spectra for addition of 3NP into MQQ1325 (at 20°C, λex=545nm)

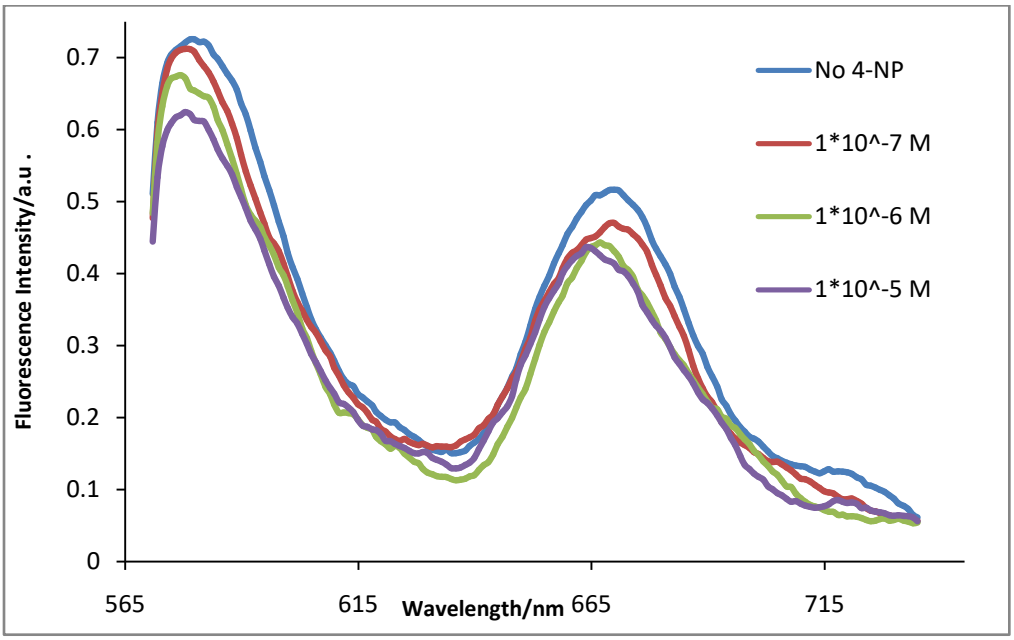

Figure 3.11 Fluorescence spectra for addition of 4NP into MQQ1325 (at 20°C, λex=545nm)

Based on the data in figure 3.10, when 3NP was added into the sensor MQQ1325 the fluorescence intensity of both donor and accepter were quenched. The data in figure 3.11 indicated the sensor was not responsive to 4NP. These results confirmed that this sensor can selectively respond to its template while ignoring isomer.

3.4 Sensor MQQ1326 based on acid-base interaction and electronic effects

3.4.1 Preparation of MQQ1326

The sensor was prepared with the same method discussed in 3.2. The only difference was the formulation of the polymer layer. A pair of anion and cation monomer was incorporated into the polymer to form another kind of non-covalent crosslinking ---electrostatic interaction. The formulation of the polymer layer was shown in table 3.2.

Sensor	NnPAM	4VP	MAA	Anion	Cation	RAFT agent	Initiator	R to T ratio
MQQ1326	75%	10%	5%	5%	5%	1%	1%	3:1

Table 3.2 Formulation for polymer layer of sensor MQQ1326

3.4.2 Thermal tests

When the temperature increased from 20℃ to 45℃, the emission intensity for the donor peak increased and the intensity for the acceptor decreased as shown in figure 3.12. This indicated when the temperature increased; the distance between those two fluorophores were increasing.

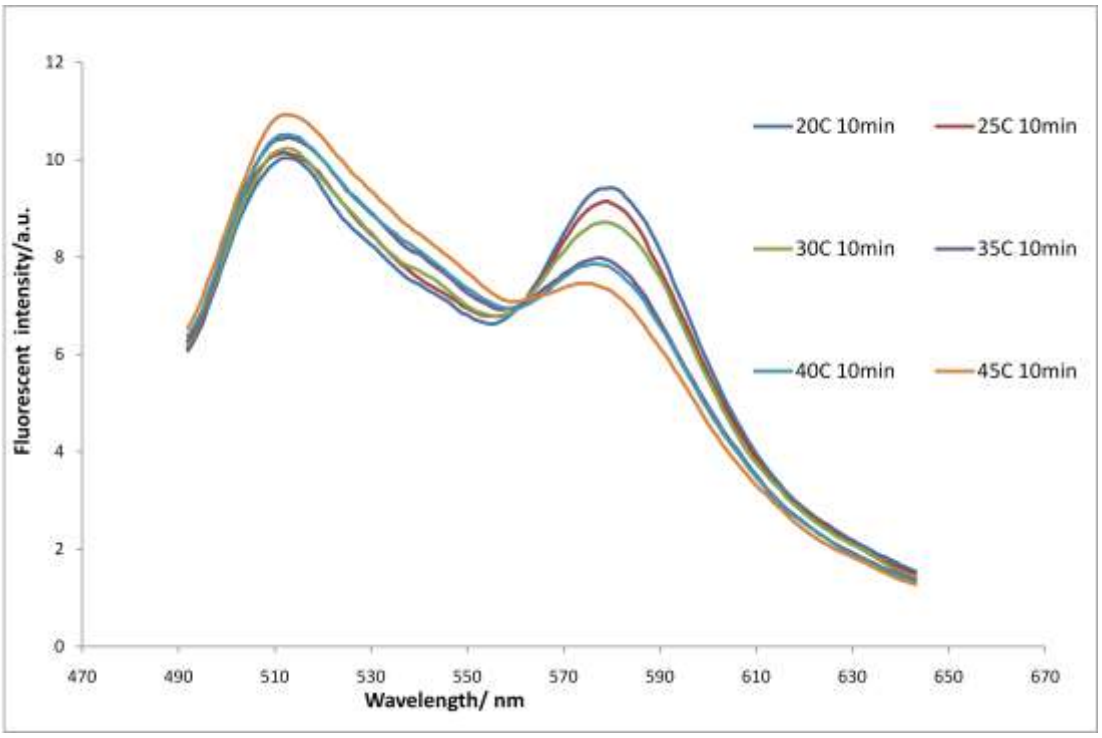

Figure 3.12 Thermal tests for the sensor MQQ1326

This phenomenon can be due to the charge attraction between cation and anion monomers. When the temperature is lower than the LCST, the polymer chain is hold tight by electrostatic attraction. The distance between the donor and acceptor is small at this point. When the temperature was increased, the kinetic energy inside the polymer increases, and overcomes the attraction between the anion and cation, so the polymer chains started to detangle. The distance between these two fluorophores begins to increase. The energy transfer efficiency between those two fluorophores decreases. Therefore, with the increasing of temperature the peak of the accepter decreased and the peak of the donor increased.

3.4.3 Sensing experiments

In the sensing experiments, template 4NP was added into the sensor solution. The addition of the template didn't cause instant change. So fluorescent emission spectra were collected at different time for 240 min. In figure 3.13 below the intensity of both donor and acceptor peak were changing over time even without addition of the template. The fluorescent spectra for the pure sensor at different time were shown. The spectra for sensor with addition of template were shown in figure 3.14.

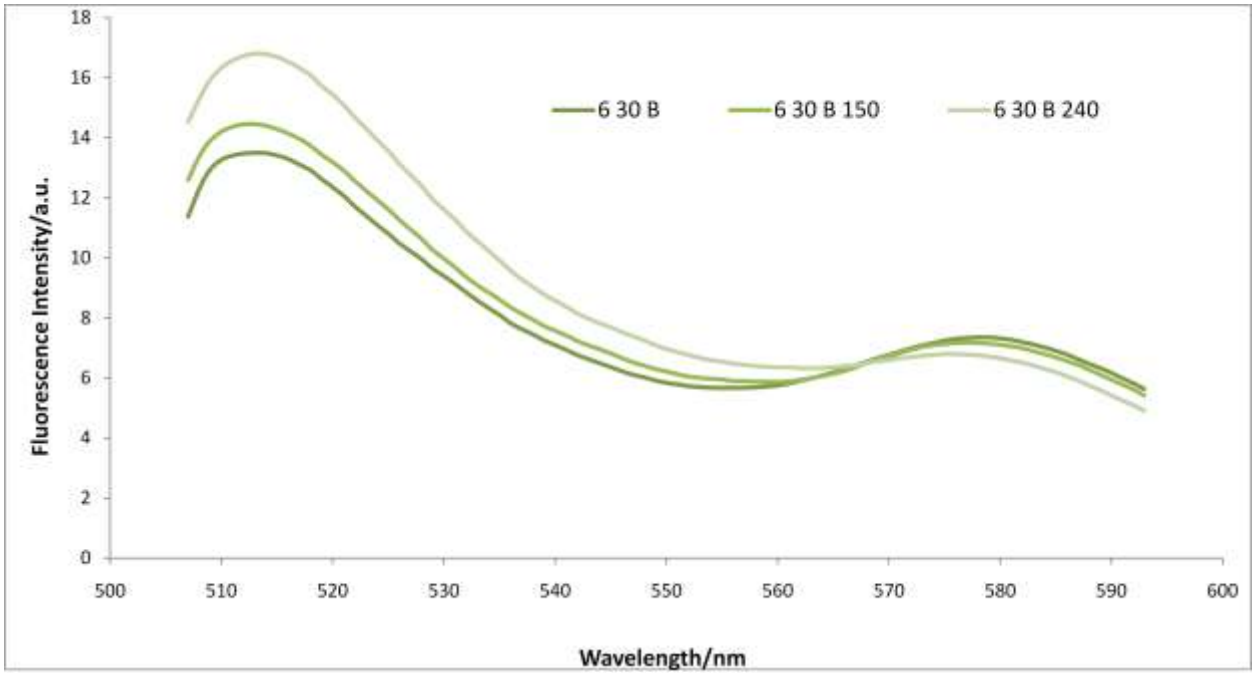

Figure 3.13 Fluorescence spectra for pure sensor MQQ1326 (at 20°C, λex=500nm)

(Fluorescent emission spectra of the pure sensor were collected at different time,150 min and 240 min.)

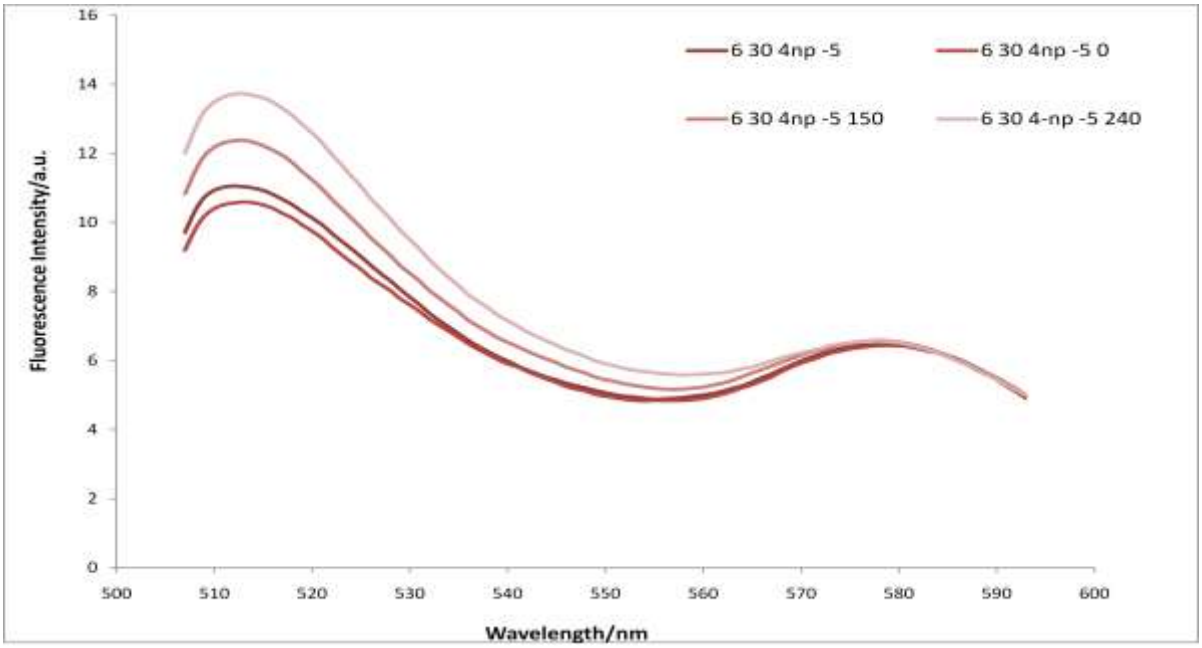

Figure 3.14 Fluorescence spectra for addition of 4NP into MQQ1326 (at 20°C, λex=500nm)

(Fluorescent emission spectra of the pure sensor were collected with the addition of 1×10^{-5} moles of the template 4NP at different time.)

The changing of fluorescent intensity with time indicated that the polymer chains were detangling even at 20°C. The difference A to D ratio for pure sensor after 240 min is -0.16. The difference for sensor with addition of 4NP is -0.11. The addition of the template seems to delay the untangling of the polymer chains.

For selectivity information, same amount of 3NP was added into the sensor. The fluorescent spectra were shown in figure 3.15. The difference of A to D ratio was -0.11. The sensor MQQ1326 respond to both 3NP and 4NP. The selectivity for sensor MQQ1326 is low.

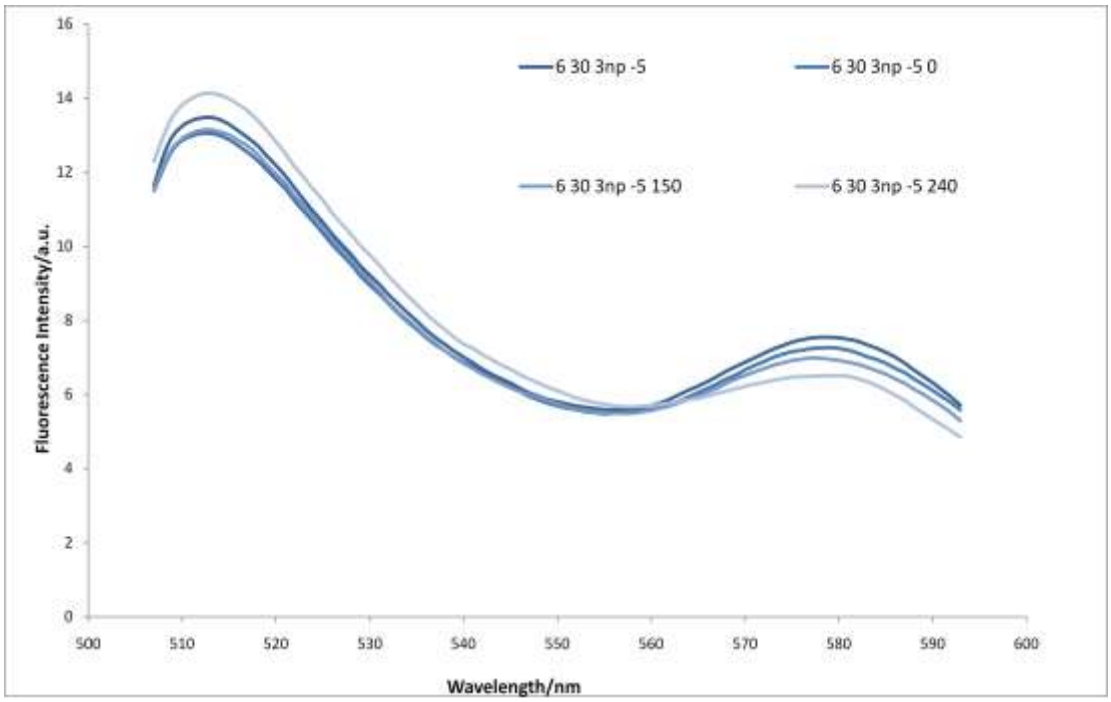

Figure 3.15 Fluorescence spectra for addition of 3NP into MQQ1326 (at 20°C, λex=500nm)

(Fluorescent emission spectra of the pure sensor were collected with the addition of 1×10^{-5} moles of the isomer 3NP at different time.)

3.5 Sensor MQQ1327 based on π-π interaction and electronic effects

3.5.1 Preparation of MQQ1327

The sensor was prepared with the same method discussed in 3.2. The non-covalent interactions used in this sensor were π-π interaction and electrostatic effects. The formulation of the polymer layer was shown in table 3.3.

Sensor	NnPAM	BMA	Anion	Cation	RAFT agent	Initiator	R to T ratio
MQQ1327	85%	5%	5%	5%	1%	1%	3:1

Table 3.3 Formulation for polymer layer of sensor MQQ1327

3.5.2 Thermal tests

When the temperature increased from 20℃ to 45℃, the emission intensity for the donor peak increased and the intensity for the acceptor decreased. This was same with the trend of sensor MQQ1326.

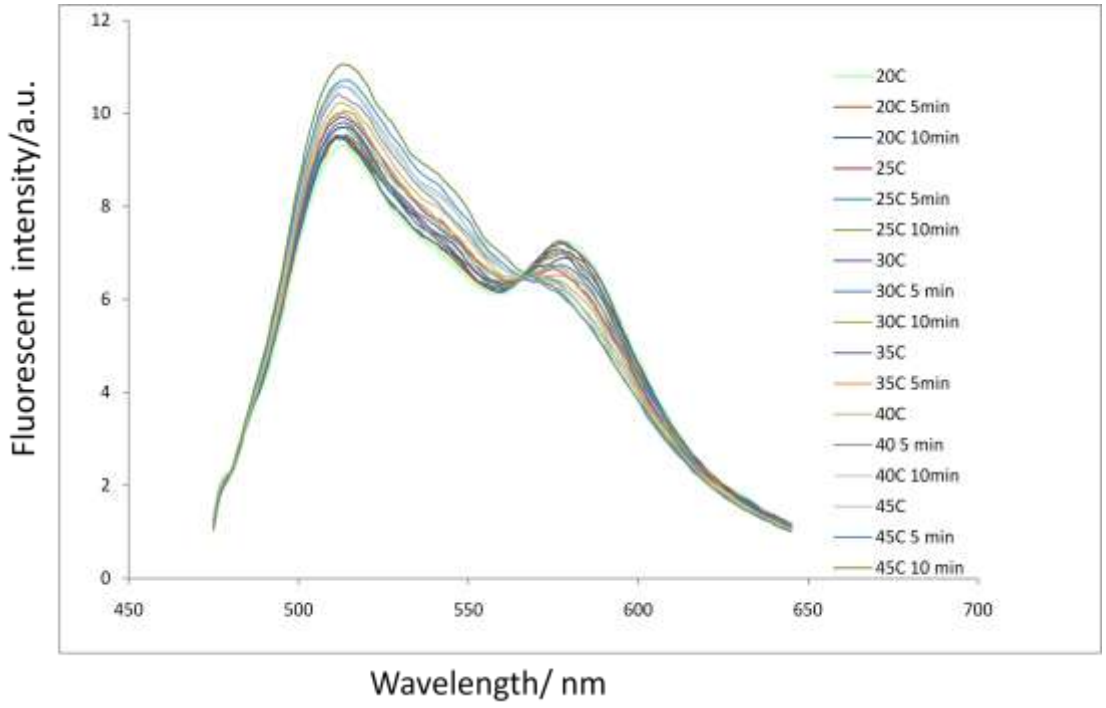

Figure 3.16 Thermal test for sensor MQQ1327

3.5.3 Sensing experiments

In the sensing experiments, same amounts of template 4NP and 3Np were added into the same amount of sensor. The emission spectra for the pure sensor are shown in figure 3.17. The emission spectra for the addition of 4NP are shown in figure 3.18. The emission spectra for the addition of 3NP are shown in figure 3.19.

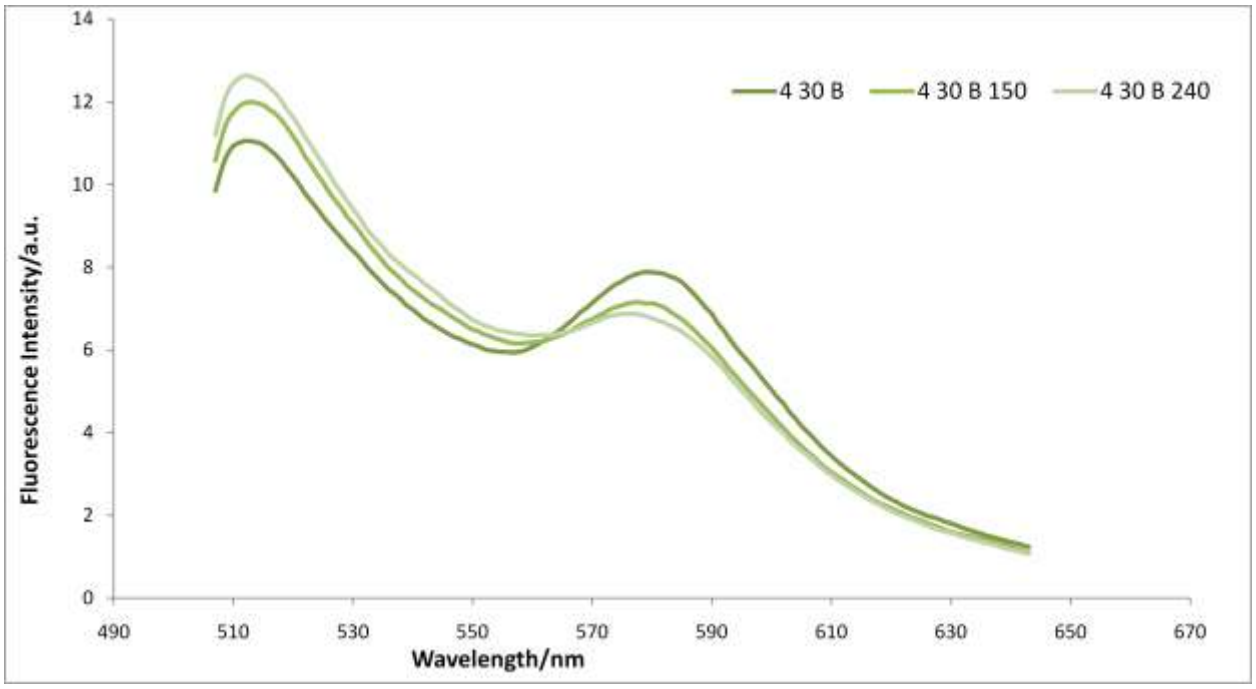

Figure 3.17 Fluorescence spectra for pure sensor MQQ1327 at different time (at 20°C, λex=500nm)

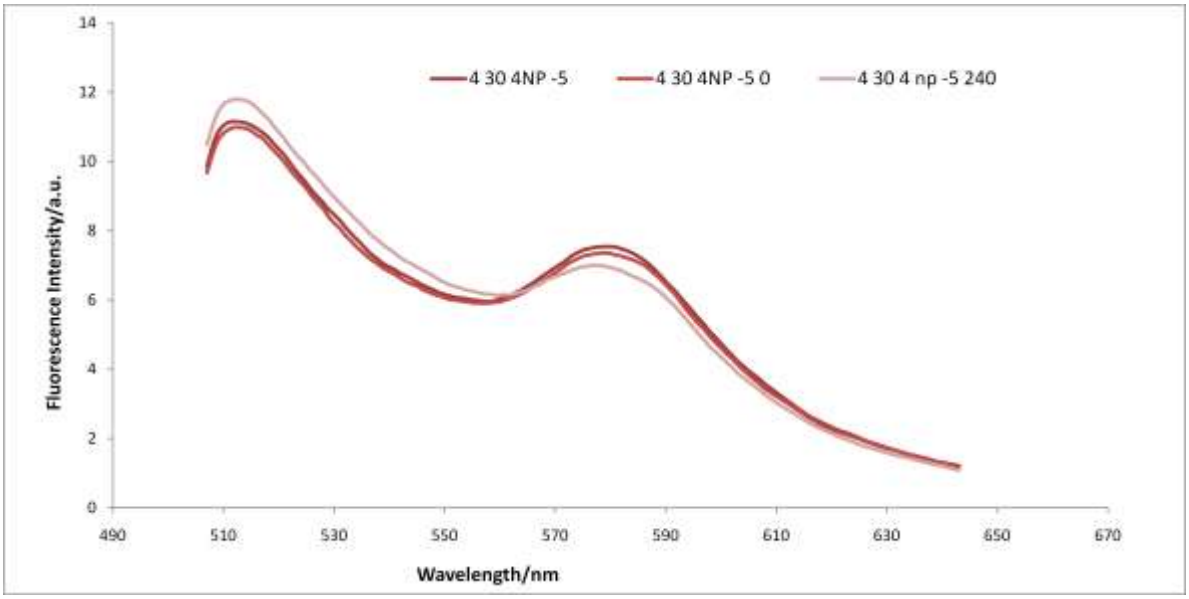

Figure 3.18 Fluorescence spectra for sensor MQQ1327 with addation of 1×10^{-5} Molar 4NP at time 0 min and 240 min. (at 20°C, λex=500nm)

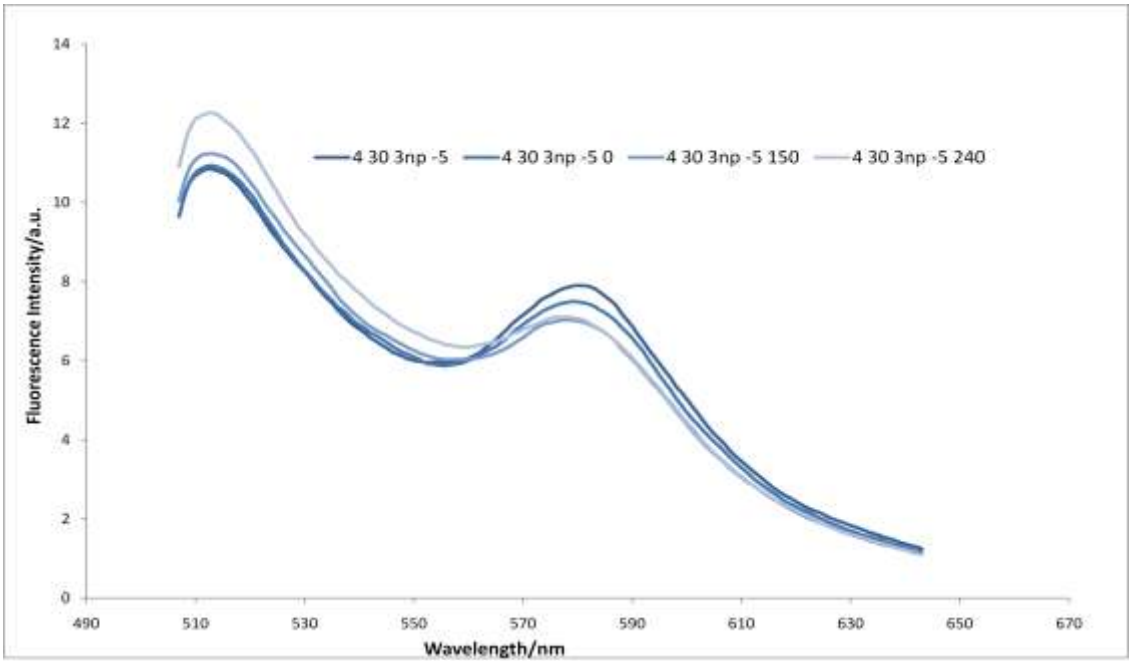

Figure 3.19 Fluorescence spectra for sensor MQQ1327 with addiation of 1×10^{-5} Molar 3NP at different time 0 min,150min, and 240 min. (at 20°C, λex=500nm)

The difference of A to D ratio for pure sensor MQQ1327 after 240 min was -0.15. The difference after addition of 4NP was -0.08. The difference after addition of 3NP was -0.13. The sensor MQQ1327 responded to both 3NP and 4NP with delayed detangling process. The delayed effect for the template 4NP was stronger than its isomer 3NP.

3.6 Conclusion

The Sensor MQQ 1324 and MQQ1325 prepared by combining the acid base covalent crosslinking with π-π interactions can selectively detect the template with high affinity and selectivity. The binding of the template to the MIPs on the sensor quenched the fluorescence of both fluorophores. However the intensity ratio of the acceptor and the donor fluorophore was not changed with the binding as expected.

The Sensor MQQ 1326 and MQQ1327 respond to the nitrophenols by delaying its untangling process. However, these sensors cannot distinguish between 3NP and 4NP. The fluorescence signals of the pure sensor were changing with time. This may due to the polymer chains were tangled up on the nanoparticle surface during the polymerization. The tangled polymer chains started to untangle with time. The untangling process caused the increased fluorescence intensity for donor fluorophore and decreased fluorescent intensity for acceptor fluorophore.

Due to the complexity of the sensor, the completely understanding of the sensing mechanism between MIPs and the template were difficult. To investigate the binding process between the MIPs and the template, MIPs without any fluorophore and substrates were developed in next chapter.

CHAPTER 4

DEVELOPMENT OF BIO MIMETIC RECEPTOR (I)

---Investigations of polymerization

4.1 Introduction

The results from chapter 3 indicated that MIPs grown from the silica surface can recognize the template molecules among structure analogues with high selectivity. However there are many problems cannot be completely explained, such as the shifting fluorescent signal with time and the decreasing A to D ratio with increased temperature.

To simplify the problem, demonstrate the concept of molecular imprinting, novel bio mimetic molecularly imprinted polymers were developed in this chapter.

Unlike the traditional MIPs with high percentage of covalent crosslinking, the MIPs developed in this chapter contained only up to 5% mole of covalent crosslinking, which acted like the disulfide bonds in bio receptors. These covalent crosslinking connected two portions of the polymer and ensured the polymer to return back to same topology after phase transition.[103,104] The solubility of the MIPs increased with the decreased percentage of covalent crosslinking.

To maintain the configuration of the binding sites, 5% to 10% of acid-base crosslinking was added. The hydrogen bonds between the acid and base monomers provided most of the directional interactions that underpin the folding of the polymer. The accepted(and most frequently observed) geometry for a hydrogen bond is a distance of less than 2.5 Å (1.9 Å) between hydrogen and the acceptor and a donor-hydrogen-acceptor angle of between 90° and 180° (160°).[105]

The polymer backbone was PNIPAm. At the LCST, the phase transition of PNIPAm from random coil to globule occurs. With the direction of the covalent crosslinking and the hydrogen bonds, the MIPs can be folded to specific tertiary structures like that in proteins as shown in figure 4.1. This specific tertiary structure is responsible for the recognition of the template.

Figure 4.1 Three-Dimensional arrangements of antibody (left) and PNIPAm (right)

The results from chapter 3 indicated that MIP with only non-covalent crosslinking can distinguish the template from isomers with high selectivity. The study by Casey Grenier shows that a polymer with low mole percent of covalent crosslinking can bind the template with high affinity. Therefore, it is expected that an MIP sensor with a combination of covalent crosslinking and non-covalent crosslinking would show both high selectivity and binding affinity.

A fluorescent template, 7-hydroxycoumarin (7CM) was exploited in this chapter. 7CM is the metabolite of coumarin, which is used in the treatment of cancer, brucellosis, rheumatic disease and burns. [106,107] 7CM can be detected by fluorescence at concentration as low as 10nM with our instrument. This made it possible to investigate the binding process at lower concentration. [108]

The initial formulations for the MIP and NIP are shown in table 4.1.

	NIPAM	**4VP**	**MBA**	**MAA**	**RAFT Agent**	**Initiator**	**Template**
MIP Sensor	83%	5%	2%	8%	0.1%	0.1%	7CM
NIP Blank	83%	5%	2%	8%	0.1%	0.1%	N/A

Table 4.1 Initial formulations (mole-%) of MIP and NIP

4.2 Characterization of the MIP and NIP

After removal of the template, the MIP and NIP were lyophilized to dry powder. ^{1}H NMR spectra of both polymers were taken for the structural analysis. The phase transitions of

both polymers were studied by dynamic light scattering. The polymer chain lengths were estimated by UV-Vis.

4.2.1 NMR spectra of MIP and NIP

The samples for NMR tests are prepared by dissolving 5mg of polymer powder into 1ml D_2O. The ^1H NMR spectra for MIP and NIP are shown in figure 4.2 and 4.3.

The broad peak at 8.27 ppm is from the hydrogen (c) on the carboxylic group of MAA; the broad peak at 7.04 is from the 4 hydrogens (b) on the aromatic ring of 4VP; the broad peak at 6.48 is from the hydrogen (a) on the amide group of NIPAM; the broad peak at 3.72 is from the hydrogen (d) on the isopropyl group of NIPAM. From the integral of peak b and peak d, the mole ratio of NIPAM to 4VP in MIP is 12.5 : 1, while in NIP is 14.6 : 1. This means there is higher percentage of 4VP in the MIP. This is due to the interaction of template with 4VP during the polymerization, which affected the reactivity of the 4VP.

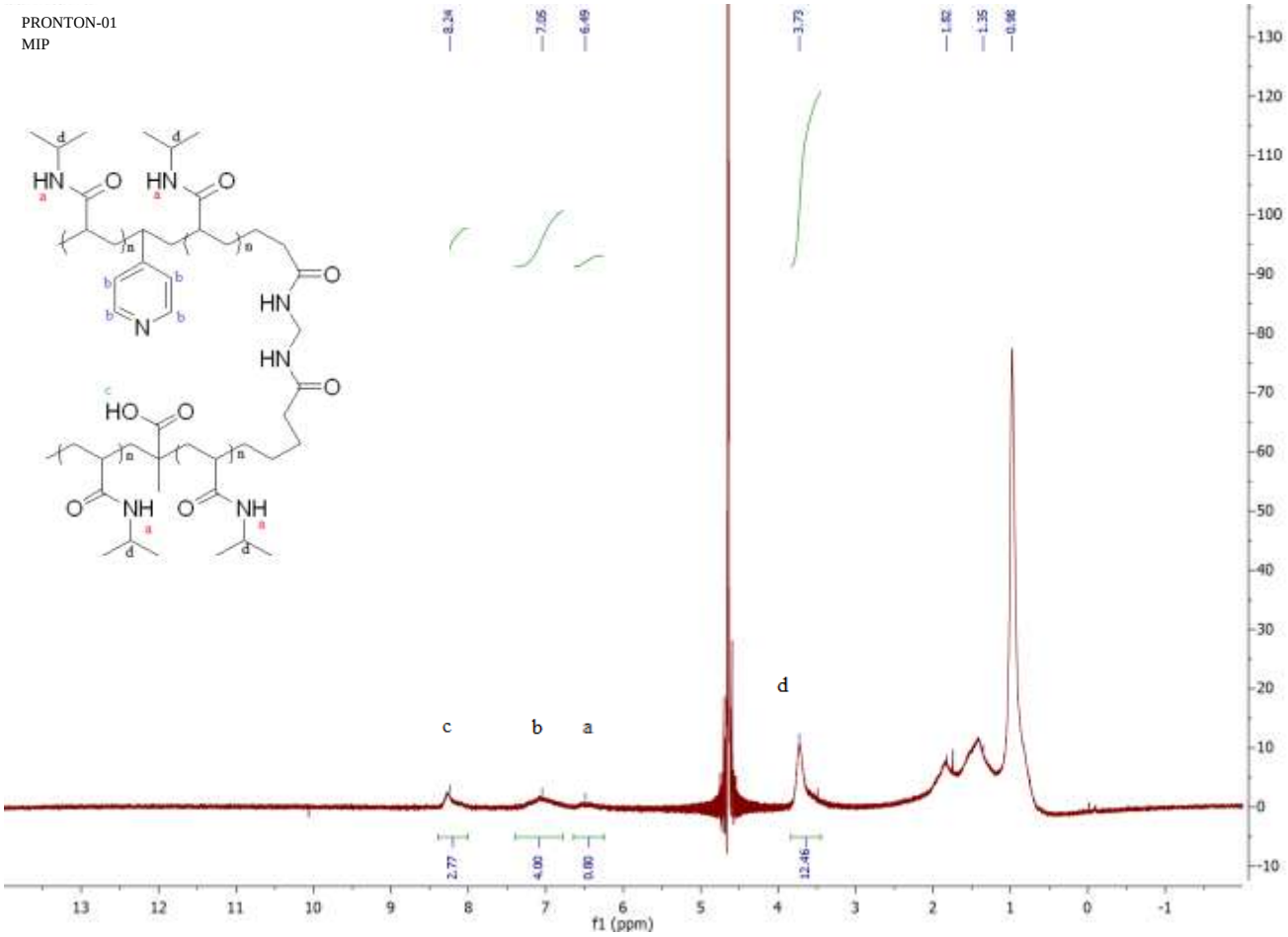

Figure 4.2 ^{1}H NMR spectrum of MIP ($D_2$0, 400 MHz): δ 8.24 (br s), 7.05 (br s), 6.49 (br,s), 3.73 (br s), 1.82 (br s), 1.35 (br s), 0.98 (br s).

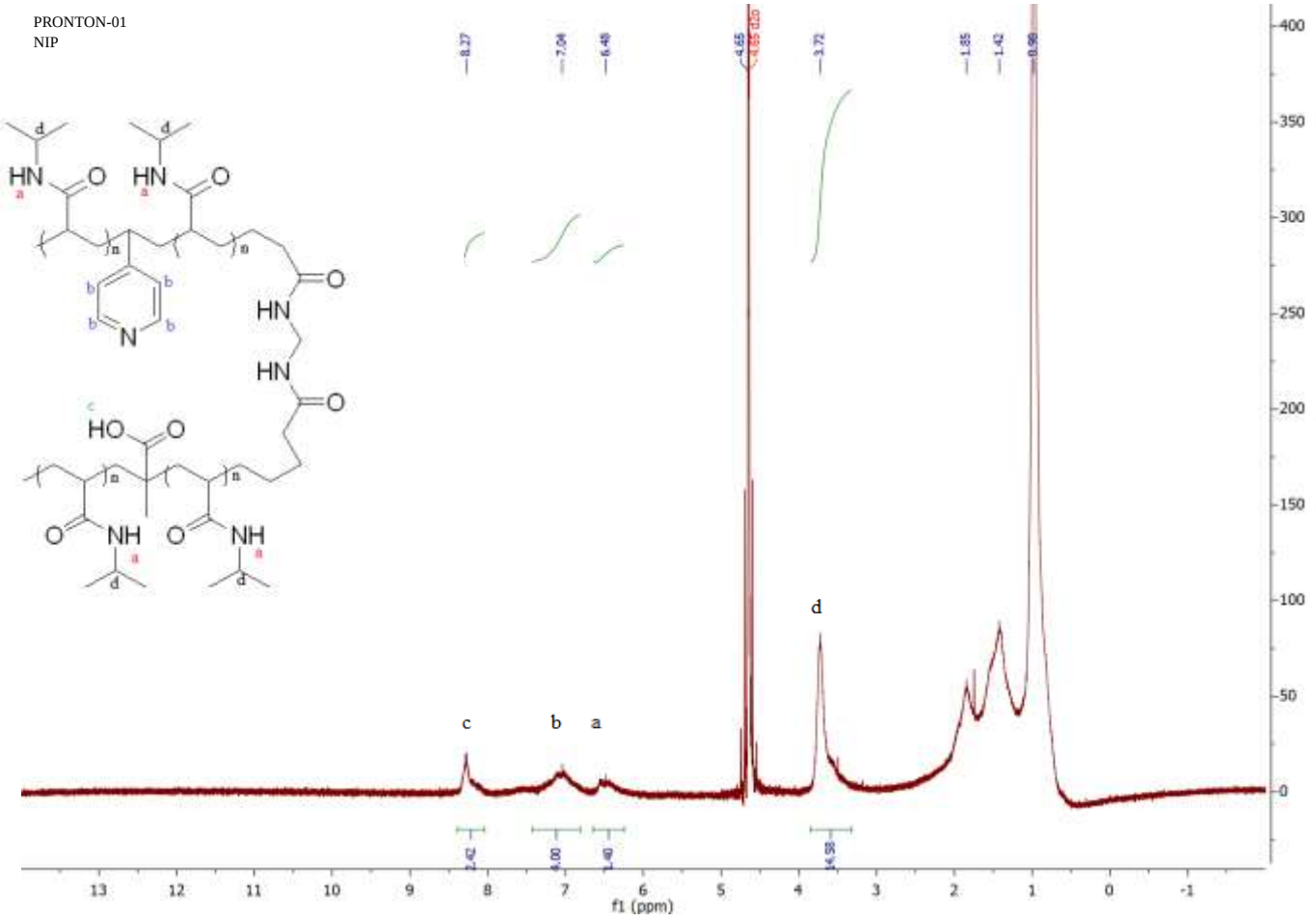

Figure 4.3 ^{1}H NMR spectrum of NIP (D_20, 400 MHz): δ 8.27 (br s), 7.04 (br s), 6.48 (br,s), 3.72 (br s), 1.85 (br s), 1.42 (br s), 0.90 (br s).

c

4.2.2 UV-Vis spectra of MIP and NIP

The UV-Vis spectra of the polymers were measured by dissolving 0.002 grams of polymer powder into 0.5 ml of methanol first. Then 100ul of the polymer solution was added into 3ml methanol in a quartz cuvette for the UV-Vis measurements. The UV-Vis spectra for MIP and NIP are shown in figure 4.4.

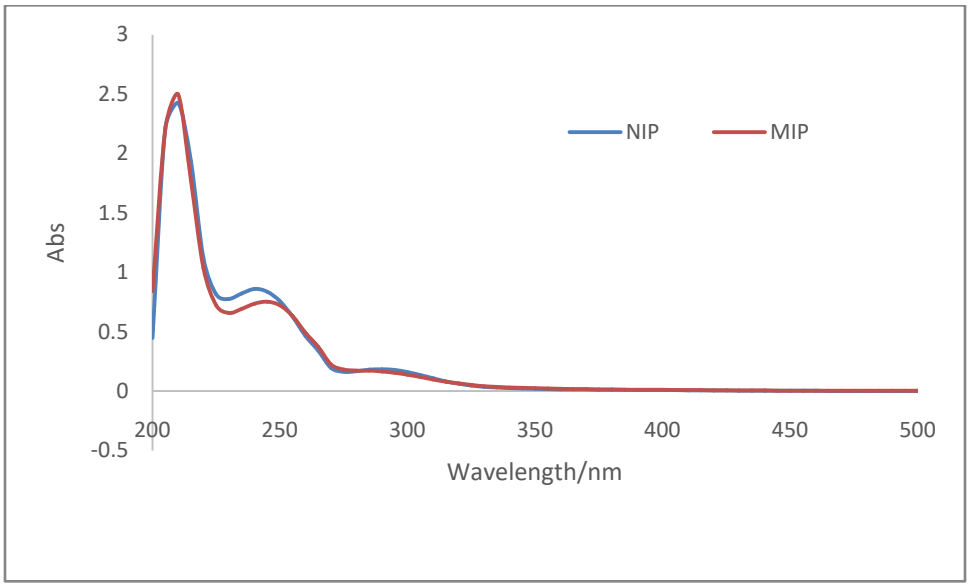

Figure 4.4 Absorbance of MIP (red) and NIP (blue) from UV-Vis measurement scanned from 200nm to 500nm.

The peak around 200 nm is due to the absorption of NIPAM. The peak around 300 nm is from the absorption of the RAFT agent. With these the UV-Vis spectrum, the polymer chain length can be estimated by the method developed by John Csoros with minor modification. [109] The calculation for chain length MIP is shown as following:

The absorbance of the RAFT agent is: 0.173

Molar absobtivity is (reported by Skrabania et al. [109]): 158,00 $M^{-1}cm^{-1}$

Concentration of the RAFT agent in the cuvet is: $\frac{0.173}{15800} = 1.1 \times 10^{-5}$moles

Moles of RAFT agent in the polymer is: $1.1 \times 10^{-5} \times 31 \times 0.0005$

$=1.7\times 10^{-7}$moles

Molar mass of the MIP is: $\frac{0.0025}{1.7\times 10^{-7}} =$14,000 g/mole

The molecular weight for NIP can be estimated around 14,000 g/mole using the same method.

4.2.3 Dynamic light scattering of MIP and NIP

The phase transition of the MIP and NIP can be investigated by the dynamic light scattering. 1mg polymer dissolved in 1ml water, filtered twice with a poly (styrene) 0.45 μm syringe filter. The z-average radius of the polymer at each temperature was measured 3 times from 30°C to 50 °C. The data for MIP was shown in figure 4.5 and NIP in figure 4.6.

The phase transition of MIP began at 44 °C, where the polymer chains started to form random coils. At the end of the phase transition at 50 °C, the polymer random coils aggregated and the solution became cloudy. The phase transition for NIP started at 37 °C and end at 45 °C, which is at lower temperature range than that of MIP. This may due to less MAA and 4VP were incorporated into the NIP polymer chains than MIP as indicated in the NMR spectra.

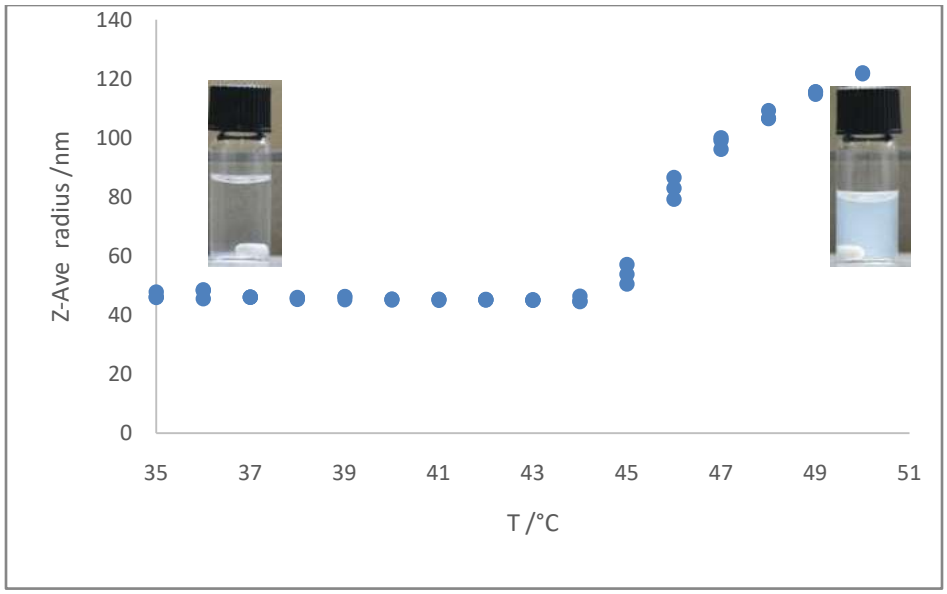

Figure 4.5 Z-average radius versus temperature for MIP obtained from DLS. MIP concentration was 1 g/L in water. Each temperature was held constant for 5 minutes. Three measurements were taken and averaged.

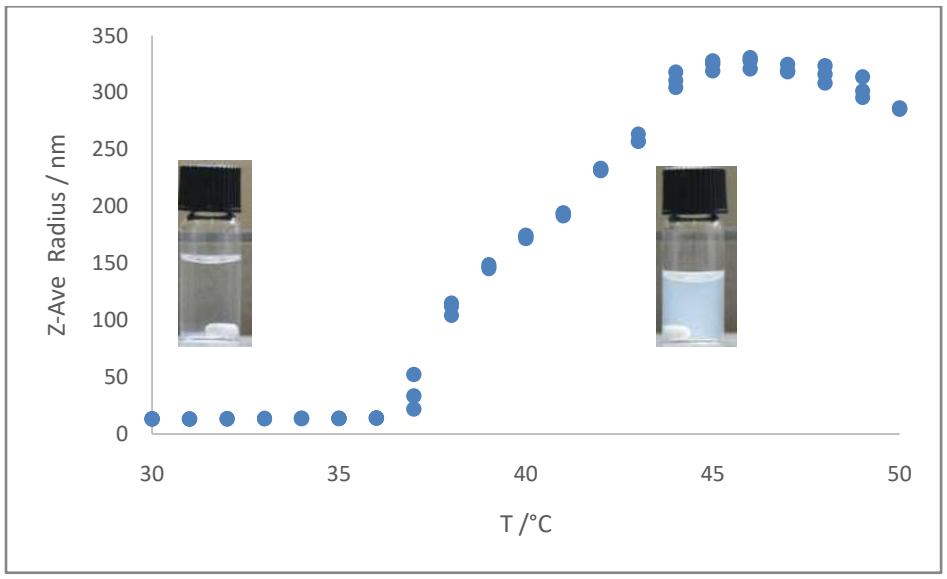

Figure 4.6 Z-average radius versus temperature for NIP obtained from DLS. MIP concentration was 1 g/L in water. Each temperature was held constant for 5 minutes. Three measurements were taken and averaged.

4.3 Template removal process

After polymerization, the polymers need to be separated from the un-reacted monomers. This was achieved by adding hexane into the polymerization mixture. Due to the different solubility, the polymers precipitated out while the monomers stayed in solution. After centrifugation at 6000 rpm, the polymers were collected by decanting supernatant. Then the NIP was dried under vacuum for future tests. The MIP was dissolved back into dioxane for more rounds of precipitation to remove the template. After each round of precipitation, part of the polymer was dried for fluorescence test to monitor the residual template level. The fluorescent intensity for MIP after first round of precipitation is over 1000 units. After the 2^{st} precipitation, the fluorescence dropped to 45 units, which means over 90% of template molecules had been removed. The fluorescent intensities for MIP samples after 4^{th} and 7^{th} round of precipitation are similar. The residual template molecules bond strongly with the binding sites inside the MIP, the precipitation method could not remove these molecules.

Then 1 gram of the MIP from the 7^{th} precipitation was dissolved in 50 ml of pH 10 sodium hydroxide solution in dialysis bag with molecular weight cut off (MWCO) pore size at 45000 placed in a beaker of pH 10 solution. The dialysis went 1 week with solution changed every 12 hours. After 2 more days' dialysis with D.I. water, the MIP was lyophilized to form white powder. After measuring the fluorescence, this MIP was dialysis in pH 3 hydrochloric acid solution for another week, in D. I. water 2 days. Then the MIP was lyophilized again for fluorescence measurements. Based on the fluorescence intensity, some of the template molecules had been removed after each dialysis and phase change from powder to solution.

However, there are still some template molecules left over inside the MIP. To completely remove the template, the MIP was first refluxed in 0.1 M sodium hydroxide and methanol (V:V=30:70) mixture for 6 hours, then flowed by dialysis in pH 10 sodium hydroxide solution for 2 days and D.I. water for 1 day. After lyophilizing, the fluorescent intensity was measured. Based on the fluorescence, this combination of refluxing and dialysis is more efficient than just dialysis in base of acid. Another round of refluxing was conducted for 72 hours, the template was finally removed completely from the MIP. The fluorescent intensity for each measurement is shown in figure 4.7.

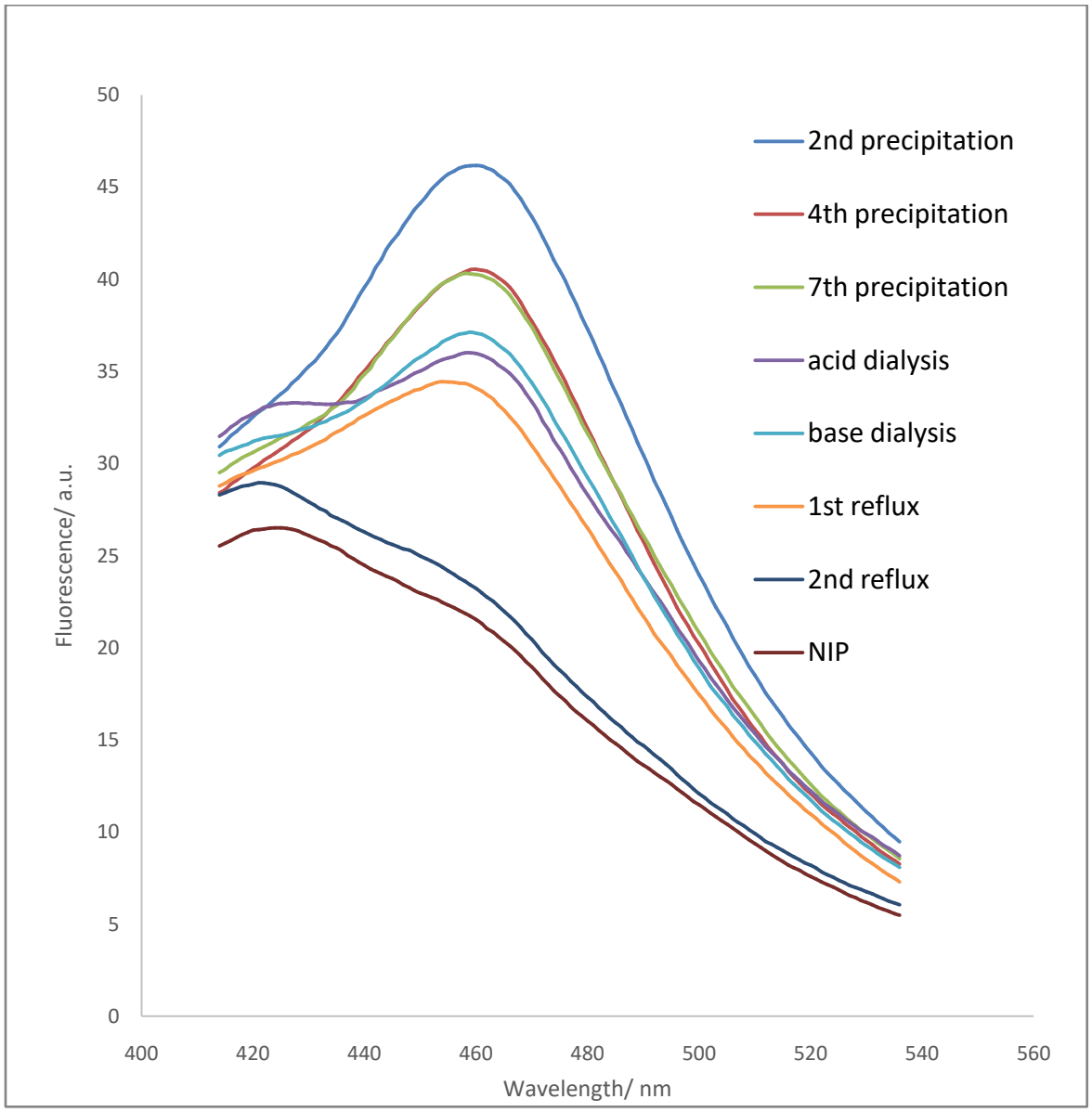

Figure 4.7 Template removal process for MIP (with 7 rounds of precipitation in hexane, 1 round of dialysis with acid, 1 round of dialysis with base, and 2 rounds of reflux in sodium hydroxide and methanol.)

4.4 Investigation of acid base interaction between MAA and 4VP by NMR

To mimic the non-covalent crosslinking in protein, reduce the mole percentage of covalent crosslinking, and increase the solubility of the MIP, MAA and 4VP were added to form acid base interaction. The pKa for MAA is 4.65 [110]; for protonated 4VP is 5.62[111] . When mixed together, the hydrogen (a) in the carboxylic acid group in MAA can behave as a hydrogen bond donor, the nitrogen (b) in aromatic ring of 4VP act as a hydrogen bond acceptor as shown in figure 4.8.

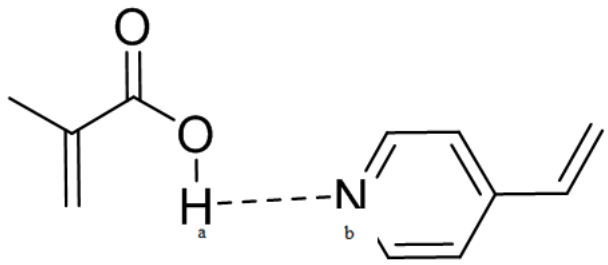

Figure 4.8 The formation of hydrogen bond between MAA and 4VP

Formation of hydrogen bonds would cause the actual electron density change around hydrogen (a). Therefore, in NMR spectrum, the peak of hydrogen (a) should move to a higher frequency (higher ppm). The NMR spectrum of pure MAA, 4VP and a mixture of the two are shown in figure 4.9.

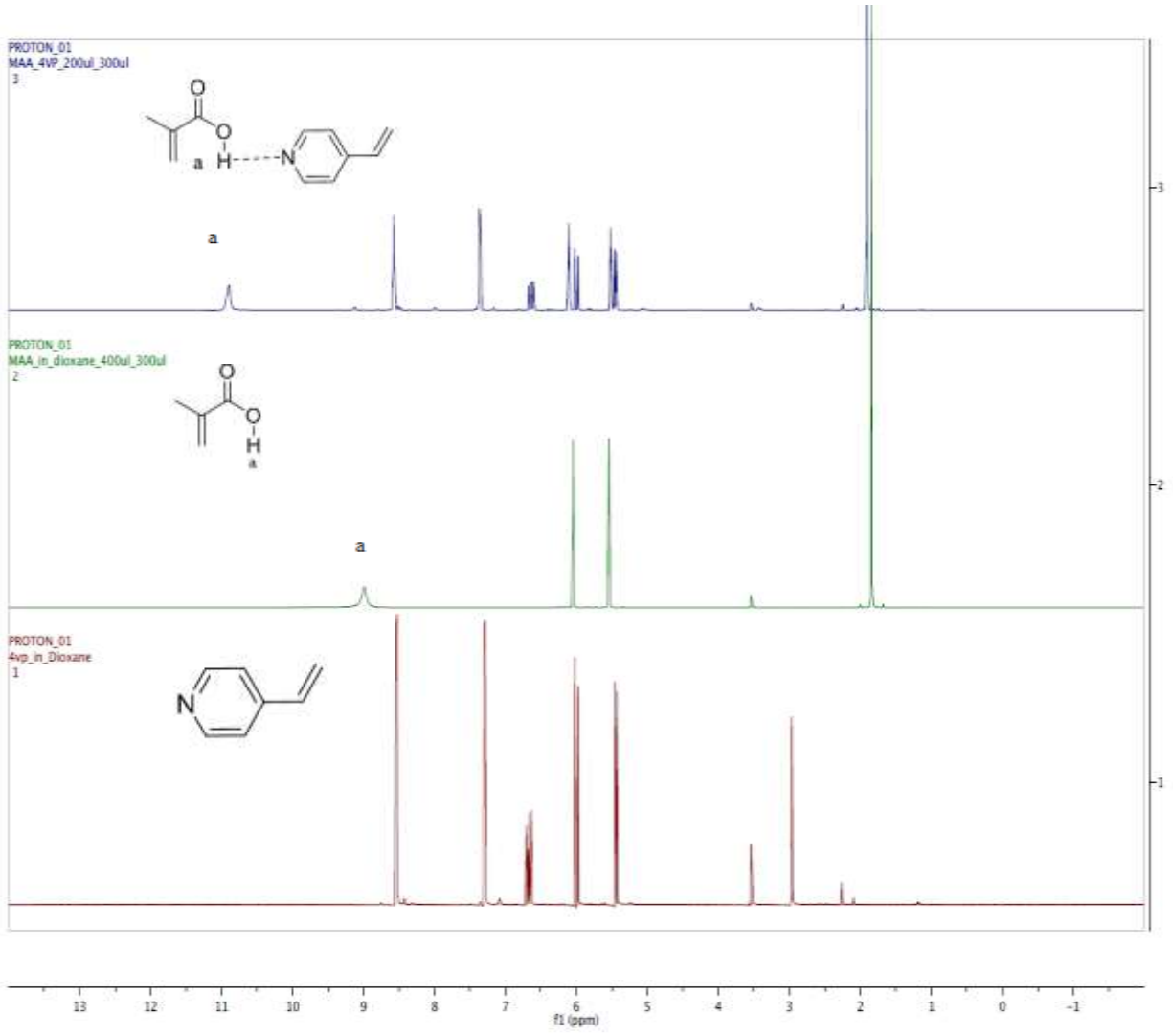

Figure 4.9 ^{1}H NMR spectra of 4VP (Bottom), MAA (Middle), and mixture (Top)

(1,4-Dioxane-d_8 , 400 MHz).

Based on the NMR spectrum, the peak of hydrogen (a) in MAA shifts from 9ppm to 11ppm. This indicates the MAA and 4VP interact strongly in dioxane during the formation of MIP.

To confirm the existence of acid base interaction in the MIP, MIP-NMR reference 1 (PNIPAM-co-MAA) was made without addition of 4VP and MIP-NMR reference 2 (PNIPAM) was made without either MAA or 4VP.

	NIPAM	**4VP**	**MBA**	**MAA**	**RAFT Agent**	**Initiator**	**Template**
MIP-NMR reference 1	78%	0%	2%	20%	0.1%	0.1%	7CM
MIP-NMR reference 2	98%	0%	2%	0%	0.1%	0.1%	7CM

Table 4.2 Formulation of MIP-NMR reference 1 (PNIPAM-co-MAA) and 2 (PNIPAM)

The ^{1}H NMR spectra for MIP and MIP NMR reference 1 and 2 were made by 5mg of polymers in 1 ml D_2O. The spectra were shown in figure 4.10.

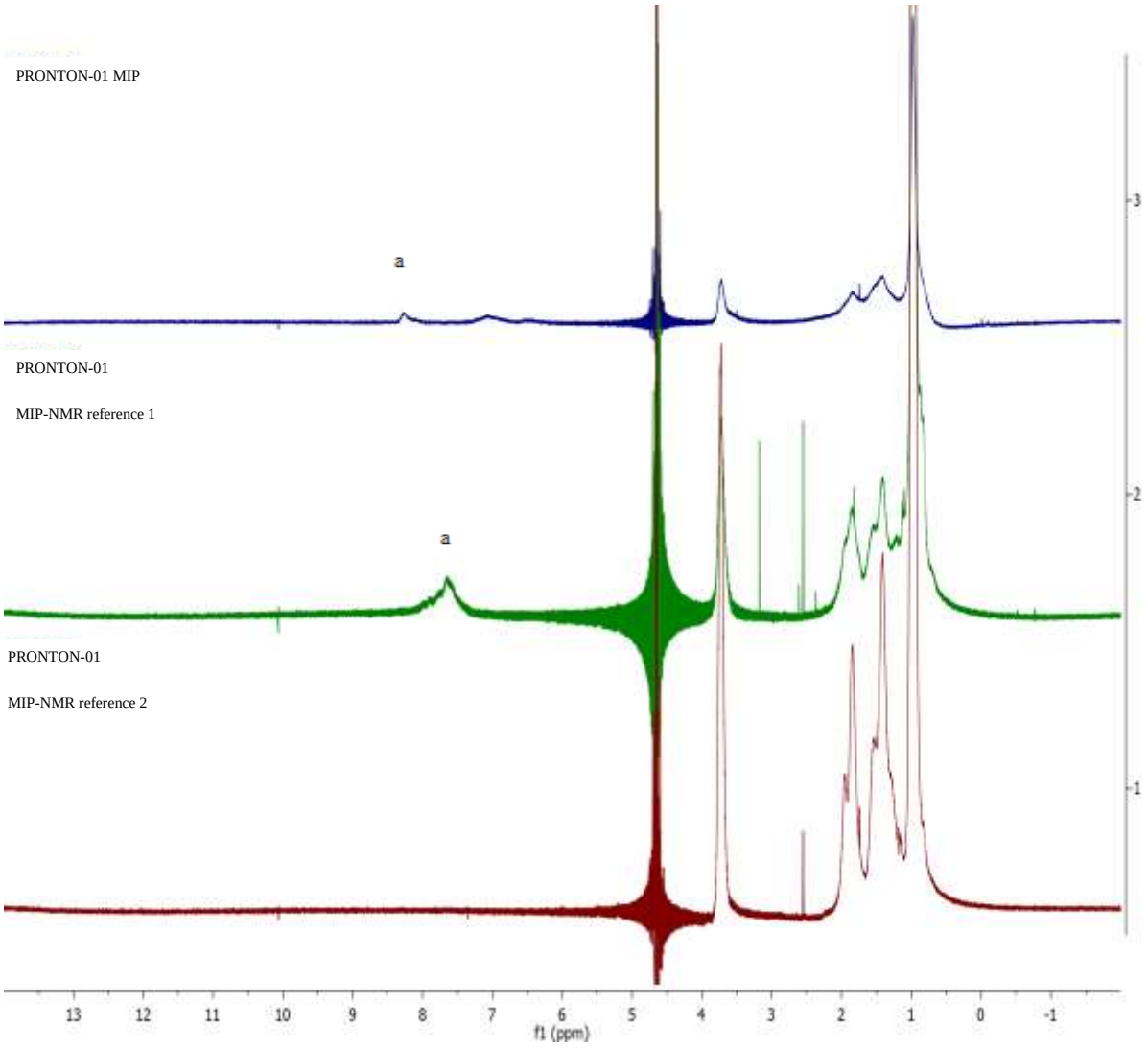

Figure 4.10 ^{1}H NMR spectra of MIP (Top), MIP-NMR reference 1 (Middle), and MIP-NMR reference 2 (Bottom) (D_2O , 400 MHz).

Based on the spectra in figure 4.8, the peak of hydrogen (a) in MIP-NMR reference 1 was at 7.59, while in MIP was shift to 8.26. This indicated that the addition of 4VP inside the polymer formed hydrogen bonds with MAA, causing the shift. This confirmed that there are acid-base noncovalent crosslinking in the MIP.

4.5 Investigation of the polymerization

The polymerization process of the MIP and NIP took 5 days and with a low yield. The estimated polymer chain length is much lower than the theoretical value. To improve the polymerization yield and know more about the polymerization process, polymers with 100 monomer units (100mer) and 500 monomer units (500mer) were synthesized using the following formulation.

	NIPAM	**4VP**	**MBA**	**MAA**	**RAFT Agent**	**Initiator**	**Template**
500 mer	83%	5%	2%	5%	0.2%	0.2%	7CM
100 mer	83%	5%	2%	5%	1%	1%	7CM

Table 4.3 Formulation for 100mer and 500mer

20 mmoles of monomers were dissolved in 50 ml dioxane. During the polymerization, 5 ml of solution was removed from the polymerization mixture at various time. Then 15 ml of hexane was added to precipitate the polymer. The polymer was then dried under vacuum over night. The dry polymer powder was weighed and then dissolved in 1 ml methanol for UV-Vis analysis.

The mass of the 100mer polymer powder at different time is plotted versus time in figure 4.11. Based on figure 4.11, 0.1338g of polymer was precipitated out of solution from 0.285g feeding monomer at 6hrs. 0.2342 grams of polymer was collected at 48 hrs. The yield reached maximum at 48 hrs and then leveled off, which means that the polymerization was complete at 48 hours. The molecular weight of 100mer polymer at different time was estimated by UV/Vis and is plotted in figure 4.12. The molar mass of the polymer reached a maximum at 48 hours.

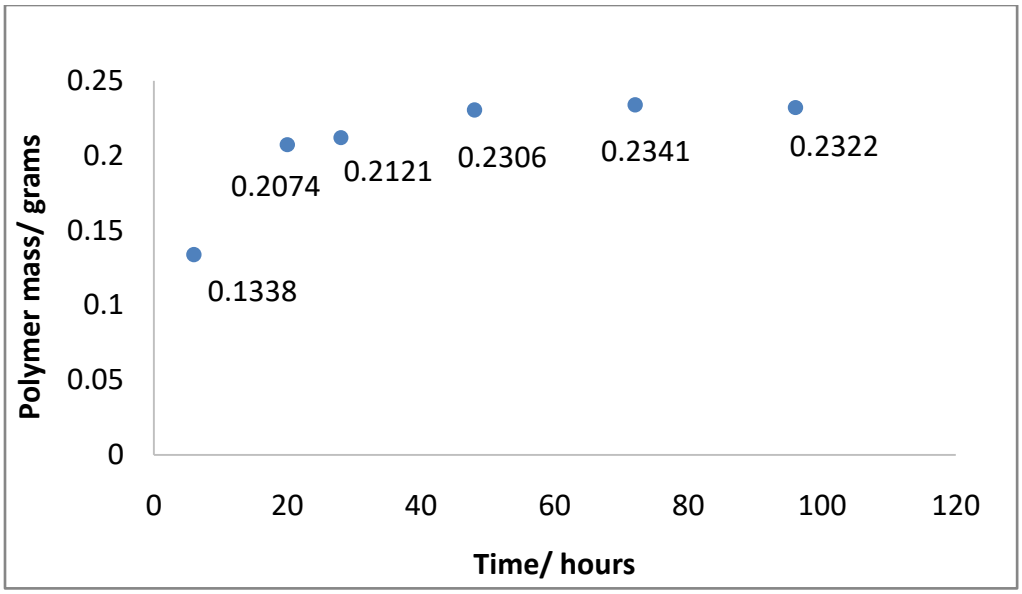

Figure 4.11 Mass of 100mer at different time after initiating polymerization

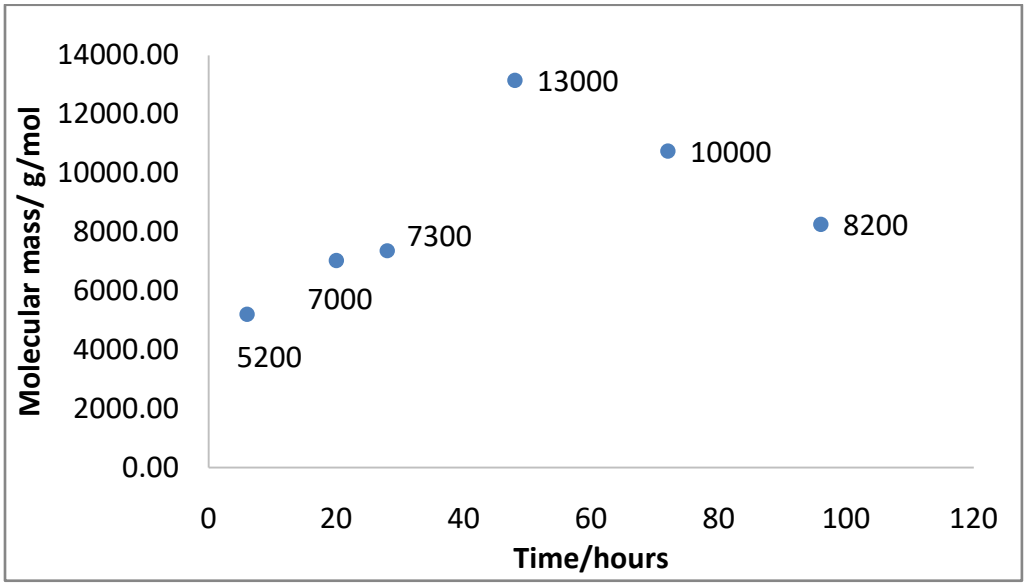

Figure 4.12 Molecular weight of 100mer polymer estimated by UV-Vis using the method discussed in 4.2.2

The mass of the 500mer polymer powder at different time was plotted verses time in figure 4.13. The molecular weight of 500mer polymer at different time was estimated by UV/Vis. and plotted in figure 4.14.

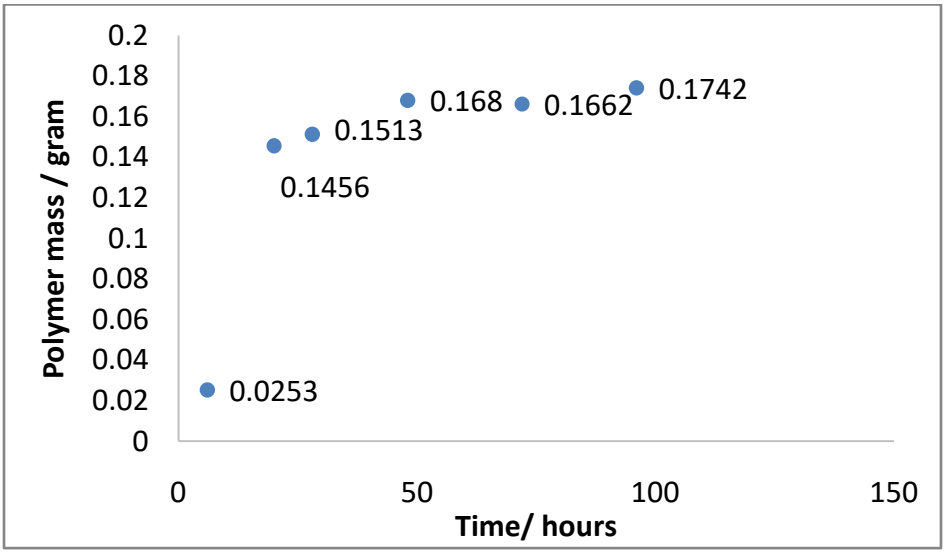

Figure 4.13 Mass of 500mer at different time

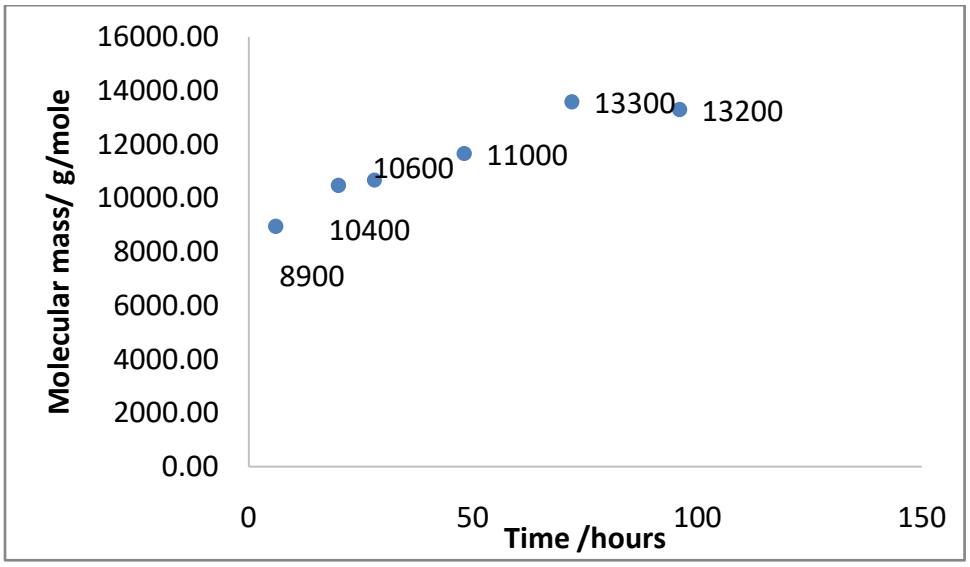

Figure 4.14 Molecular weight of 500mer polymer estimated by UV-Vis using the method discussed in 4.2.2

By comparing the data, polymers with less percentage of RAFT agent and initiator would grow slower and produce a smaller yield. The actual molecular weight for 100mer (13000g/mole) and 500mer (13000g/mole) was close to that of 1000mer (14000g/mole). This may due to the different reactivity of different monomers that stops the propagation of the polymer chain.

4.6 Optimization of polymer formulation

Many factors can affect the binding affinity between the polymer and the template, such as the percentage of the covalent crosslinking, non-covalent crosslinking, recognition monomers, and recognition monomer to template ratio. To get the strongest binding, different combinations were investigated.

4.6.1 Determination of percentage of crosslinking

MIPs with different percentage of crosslinking were prepared. There was 2% covalent and 5% non-covalent crosslinking in MIP 6302, just 2% covalent crosslinking in 6303, and 10% non-covalent and 2% covalent crosslinking in 6304. The formulation of each polymer is shown in table 4.4.

	NIPAM	4VP	MBA	MAA	RAFT Agent	Initiator	Template
MIP 6302	85%	5%	2%	8%	0.1%	0.1%	7CM
MIP 6303	95%	0%	2%	3%	0.1%	0.1%	7CM
MIP 6304	75%	10%	2%	13%	0.1%	0.1%	7CM

Table 4.4 MIP formulations for determination of percentage of crosslinking

After polymerization and complete removal of template, the 4 mg of the polymers was dissolved into 4 ml of 400 nm 7hydroxycoumarin solution and stored in the dark at room tempreture for 1 week. Then 1 ml the solution was loaded in one side of the equilibrium dialysis block with another side filled with 1ml water. The blocks were kept in 42 C water bath for 5 days. Then the fluorescence of the water side was measured and the distribution ratio (D ratio) was determined based on the standard curve of 7CM. The D ratio of each polymer from three blocks were averaged and listed in table 4.5.

Polymer	Polymer (g/l)	7 CM (nM)	Distribution Ratio at the LCST
MIP 6302	1	400	2.33 ± 0.001
MIP 6303	1	400	1.05 ± 0.005
MIP 6304	1	400	1.69 ± 0.0032

Table 4.5 Average D ratio of MIPs for determination of percentage of crosslinking

The data in table 4.5 indicated that the MIP with of 2% covalent crosslinking and 5% acid-base crosslinking binds more template molecules than other MIPs under the same condition. The D ration for MIP 6303 is 1.05 which is close to 1, indicating that the polymers merely bind any templates.

4.6.2 Determination of recognition to template ratio

MIPs with different recognition to template ratio (R to T ratio) were made. The R to T ratio is 6:1 in MIP 6306, 4:1 in 6307, and 3:1 in 6304. The formulation of each polymer was shown in table 4.6. The D ratio of each polymer from three blocks were averaged and listed in table 4.7.

	NIPAM	4VP	MBA	MAA	RAFT Agent	Initiator	Template
MIP 6306	82%	5%	2%	11%	0.1%	0.1%	7CM
MIP 6307	84%	5%	2%	9%	0.1%	0.1%	7CM
MIP 6304	85%	5%	2%	8%	0.1%	0.1%	7CM

Table 4.6 MIP formulations for determination of recognition to template ratio

Polymer	Polymer (g/l)	7 CM (nM)	Distribution Ratio at the LCST
MIP 6306	1	400	2.18 ± 0.0027
MIP 6307	1	400	2.56 ± 0.001
MIP 6304	1	400	2.33 ± 0.0052

Table 4.7 Average D ratio of MIP for determination of recognition to template ratio (R to T ratio)

The data in table 4.7 indicated that the R to T ratio didn't show much affect on the D ratio. However, higher R to T would cause nonspecific binding. (reference) So the R to T ratio is control at 4:1.

4.6.3 Determination of recognition monomer

MIPs with different recognition monomers were made. The recognition monomer in 6308 is 3VA, in 6309 is 4VP, and in 6307 is MAA. The formulation of each polymer was shown in table 4.8. The D ratio of each polymer from three blocks were averaged and listed in table 4.9.

	NIPAM	4VP	MBA	MAA	3VA	RAFT Agent	Initiator	Template
MIP 6308	82%	5%	2%	5%	4%	0.1%	0.1%	7CM
MIP 6309	84%	9%	2%	5%	0%	0.1%	0.1%	7CM
MIP 6307	85%	5%	2%	9%	0%	0.1%	0.1%	7CM

Table 4.8 MIP formulations for determination of recognition monomer

Polymer	Polymer (g/l)	7 CM (nM)	Distribution Ratio at the LCST
MIP 6308	1	400	3.47 ± 0.0026
MIP 6309	1	400	1.78 ± 0.0082
MIP 6307	1	400	2.56 ± 0.0043

Table 4.9 Average D ratio of MIP for determination of recognition monomer

Based on the data in table 4.9, the MIP with 3VA as recognition monomer can bind more template molecules than other MIPs under the same condition.

4.7 Other factors that affect D ratio

4.7.1 Concentration of MIP

The concentration of MIP can affect the D ratio. Theoretically, MIP with higher concentration contains more binding sites in the polymer side, thus the distribution ratio would be higher. The D ratios of MIP at different polymer concentration were listed in table 4.10.

Polymer	Polymer (g/l)	7 CM (nM)	Distribution Ratio at the LCST
MIP 6308	1	400	3.47 ± 0.001
MIP 6308	0.01	400	2.74 ± 0.0045
MIP 6308	0.001	400	2.41 ± 0.0065

Table 4.10 Average D ratio of MIP at different polymer concentrations

The D ratio was not proportional to the concentration. When concentration was increased by a factor of 10, the D ratio just slightly increased. This indicated that most of the binding sites were buried inside the polymer structure and were not accessible to template molecules

4.7.2 Effect of detangling extent

Since most of the binding sites were buried inside the polymer structure, it may be useful to dissolve the MIP 6308 in water and store the solution for 6 month. The D ratio of this sample was compared to the freshly made MIP 6308 solutions in table 4.11

Polymer	Polymer	7CM (nM)	Distribution Ratio at the LCST
MIP 6308 fresh	0.001	400	2.41 ± 0.0083
MIP 6308 6 month	0.001	400	4.52 ± 0.0059

Table 4.11 Average D ratio of MIP at different detangling time

The D ratio of MIP 6038 after stored for 6 month is significantly larger than that of fresh made MIP solution. It is believed that the polymer chains are tangled up during the polymerization and were detangling slowly in solution. This detangling process made the binding sites more accessible to template molecules.

4.8 Conclusion

It was determined that the MIP with 2% (mole) covalent crosslinking and 5% (mole) non-covalent crosslinking can bind strongly with the template. The recognition monomer 3VA interacted more efficiently with the template than MAA and 4VP.

Lower the concentration of the MIPs in solution can help the detangling of the polymer and more binding sites were accessible to the template. The extent of the detangling affected the amount of accessible binding sites.

CHAPTER 5

DEVELOPMENT OF BIO MIMETIC RECEPTOR (II)

--- Determination of the binding affinity and exploration of binding process

5.1 Introduction

The equilibrium dialysis can only estimate the binding capacity of the polymers. The actual binding affinity and capacity of the MIPs developed in chapter 4 can be determined by titration. First, the MIPs were coated onto nano substrates. Then the composite nanoparticles were exposed to different concentration of template molecules.

The spin-down experiments were designed to titrate the MIP with the template as shown in figure 5.1. First the composite nanoparticles were equally distributed into 1.5 ml micro centrifuge tubes. Then 6 standard template solutions with different concentration were added into different tubes. After mixing well and equilibrating for 15 min at LCST, the MIPs on the nanoparticles interacted with the template. After centrifugation, the bound template molecules moved with the nanoparticles to the bottom of the tube as pellets, while the unbound template molecules stayed in the supernatant. The fluorescent emission spectra of the supernatant were collected. The intensity of the emission was proportional to the concentration of the template. So moles of unbound template molecules can be calculated. The concentration difference between the supernatant and the initial standard solution was the bound template molecules.

Silica nanoparticles, magnetic iron oxide nanoparticles and gold nanoparticles were investigated as subtracts for this project.

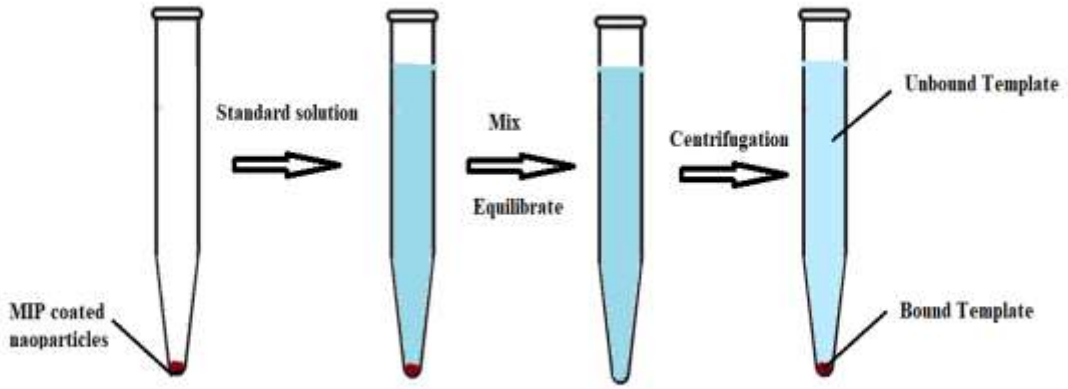

Figure 5.1 Scheme of spin-down experiments

To explore the binding process, the MIPs developed in chapter 4 were attached to fluorescein doped silica nanoparticles. 7CM and fluorescein are a FRET donor and acceptor pair. The emission spectrum of the 7CM overlaps with the excitation spectrum of the fluorescein.[112]

In the event of binding, the 7CM, which is the donor fluorophore and also is the template molecule, can bind to MIPs on the nanoparticle surface and transfer energy to the fluorescein acceptor inside the silica nanoparticles as shown in figure 5.2. In this case, the excitation spectrum of the acceptor fluorescein would be affected at the wavelength where the donor emitted energy. In the absence of binding, 7CM molecules would stay mainly in solution, far away from the fluorecein. So there will not be energy transfer. The excitation spectrum of the fluorescein will not be affect.

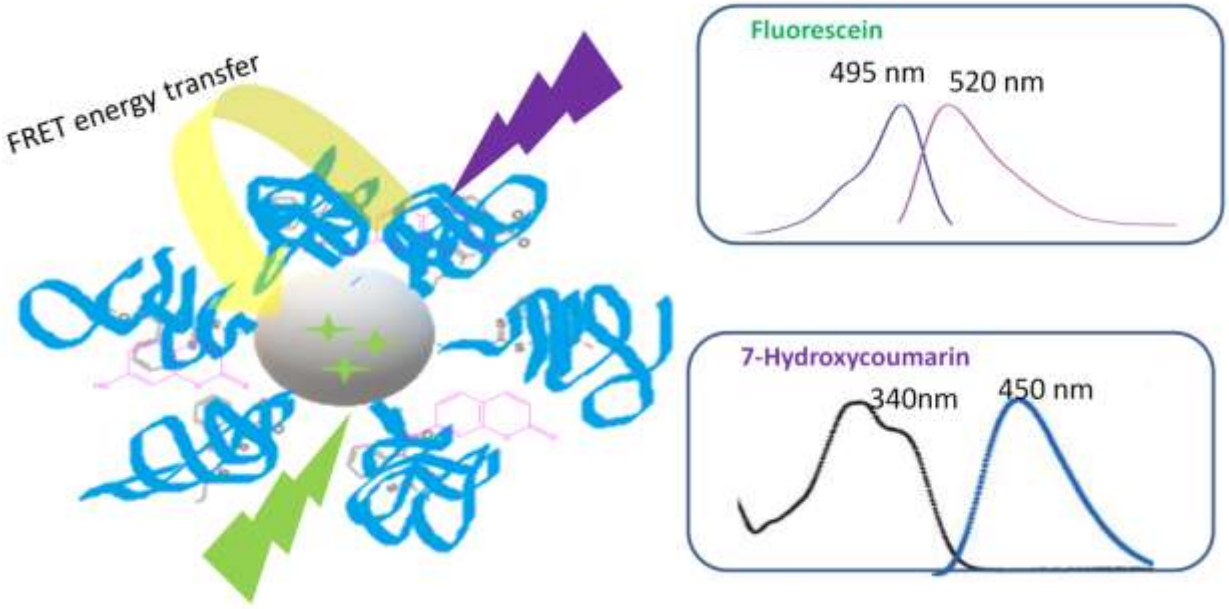

Figure 5.2 FRET triggered by the binding process between the template and MIPs

5.2 Determine the binding affinity

5.2.1 Attaching polymer onto Arosil 200 silica nanoparticle

After polymerization MIP 6308 was attached to the aminated silica nanoparticles made by the same method introduced in chapter 3.2.1 by NHS ester conjugation introduced in chapter 2.6. The NHS ester end of the polymer reacted with the amine groups on the silica nanoparticles. After rinsing with 5% (v:v) acetic acid methanol solution to remove the template, the composite nanoparticles were equally distributed into 1.0 ml of standard solutions to interact with template. After 1 hour of equilibrating, the nanoparticles were spin down, and the fluorescence of the supernants was measured. The results are shown in figure 5.3.

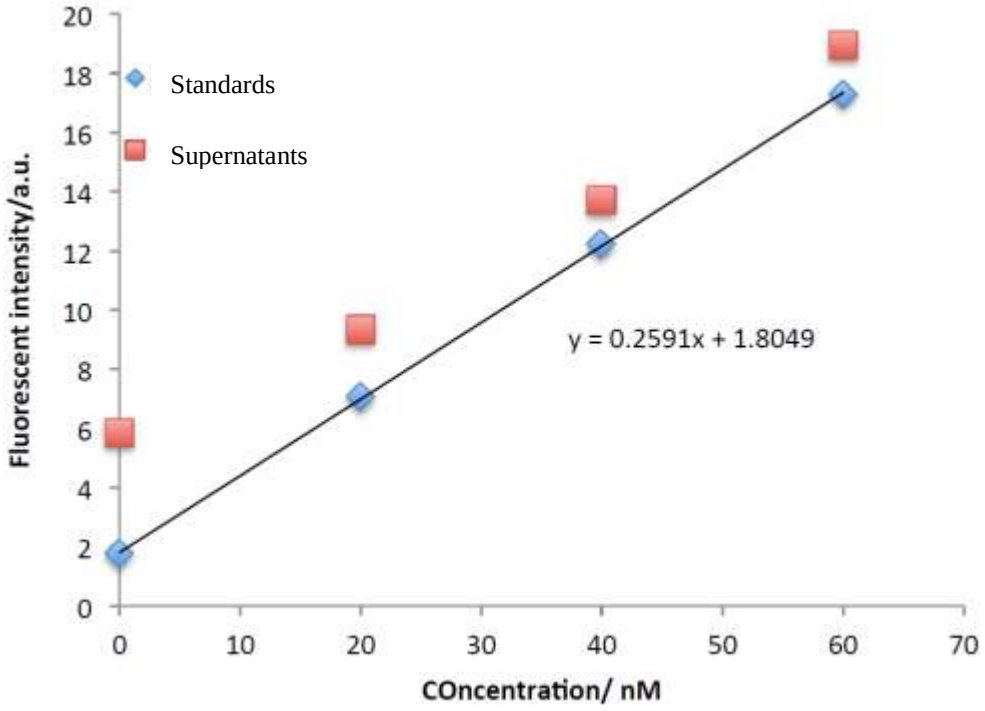

Figure 5.3 The spin-down experiments for MIP 6308 coated arosil 200 silica nanoparticles

Based on Figure 5.3, the slope of the supernatants is smaller than the standard curve, this indicated the composite silica nanoparticle did bind with the template molecules. However, the fluorescence for the first supernatant without addition of any template is higher than the standard. This is due to the scattering of silica nanoparticles stayed in the supernatant. The small size and low density made it impossible to completely spun down all silica nanoparticles. Because of this, the silica nanoparticle is not suitable for the spin-down experiments.

5.2.2 Attaching polymer onto magnetic nanoparticle

To address the density problem with silica nanoparticles, magnetic nanoparticles with were synthesized by a slightly modified micro-emulsion method developed by Du et al.[113]

First, 1.4578g of CTAB, the surfactant, was dispersed into 30 g of anhydrous toluene in a round bottom flask under vigorous stirring. Afterwards, 0.2056 g of $FeCl_2 \cdot 4H_2O$ and 0.5592g of $FeCl_3 \cdot 6H_2O$ were dissolved in 5.6638 g of DI water, and this $FeCl_2$ /$FeCl_3$ solution was slowly dropped into the toluene suspension under nitrogen. After that, the system was stirred continuously for 4h. Then 1.3 ml of ammonia solution was slowly added to the microemulsion system under a nitrogen atmosphere.2 hours later, 1.3870g of TEOS was slowly added into the flask. The mixture was then stirred continuously for 5 days to allow the formation of silica shell. The products were washed by ethanol 3 times followed by refluxing in ethanol for 12 hours. The size of the magnetic nanoparticles was determined as 11 nm by TEM; the TEM images were shown in figure 5.4.

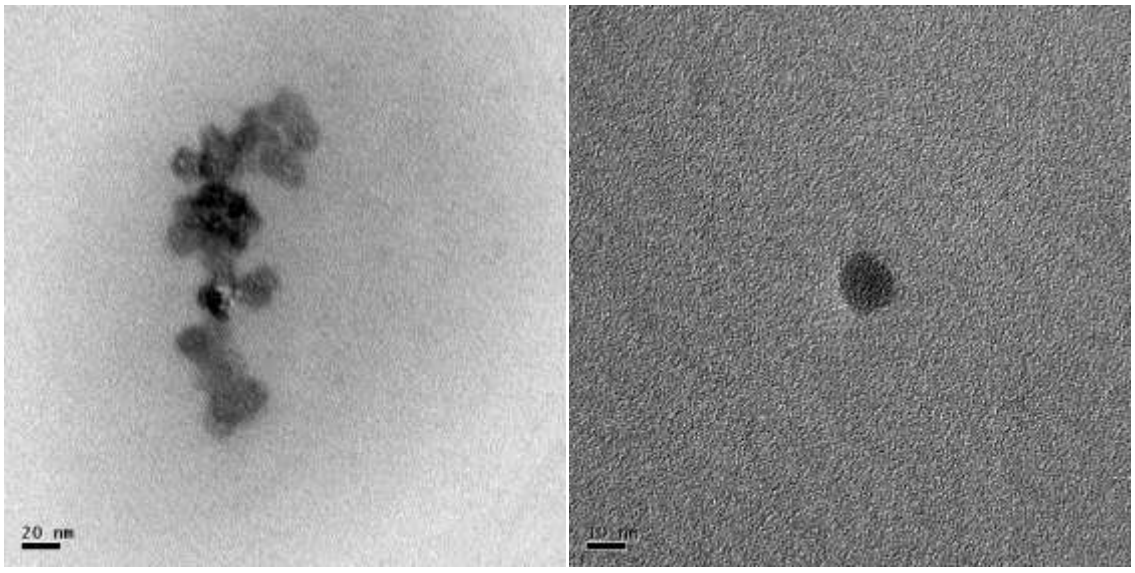

Figure 5.4 The TEM images of magnetic nanoparticles

The magnetic nanoparticles were aminated by reacting with excess APTES in anhydrous toluene. Then the MIP 6308 was coated on the aminated magnetic nanoparticles through the NHS ester conjugation reaction. The TEM images of the MIP coated magnetic nanoparticles were shown in figure 5.5.

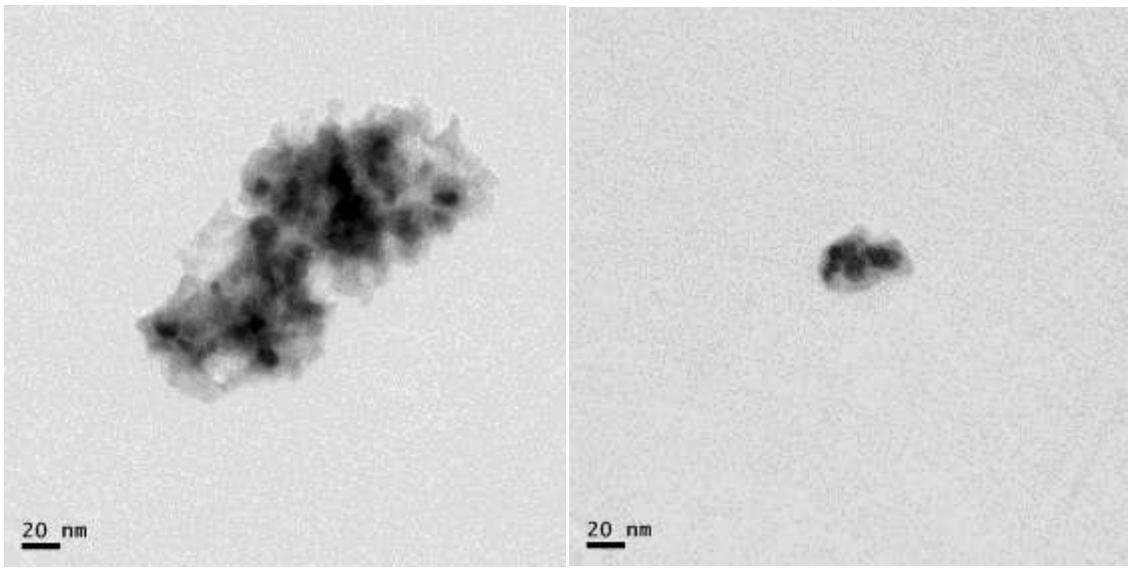

Figure 5.5 the TEM images of MIP coated magnetic nanoparticles. The grey shades around the black spherical nanoparticles are the MIPs.

After completely removing the template, the spin-down experiments were conducted. The data are shown in figure 5.6

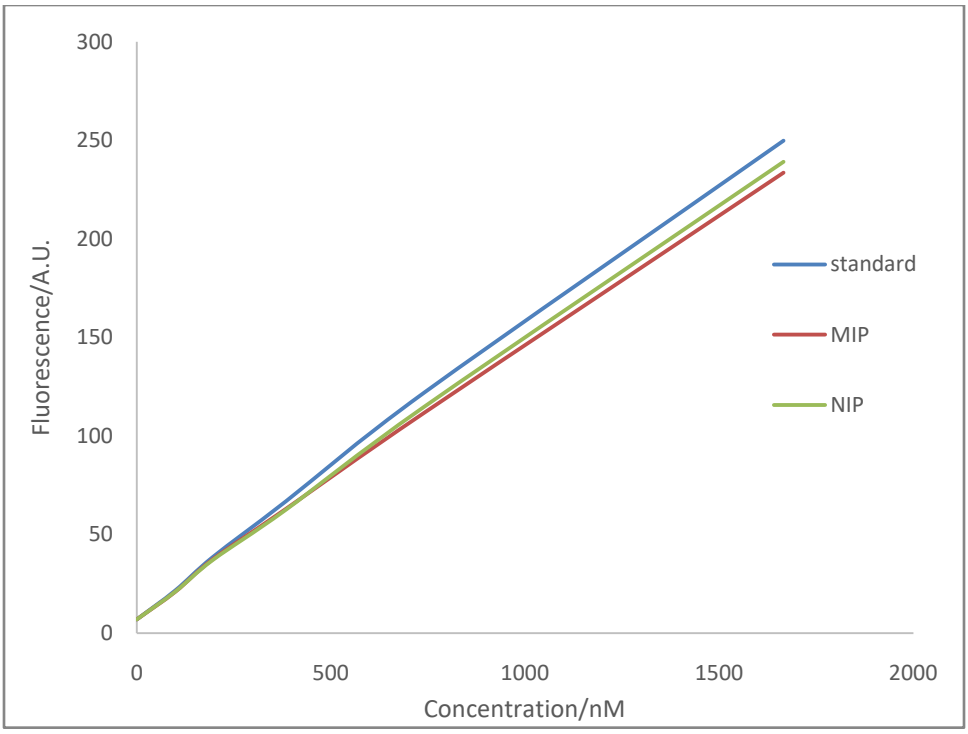

Figure 5.6 The spin-down experiments for MIP 6308 coated magnetic nanoparticles

The magnetic nanoparticles can be spun down completely however the MIP coated polymer didn't bind more template molecules than the NIP coated magnetic nanoparticles. This may due to excess the amine groups on nanoparticle surface. These amine groups can interact with the template molecules and cause significant non-specific binding.

5.2.3 Attaching polymer onto gold nanoparticle

The problem of non-specific binding of magnetic nanoparticles to template molecules can be addressed by attaching MIP onto gold nanoparticles.

After polymerization a dithioester end group is left on one side of the polymer chain. This dithioester end groups can be reduced by sodium borohydride to a thiol end group. In aqueous media at ambient temperature, the thiol reacts with gold nanoparticles (Figure 2.6).

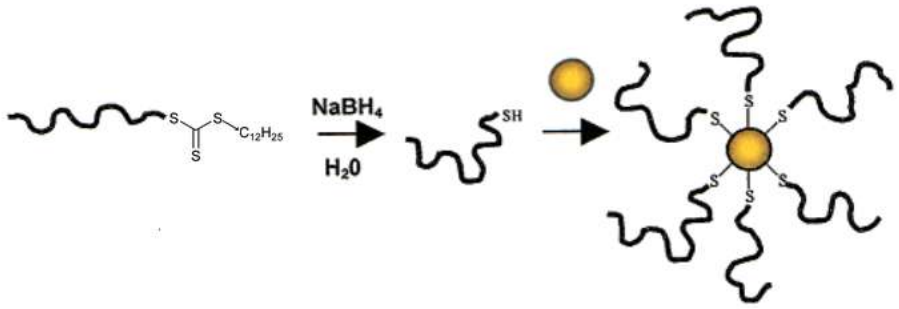

Figure 5.7 Attachment of MIP to a gold nanoparticle using sodium borohydride [93](Copyright © 2005 American Chemical Society)

The MIP coated gold nanoparticles were prepared by the coating process developed by Casey Grenier with minor modification. 100ul of 0.001 g/l MIP 6308, 10 ul of 0.006g/l sodium borohydride were added into 1 ml of gold nanoparticle solution and mixed well. The reaction went 4 hours at room temperature. Then the gold nanoparticles were spun down and washed with D.I. water 3 times to remove the excess polymer. The TEM images for the polymer coated nanoparticles and bare gold nanoparticles were shown in figure 5.8.

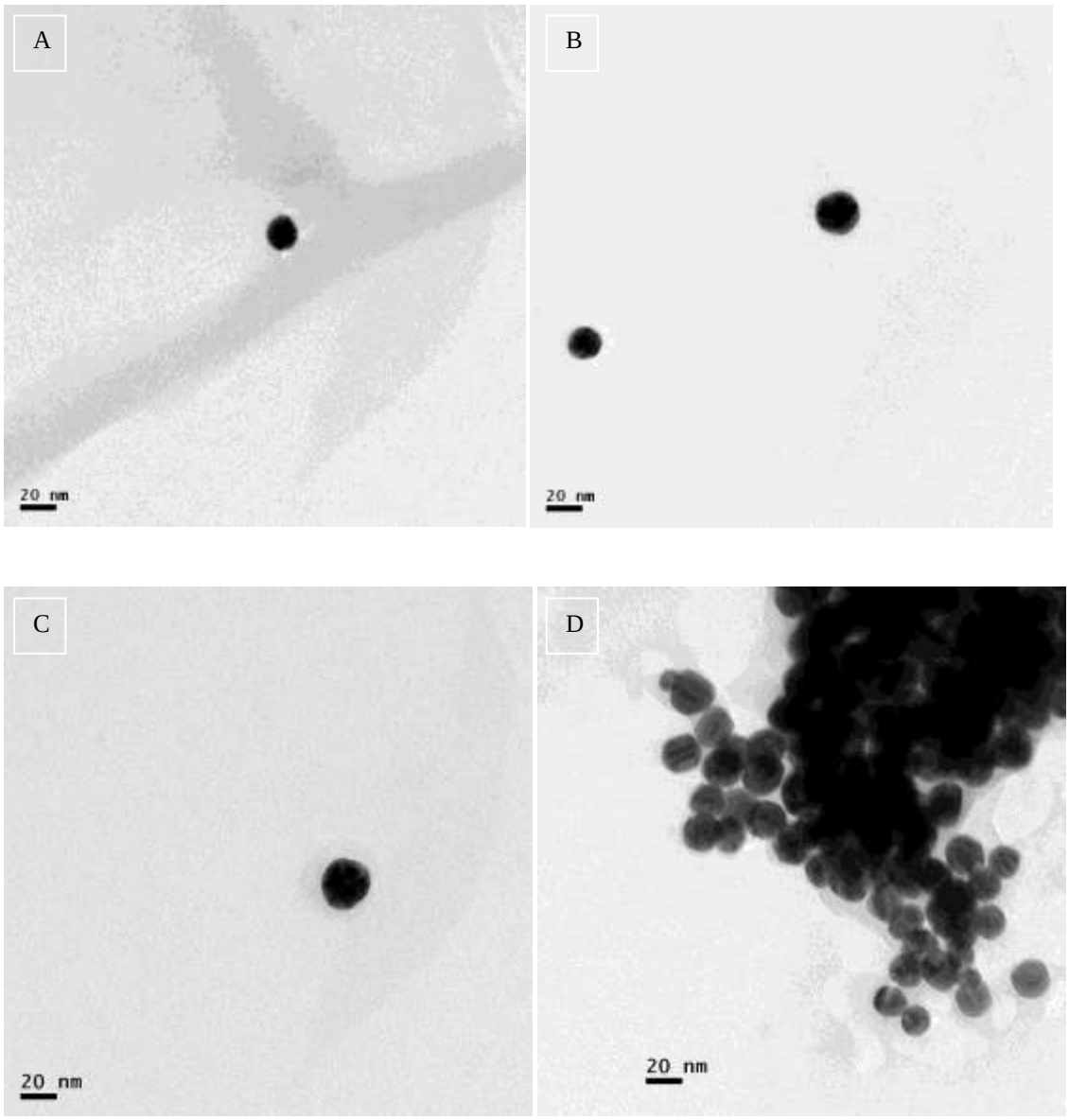

Figure 5.8 TEM images for bare gold nanoparticles (A and B) and MIP coated gold nanoparticles (C and D)

The data for the spin-down experiments of gold nanoparticles were shown in figure 5.9. The amounts of bound template molecules at different concentration were calculated in figure 5.10.

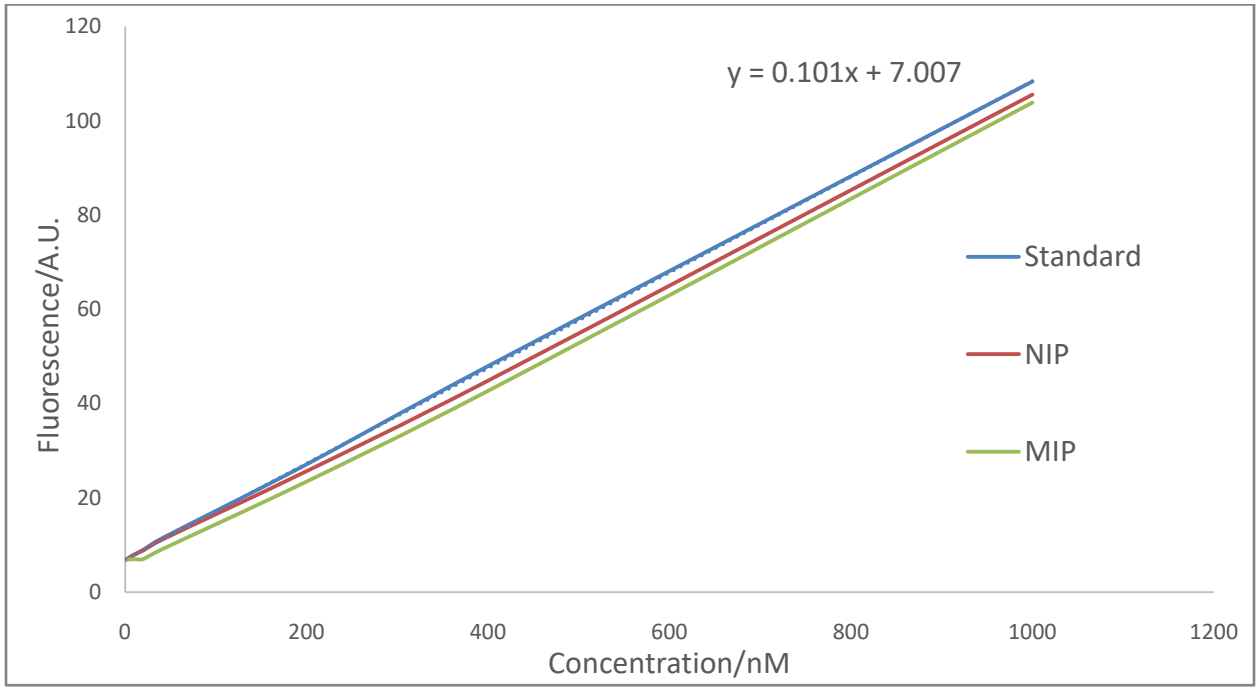

Figure 5.9 The spin-down experiments for MIP 6308 coated gold nanoparticles

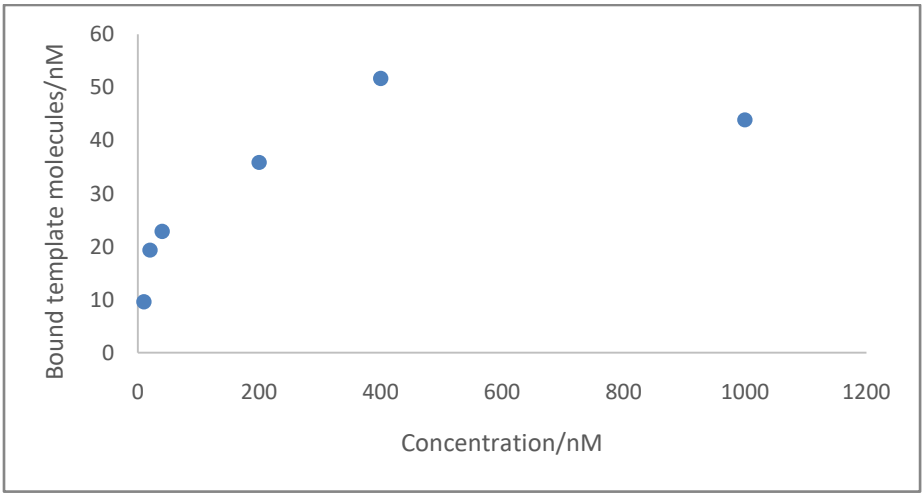

Figure 5.10 Amount of Template Bound to MIP coated gold nanoparticle

The binding constant can be calculated by the following equation:

$$K_{Binding} = \frac{Bound\ \ template}{Free\ Template\ \ x\ MIP\ open\ \ bidning\ \ sites}$$

The calculation for 20nM (Initial Concentration=$2.000x10^{-8}$M) spin-down experiment is:

1) Concentration of free Template = $\frac{Fluorescence\ \ \ Intensity - Y\ intercept}{Slope\ \ of\ the\ Calibration\ \ \ Curve}$

$$= \frac{7.244 - 7.007}{0.1014} = 2.337x10^{-9}\ M$$

2) Concentration of bound template =Initial Concentration– concentration of free template $=2.000x10^{-8}$ M-$2.337x10^{-9}$M=$1.766x10^{-8}$

3) MIP open binding sites = Bound template in 1000nM spin down experiment = 44 nM

= $4.4x10^{-8}$M

4) $K_{Binding} = \frac{Bound\ \ template}{Free\ Template\ \ x\ MIP\ open\ \ bidning\ \ sites} = \frac{1.766x10^{-8}M}{2.337x10^{-9}Mx4.4x10^{-8}M} = 1.7x10^{8}$ M

5.3 Exploration of the binding process

5.3.1 Synthesis of fluorescein doped silica nanoparticles

The fluorescein doped silica nanoparticles are synthesized based on the method developed by Liu et al. with minor modification.[114] First, FITC (3.89mg, 0.01mmol) was dissolved in anhydrous ethanol (800ul) in a 50 ml round bottom flask. Then APTES (13.6 uL, 0.08 mmol) was added into the mixture, the reaction between the APTES and FITC was allowed to proceed for 20h in the dark at room temperature. Next, extra anhydrous ethanol was added along with aqueous ammonia solution (25 %, 2 mL). After continuous stirring for another 20h, TEOS (0.558 mL, 2.5 mmol) was added into the mixture. Then after 20 hours of continuous stirring, more TEOS (13.8 mL, 0.062 mmol) was added and the mixture was stirred for 5 h.

The resulting suspension was centrifuged at 15000 rpm for 10 min to remove the remaining reagents. The particles were washed with ethanol 3 times and dioxane 3 times. The SEM image and the fluorescence of the nanoparticles and are shown in figure 5.11. Based on the SEM, the size of the nanoparticles is around 80 nm. After thoroughly washing, the nanoparticles still had strong fluorescence. The fluorescein was successfully doped into the silica naoparticles.

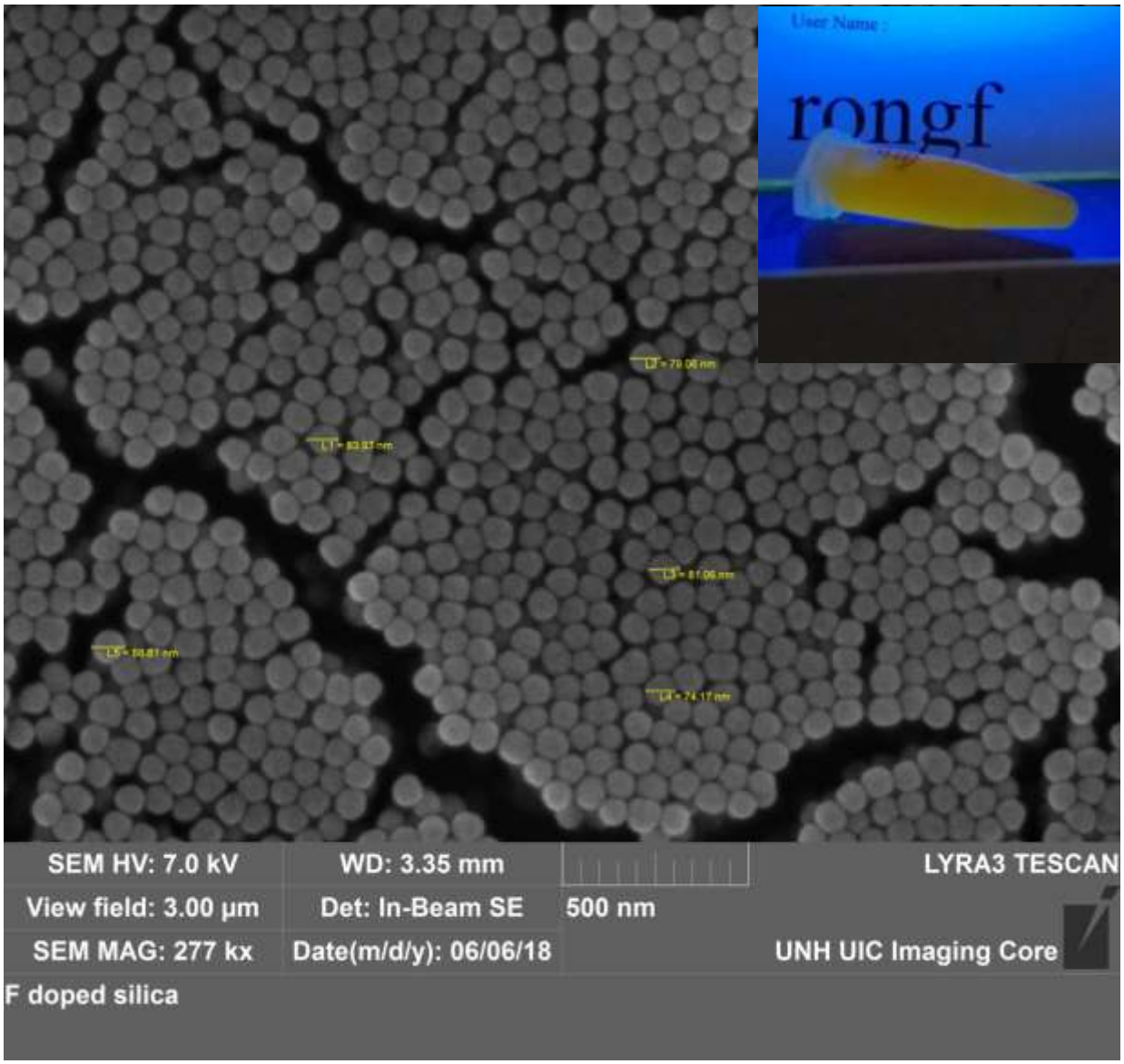

Figure 5.11 SEM image and fluorescence of the fluorescein doped nanoparticles

5.3.2 Synthesis of MPTT RAFT agent

The silanol reactive RAFT agent (MPTT) containing a trimethoxysilyl end group was synthesized based on the method developed by Zhao and Perrier with minor modification.[115]

The reaction was conducted at ambient temperature under nitrogen. In a typical run, a solution of sodium methoxide in methanol (25 wt %, 6.48 g, 30 mmol) was added drop wise into the solution of 3-(mercaptopropyl)trimethoxysilane (95%, 6.20 g, 30 mmol) in 50 mL of anhydrous methanol under nitrogen and the mixture was stirred for 30 min.Then, CS2 (3.05 g, 40mmol) was added dropwise and a yellow solution was formed immediately. The mixture was stirred continuously for 5 h**.** After that, benzyl bromide (98%, 5.24 g, 30 mmol) was added, and the mixture was stirred overnight.

The mixture was concentrated, diluted with dichloromethane, filtered off, and concentrated under reduced pressure. The raw product was purified by silica flash column chloromatography using a gradient eluent of 4:1 hexane/dichloromethane (v/v) to pure dichloromethane and obtained as an orange oil. The NMR spectrum of the pure MPTT is shown in figure 5.12.

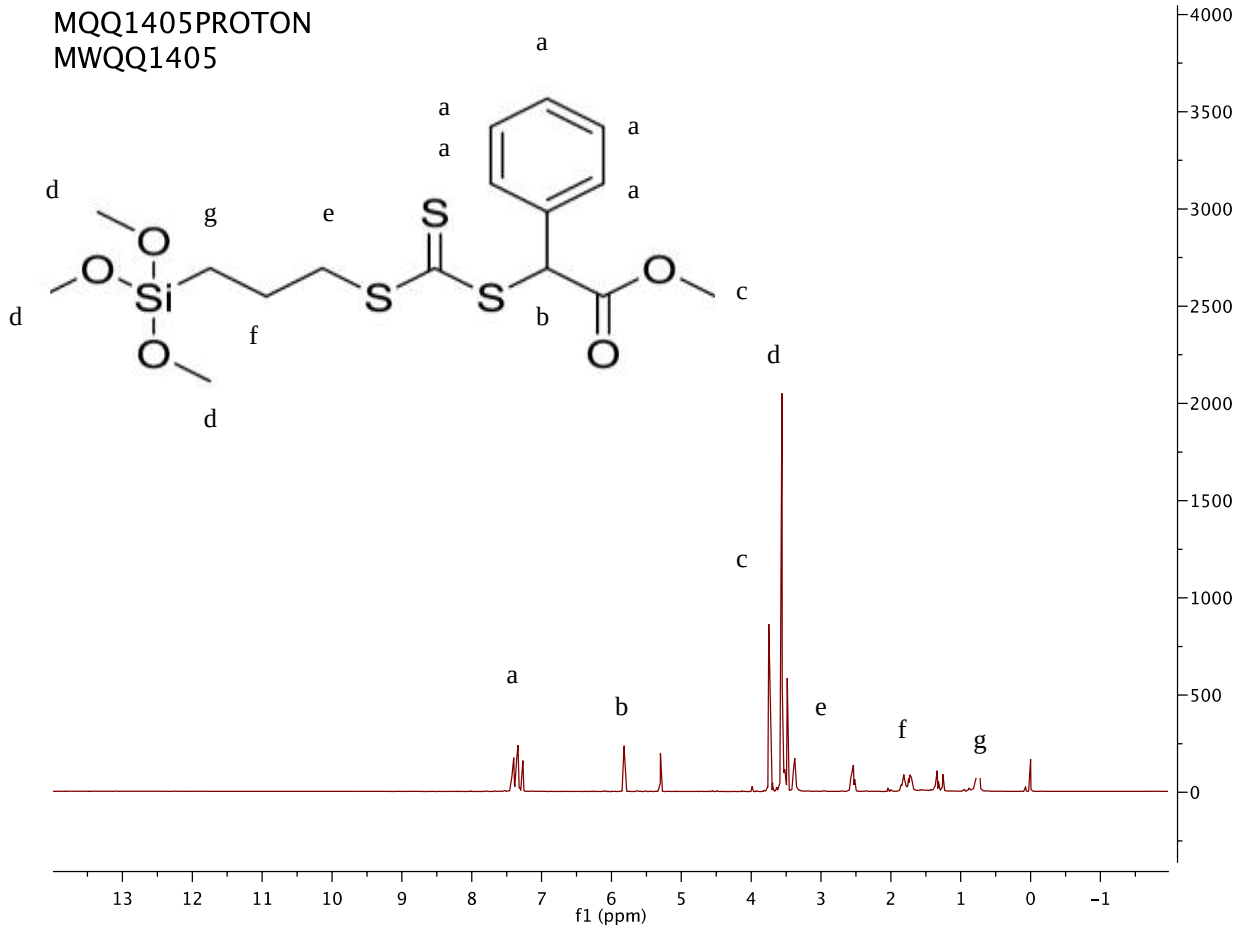

Figure 5.12 1H NMR ($CDCl_3$) of MPTT: 7.34 (m, 5 PhH), 5.81 (s, CH), 3.74 (3H, CH_3), 3.56 (s, 9H, CH_3O), 3.37 (t, 2H, CH_2S), 1.81 (m, 2H, CH_2), 0.75 (t, 2H, CH_2Si).

5.3.3 Growing polymer from the nanoparticles surface

The polymer was coated onto the dye doped silica nanoparticle by the "grown from" method. The first step was to attach RAFT agent onto the nanoparticles surface. The calculated amount of MPTT was mixed with nanoparticle in anhydrous toluene and heated to 100 C for 10 hours then the temperature was elevated to 120 C for another 2 hours. After centrifugation and

washing with dioxane for 3 times, the MPTT modified nanoparticles were used as macro RAFT agent to make MIPs.

The MIPs with the same formulation of MIP 6308 were grown from the silica surface using the standard freeze-pump-thaw methods. The polymerization went for 4 days at 70 C. After polymerization, the template was removed by washing the particles by THF, Acetic acid and methanol mixture (v:v, 10:90), and water for fluorescent tests.

The TEM image of the MIP coated dye doped silica nanoparticles is shown in figure 5.13. The grey film around the white spherical particle was considered as the polymer layer.

The NIP coated dye doped silica nanoparticles were made by the same method as MIP coated nanoparticle just without template in the polymerization.

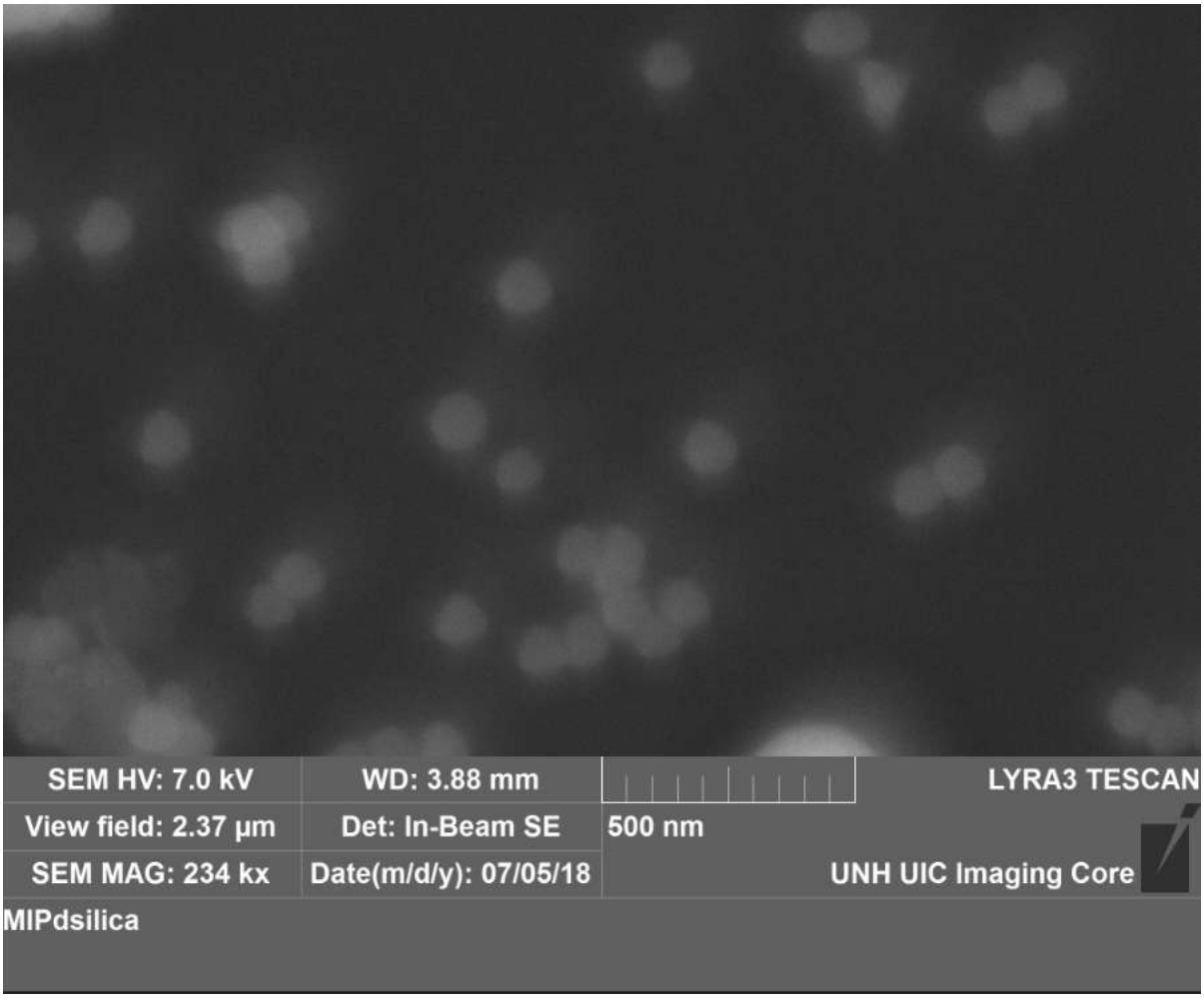

Figure 5.13 SEM image of MIP coated fluorescein doped nanoparticles

5.3.4 Exploring the binding process

To exploring the binding process, template samples with different concentrations were added into the MIPs coated silica nanoparticles. The NIPs coated silica nanoparticles were tested as control.

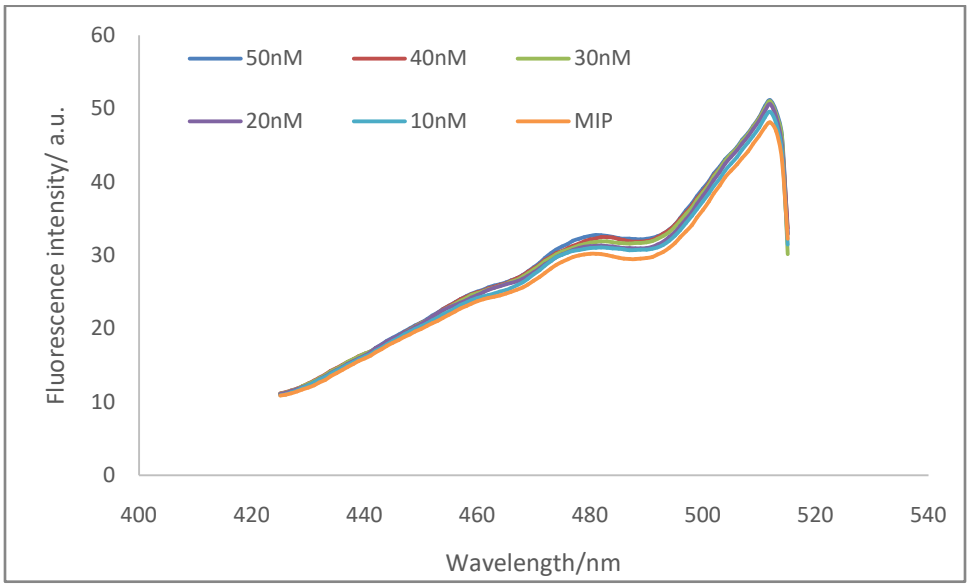

Figure 5.14 Fluorescent excitation spectra of the composite nanoparticles with addition of template at different concentrations**.** (The composite nanoparticles were made with 7CM imprinted MIP as shell and fluorecein doped silica nanopartilces as core.)

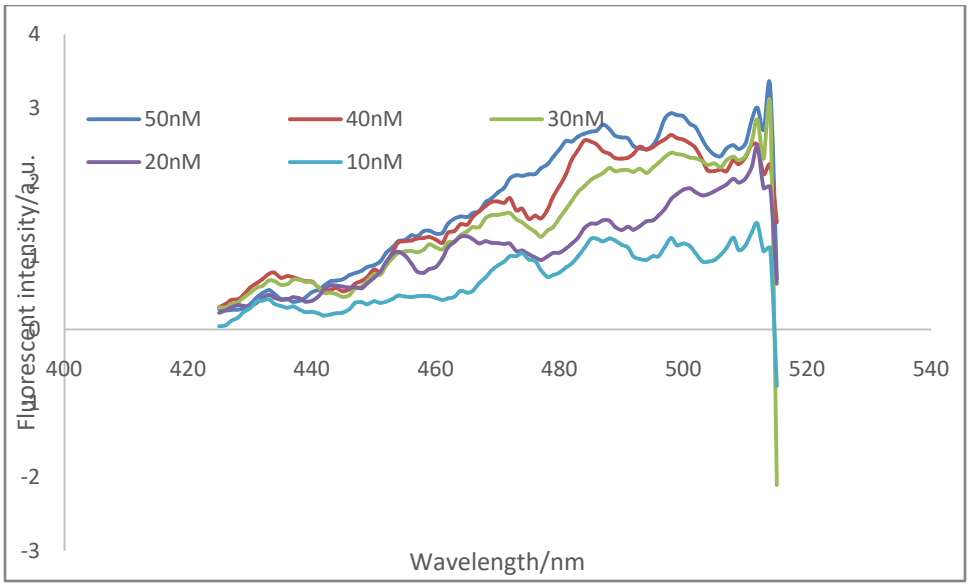

Figure 5.15 Fluorescent excitation spectra of the composite nanoparticles with addition of template at different concentration with the contribution of the initial signal subtracted

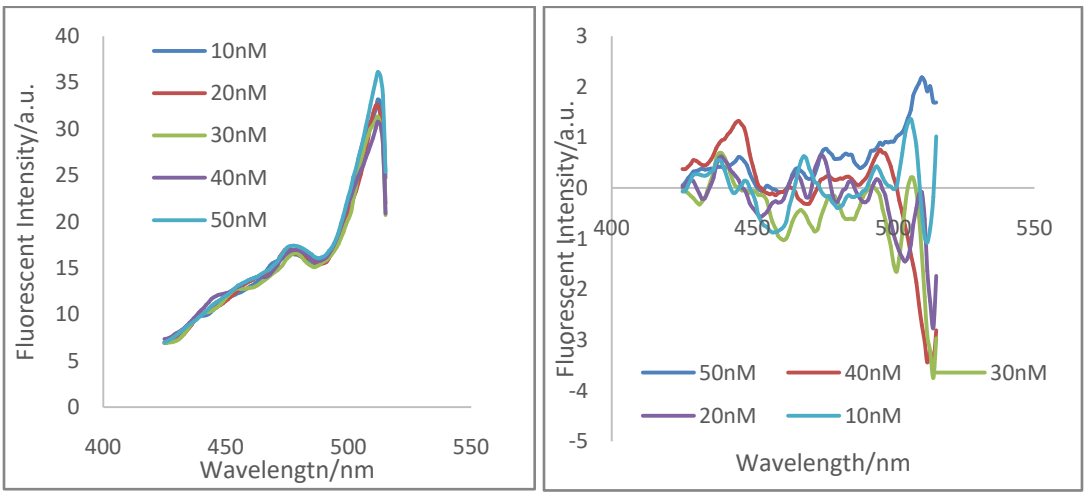

Figure 5.16 Fluorescent excitation spectra of the composite nanoparticles (Non-imprinted) with addition of template at different concentrations (left) and with the contribution of original signal subtracted **.** (The composite nanoparticles were made with Non-MIP as shell and fluorescein doped silica nanoparticles as core.)

The excitation spectra of the template imprinted composite nanoparticle at the wavelength corresponding to the contribution of template molecules were increased in the presence of the template molecule. This indicated that the template molecules in the solution could access to the binding sites inside the MIPs layer on the composite nanoparticle and transfer energy to the fluorescein inside the silica core.

The excitation spectra of the non-imprinted composite nanoparticle at the wavelength corresponding to the contribution of template molecules stayed constant in the presence of the template molecule. This indicated that the template molecules in the solution could not bind to the polymer layers.

Therefore, the FRET energy transfer can only occur in the event when the template binds to the polymer. The free template in the solution can not transfer energy to fluorescein inside the silica nanoparticles.

CHAPTER 6

DESIGN AND SYNTHESIS OF FLUORESCENT SENSOR FOR SENSITATIVE AND SELECTIVE DETECTION OF 7-HYDROXYCOUMARIN

6.1 Introduction

Fluorescent sensors developed by incorporating fluorescent dye covalently into molecular imprinted polymer matrix have been studied by many research groups all over the world because of their potential for high sensitivity and real-time monitoring. [116]

For example, Wu et al. [117] prepared a polymerizable dansyl monomer---dansyl methacrylate by coupling 2-aminoethyl methacrylate hydrochloride and dansyl chloride. A fluorescent molecularly imprinted polymer chemosensor (fMIPcs) was prepared by precipitation polymerization with this dansyl monomer as the functional monomer for monitoring bisphenol A (BPA) in tap and river water. The assay performed in 96-well plates indicated that fMIPcs can selectively bind to BPA with 60% reduction in fluorescence intensity. The limit of detection and the limit of quantification were 3 and 10 μg/L respectively.

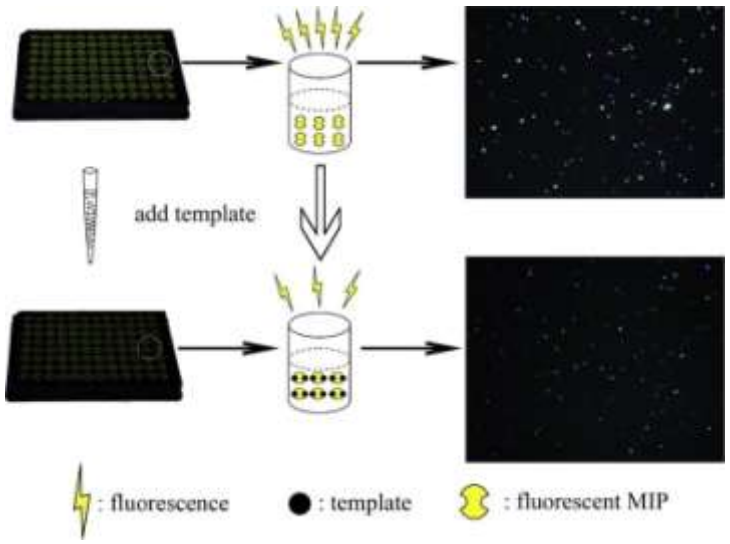

Figure 6.1 Bisphenol A detection using fMIPs with M1 in 96-well plate [117] (Copyright © 2014 Elsevier Ltd.)

Besides dansyl, the fluorescein skeleton has also been used for the design of dyadic fluorescent monomers. Gao et al. [118] synthesized a fluorescein based monomer --- allyl fluorescein by reacting fluorescein with allyl bromide. Fluorescent molecularly imprinted polymer microspheres were prepared by precipitation polymerization. Upon addition of 1.0 nM cyhalothrin template, the fluorescence of the polymer microspheres was quenched by 20%. A linear relationship could be obtained covering the lower concentration range of 0–1.0 nM with a correlation coefficient of 0.9936 described by the Stern–Volmer equation.

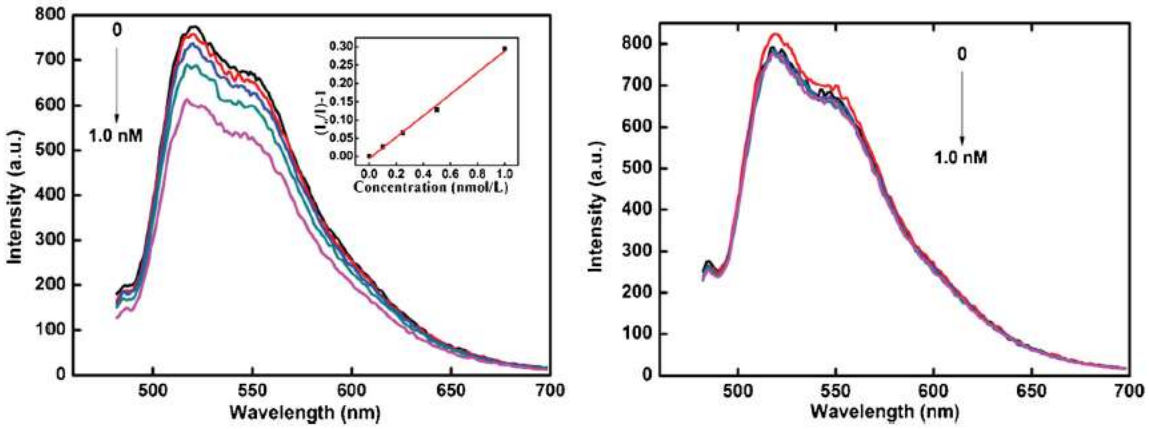

Figure 6.2 Response of the fMIP (left) microspheres and fluorescent non-imprinted polymer (NIP) (right) microspheres to cyhalothrin in a concentrationrange from 0 to 1.0 nM. [118]

(Copyright © 2014 Published by Elsevier Ltd.)

Dyadic fluorescent monomers equipped with a polymerizable functional group were used as the functional monomer for the sensing of template molecules these two researches as shown in figure 6.3. Both sensors are able to detect template molecules at low concentration. However the selectivity for both sensors is not promising. This is because of the dyadic fluorescent monomers are not capable of interacting with the template molecules in a specific pattern during the formation of binding sites. Therefore, limited amount of dyadic fluorescent monomers were effectively built inside the binding sites. Accordingly, a sizeable number of dyes are not accessible to the template molecules and generate considerable background fluorescence and signal heterogeneity.[119]

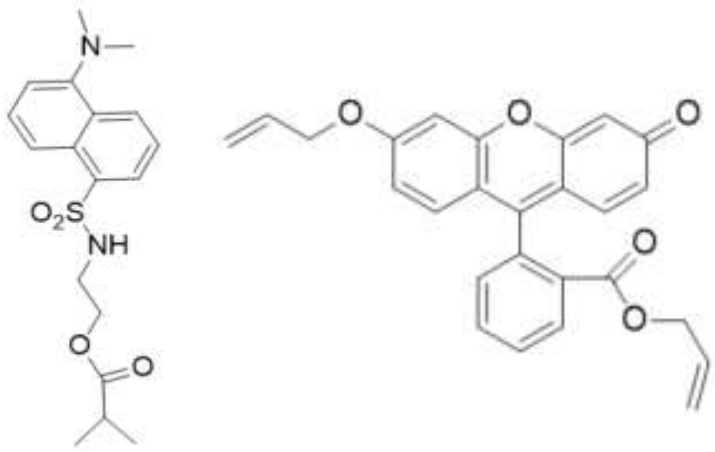

Figure 6.3 Dyadic fluorescent monomers :dansyl methacrylate(left) and allyl fluorescein (right)

The key point to solve this problem is to locate the fluorescent monomers only in the binding sites. [120]To this goal, a triadic fluorescent monomer that contains a polymerizable double bond, a functional group to specifically interact with the template molecule, and a fluorescent fragment was designed and synthesized in the following project.

6.2 Design and strategy

Lysine, an essential α-amino acid making up 5.9% of all sites in human proteins, was chosen as the backbone for the trifunctional fluorescent monomer. Besides the α-amino group and α-carboxylic acid group of all amino acids, lysine contains a lysyl group ($(CH_2)_4NH_2$) as shown in figure 6.3. The protonated ε-amino group has a significantly higher pK_a (about 10.5 in polypeptides) than the α-amino group. Therefore, it often participates in hydrogen bonding and as a general base in catalysis. [121]

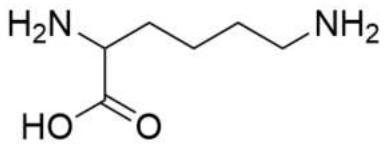

Figure 6.4 Structure of Lysine

Lysine residues are usually found on the surface of proteins increasing water solubility due to ionic character of the protonated ε-amino group. Therefore, native lysine residues are convenient targets for protein modification. [123] Many reagents have been used to react with the ε-amino, such as: ester electrophile, [124] sulfonyl Acrylate [125] and unsaturated sulfonamide-based inhibitor. [126]

Inspired by these ways of protein modification on lysine residues, I hypothesis that the two amine groups on lysine can be modified by polymerizable groups and fluorescent fragments. The modified lysine could then be incorporated into an MIP matrix and also is fluorescent. Compared to the common dyadic fluorescent monomer, the advanced point for this design is the presence of an active carboxylic acid group after the modification of these two amine groups. With a low pKa, the carboxylic groups can form hydrogen bonds with the template molecules during the formation of binding sites. Therefore, a trifunctional fluorescent monomer can be successfully constructed.

Furthermore, if the fluorescent fragment is located close enough to the carboxyl acid group and is sensitive to the microenvironment around it, the interaction between the carboxylic acid groups with the template molecules would affect the fluorescence of the fluorescent fragment. Therefore, the fluorescent fragment must be connected to the α-amino group, which is two bonds distance from the carboxylic acid group. Accordingly, the polymerizable double bond

must be attached to the ε-amino group. The proposed structure for the trifunctional fluorescent monomer is depicted in figure 6.5.

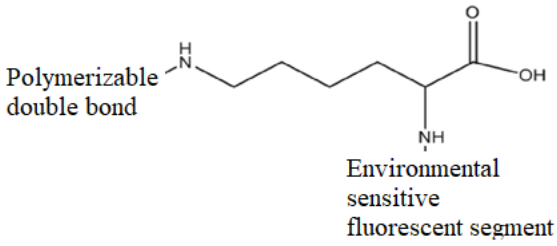

Figure 6.5 Proposed structure for the trifunctional fluorescent monomer

The fluorescence of the nitrobenzofurazan (NBD) moiety is environmentally sensitive; it is virtually nonfluorescent in water but becomes strongly green fluorescent in hydrophobic media. Because of this, the NBD moiety has been extensively used for chromatographic analysis of amino acids and low molecular weight amines. [127] In this project, 4-Chloro-7-nitrobenzofurazan (NBD-chloride) is reacted with the α-amino group in lysine. This compound is nonfluorescent until it reacts with primary to produce highly fluorescent derivatives. The excitation and emission spectra for the NBD labeled primary amine compound are shown in figure 6.6.

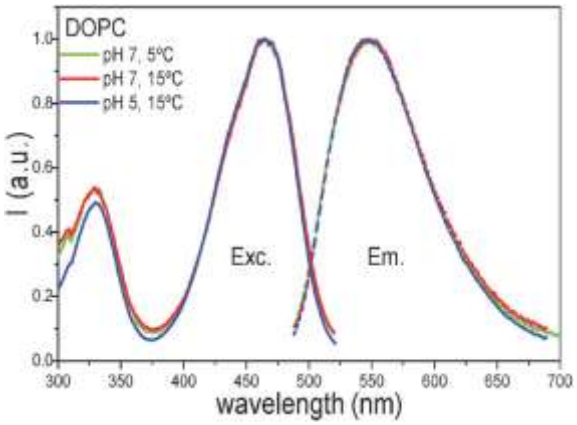

Figure 6.6 Normalized fluorescence excitation (Exc.) and emission (Em.) spectra of NBD-PS embedded in DOPC bilayers (at 1 mol%).[127]

6.3 Advantages of this strategy

With the triadic design, the trifuctional fluorescent monomer can form strong specific binding with template molecule through noncovalent interaction between the carboxylic acid group and the template molecule. It can be covalently incorporated into the polymer matrix through the polymerizable double bond. The environmental sensitive fluorescent fragment can transfer the chemical binding process into a measurable analytical signal. The predicted binding sites configuration is shown in figure 6.7.

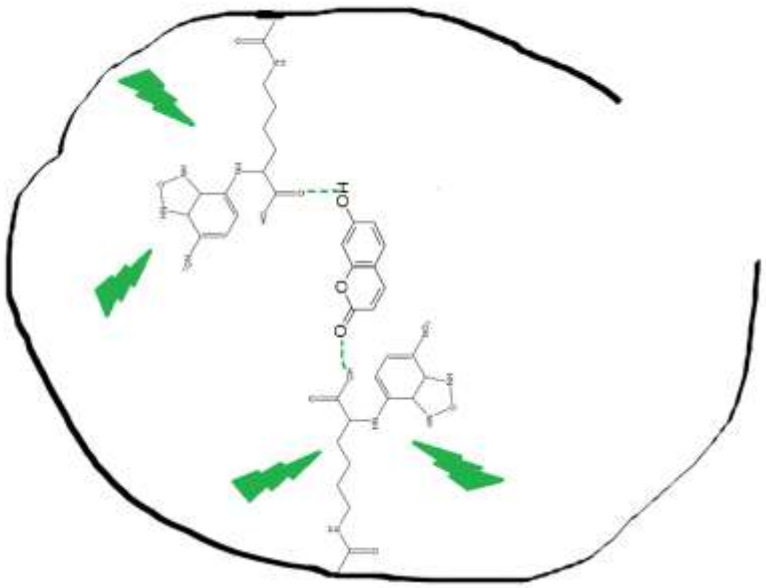

Figure 6.7 Predicted binding sites configuration

As shown in figure 6.7, after polymerization the trifuctional fluorescent monomers will only be located inside the binding sites. Because most of the fluorescent monomers are close to the template molecules, the background fluorescence can be greatly reduced. It was anticipated that the rebinding of the template with the MIP would significantly modify the output signal of

the NBD moiety. Compared to other dyadic fluorescent monomers, this trifuctional fluorescent monomer will be more sensitive and selective.

6.4 Synthesis of the trifunctional fluorescent monomer

The first part of the synthesis is to protect the α-amino group and attach polymerizable double bonds on to the ε-amino group. This was achieved by following the method developed by Nagaoka with minor modification. [128]

The α-amino group was protected by adding basic cupric carbonate to hot aqueous lysine solution to form the lysine-copper complex shown in figure 6.8. L-Lysine hydrochloride (10 g, 54.8mmol) was dissolved in water (120 ml) at 90°C. Basic cupric carbonate (6.66 g, 30.1 mmol) was added slowly to the solution and stirred for 10 min. After cooling and filtering the insoluble residue, a solution of lysine-copper complex was attained.

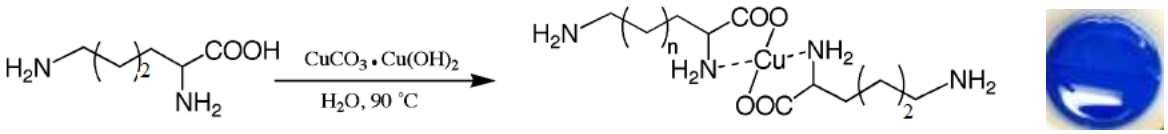

Figure 6.8 Synthesis of lysine-copper complex

The polymerizable double bonds were attached to the ε-amino by reacting acryloyl chloride with the lysine-copper complex shown in figure 6.9. First, 58 ml of acetone and 27.4 ml of 2.0 M KOH aqueous solution was added to the solution of lysine-copper complex. Then acryloyl chloride (1.38 ml, 17.1 mmol) and 7.7 ml of 2.0 M KOH aqueous solution were added every 5 min at 3°C. This procedure was repeated four times. After stirring for 12 h, the

precipitates of the acrylamide lysine-copper complex were filtrated and washed successively with water, methanol, and ether.

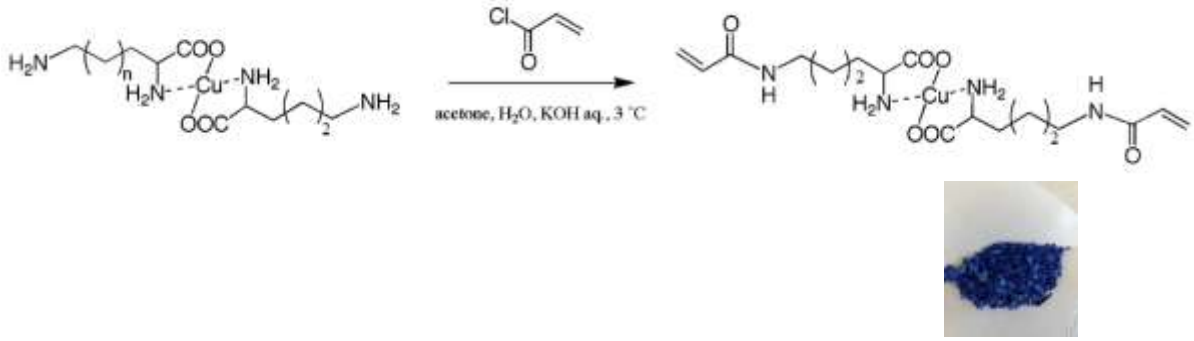

Figure 6.9 Synthesis of acrylamide lysine-copper complex

The structure of acrylamide lysine-copper complex was confirmed by their IR spectra. the peak at 3100–3400 cm^{-1} is from the N-H stretch in amide and amine; peak at 2880–2960 cm^{-1} is from the C-H stretch; the peak at 1660 cm^{-1} is from the C=O stretch in the amide.

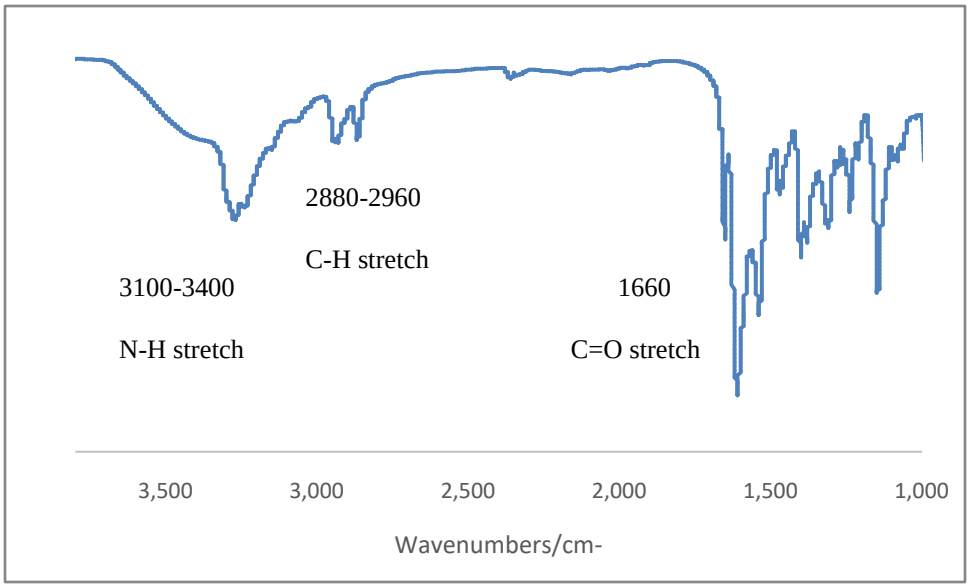

Figure 6.10 IR spectrum of acrylamide lysine-copper complex

The α-amino group was de-protected using 8-hydroxy quinoline as an organic chelate precipitant to form a complex with copper ion as shown in figure 6.11. The solid of acrylamide lysine-copper complex (21.0 g, 45.5 mmol) was ground with a mortar first, then dispersed in water (300 ml), and a chloroform solution (300 ml) of 8-quinolinol (7.91 g, 54.5 mmol) was added. After stirring overnight in a round bottom flask at room temperature, a green precipitate in the chloroform layer was produced. This was removed by filtering. Three extractions with chloroform were performed to remove traces of 8-hydroxy quinoline. The raw product acryloyl lysine was collected by the lyophilizer to dry out the water layer. Then raw product was dissolved in 5ml water with 2ml acetic acid. The white precipitate was recrystallized from teterahydrofuran. The structure of acryloyl lysine was confirmed by ^{1}H NMR shown in figure 6.12.

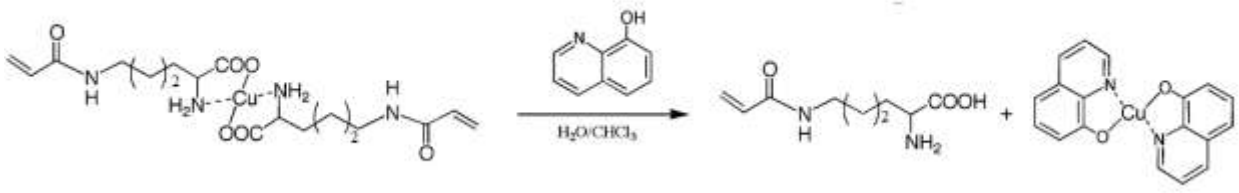

Figure 6.11 Synthesis of acryloyl lysine

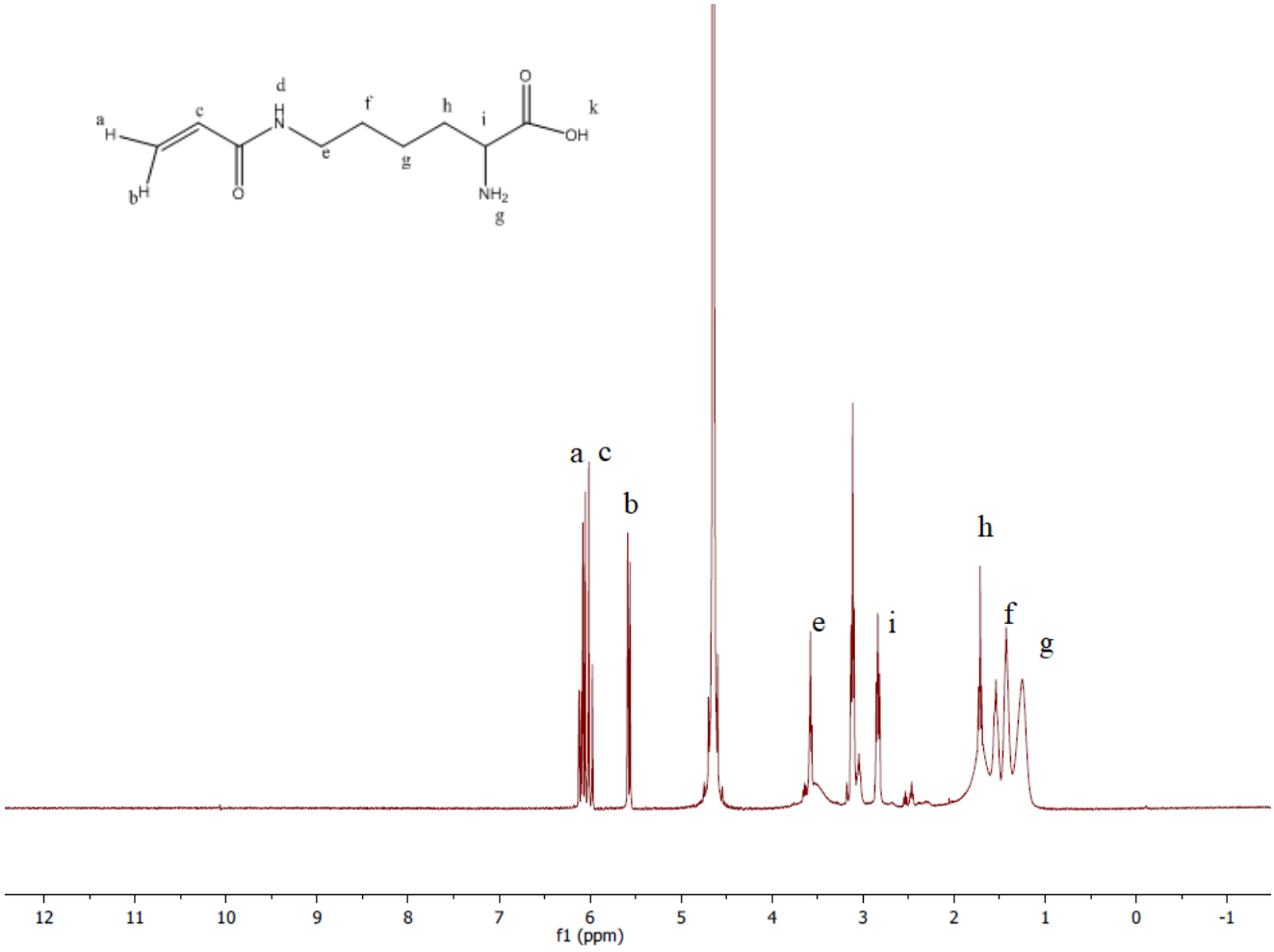

Figure 6.12 ^{1}H NMR spectrum of acryloyl lysine (D_2O, 400 MHz): 1.22 (m, 2H, CH_2), 1.42 (m, 2H, CH_2), 1.66 (m, 2H, CH_2), 2,89 (t, 1H, CH), 3.73 (t, 2H, CH_2), 5.65 (d, 1H, CH_2=CH[trans]), 6.10 (d, 1H, CH_2=CH[cis]), 6.17 (dd, 1H, CH_2=CH).

The second part of the synthesis is to graft NBD fluorescent fragment onto the α-amino group as shown in figure 6.13. (1.3g, 10mmol) acryloyl lysine was dissolved in 10ml 0.1 molar sodium bicarbonate buffer. Then a solution of (2g, 10mmol) NBD-Cl in 80 ml methanol was added. The mixture was heated up to 50C and stirred for 2hrs. After removing the methanol, the raw product was lyophilized to remove the water. The NMR spectrum of the NBD-lysine is show in figure 6.14.

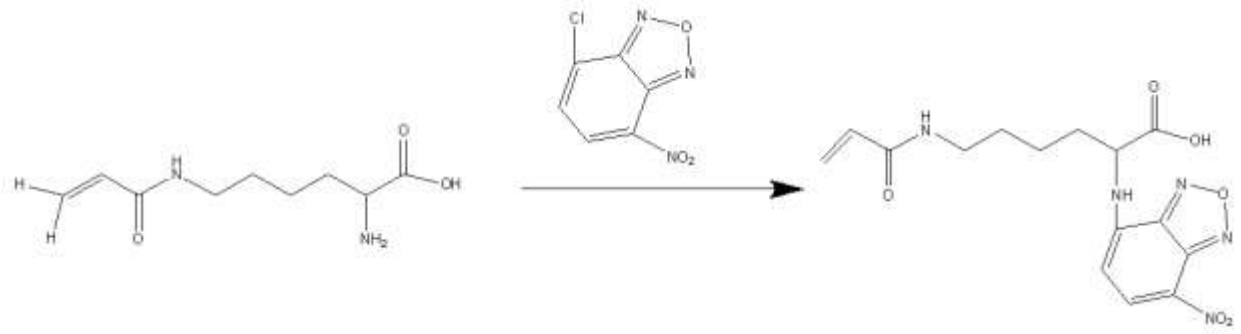

Figure 6.13 Synthesis of NBD-lysine

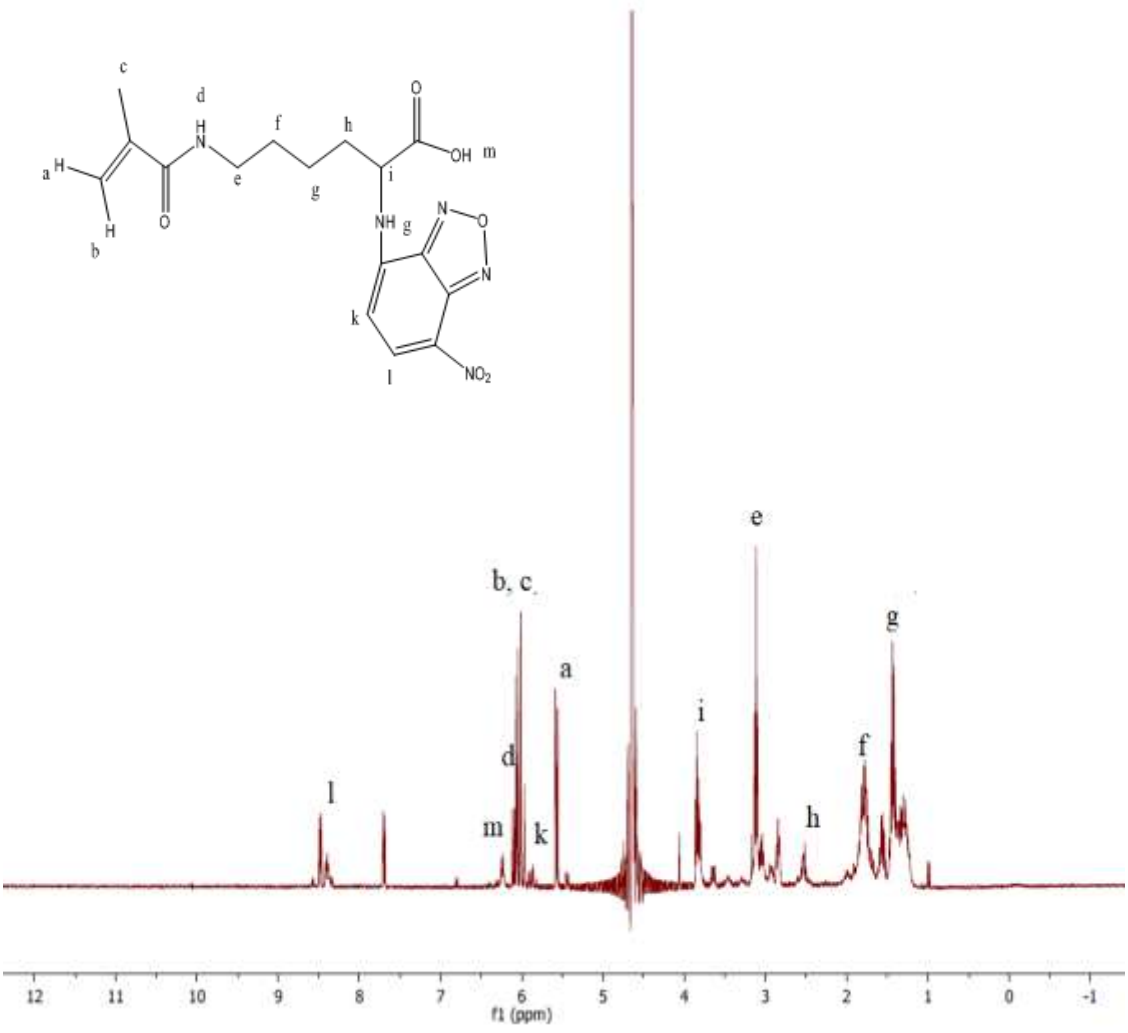

Figure 6.14 ^{1}H NMR spectrum of NBD-lysine (D_2O, 400 MHz)

The fluorescent spectra of the 0.01mg/l of NBD-Lysine in ethanol are shown in figure 6.15. The maximum excitation wavelength is 498 nm and the maximum emission wavelength is 500nm.

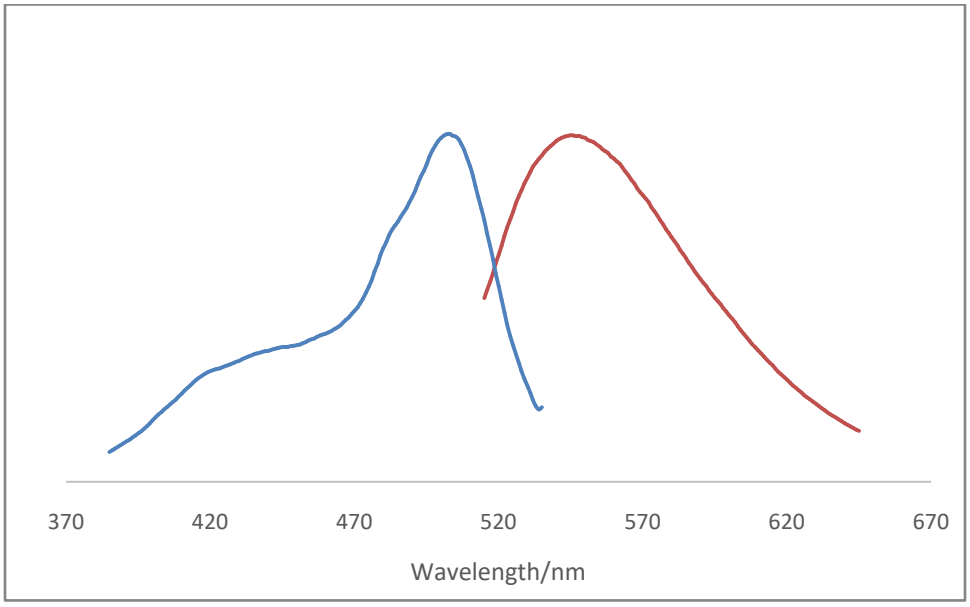

Figure 6.15 Fluorescent excitation and emission spectra of NBD-lysine

6.5 Synthesis of the fluorescent sensor

A fluorescent sensor was developed by incorporating the NBD-lysine into the MIP matrix as a recognition monomer. The MIP formulation was optimized throughout the project to ensure that the MIP would selectively bind the template with high affinity. The carboxylic acid group in NBD-lysine molecule can form hydrogen bond with the template molecule for specific recognition. The recognition monomer to template molar ratio is 5:1, to fully saturate the template's hydrogen binding sites. The MAA and 4VP were used to form acid/base non-covalent

crosslinking. Below in table 6.1 is a polymer formulation for the final optimized MIP and NIP blank.

	NIPAM	**4VP**	**MBA**	**MAA**	**Lysine - NBD**	**RAFT Agent**	**Initiator**	**Template**
MIP Sensor	83%	5%	2%	5%	5%	1%	0.1%	7CM
NIP Blank	83%	5%	2%	5%	5%	1%	0.1%	N/A

Table 6.1 Polymer formulations formulation of MIP sensor and NIP blank

The fluorescent spectra for the 0.1mg/l MIP sensor in ethanol are shown in figure 6.16. The maximum excitation wavelength is 470 nm and the maximum emission wavelength is 538 nm. The trifunctional fluorescent monomer was successfully incorporated into the MIP matrix.

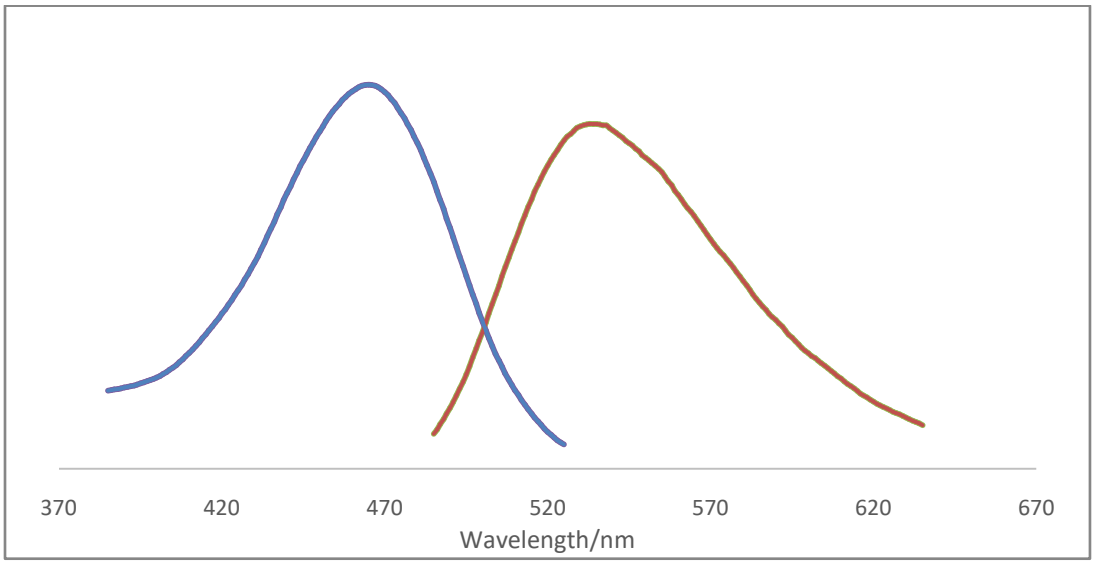

Figure 6.16 Fluorescent excitation and emission spectra of MIP sensor

6.6 Response of MIP sensor to the template

After polymerization, the MIP sensor was precipitated out by adding hexane to the polymerization mixture. Then the MIP sensor was dialyzed against THF for 4 weeks to remove the template. After the removal of the template, the MIP sensor and NIP blank were dissolved in ethanol.

The response of the MIP sensor and NIP blank to the template molecule in ethanol was measured by adding different amount of template into 0.1mg/l MIP sensor or NIP blank solutions at 38°C. The response of MIP sensor to the template is shown in figure 6.17. The excitation wave length is 450 nm, the slit width is 10nm for both excitation and emission. Upon the addition of 1 nano molar template into the MIP solution, the fluorescence of the MIP sensor was quenched. More template molecules cause stronger quenching. The quenching effect reached maximum when 1 micro molar template molecule was added. This indicates the MIP sensor can detect the template molecule in nano molar level with significant signal change. The binding sites in MIP sensor were saturated when 1 micro molar of template was added.

As a control, the response of NIP to the template molecule was also measured with the same method, shown in figure 6.18.

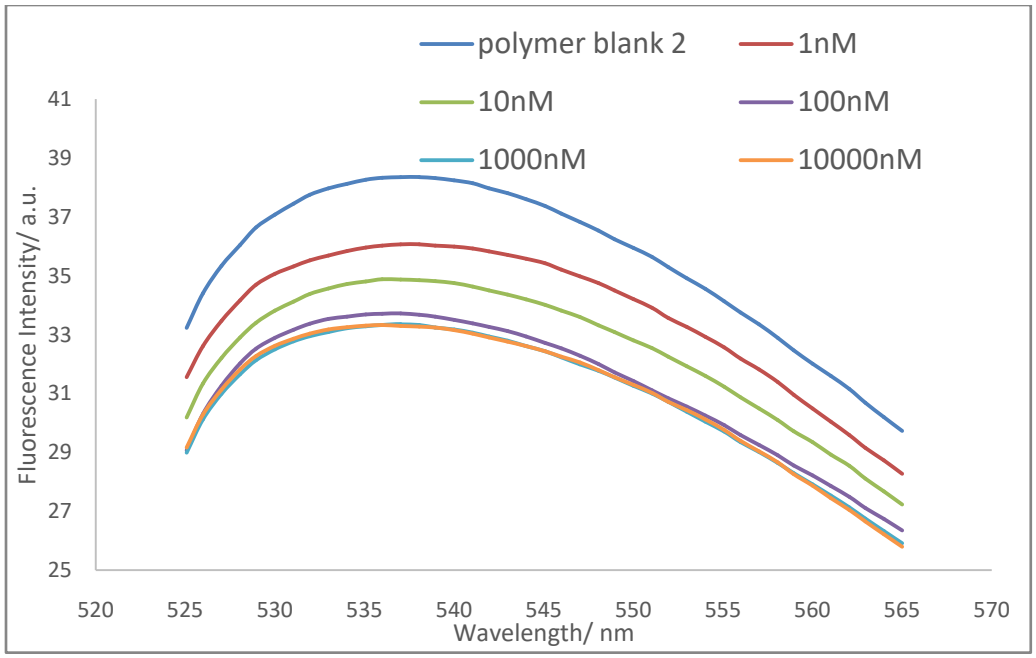

Figure 6.17 Response of MIP sensor to template (λex=450nm, at 38°C)

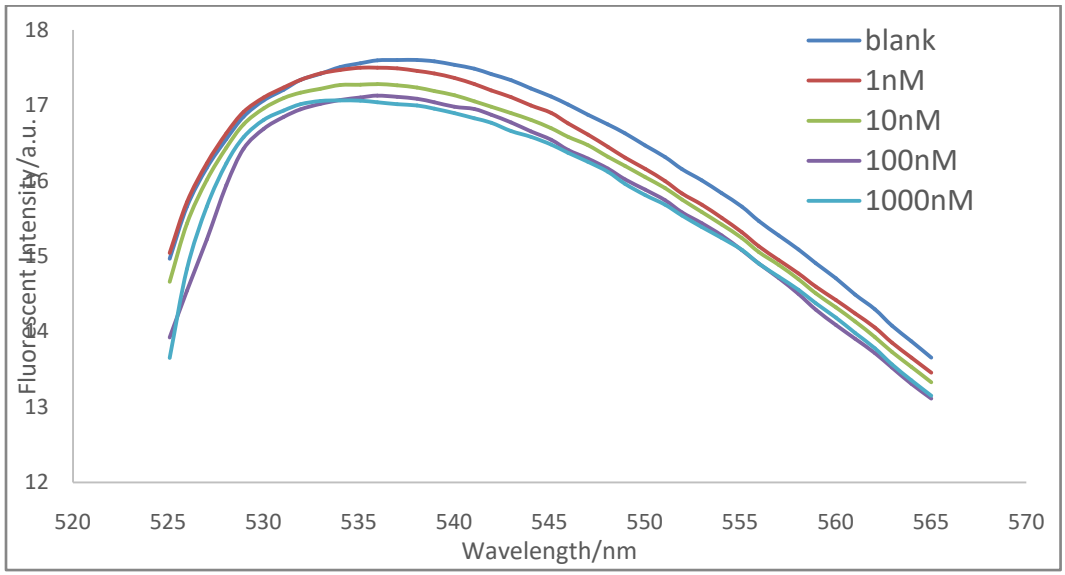

Figure 6.18 Response of NIP sensor to template (λex=450nm, at 38°C)

6.7 Selectivity Test

To investigate the selectivity of the MIP sensor, different structural analogues of the template molecules were tested. The analogues were dissolved in ethanol at a concentration of 100 nM. In the tests, 300 ul of each structural analogue solution was added to700 ul of the MIP sensor solution. The fluorescent spectra are shown in figure 6.19.

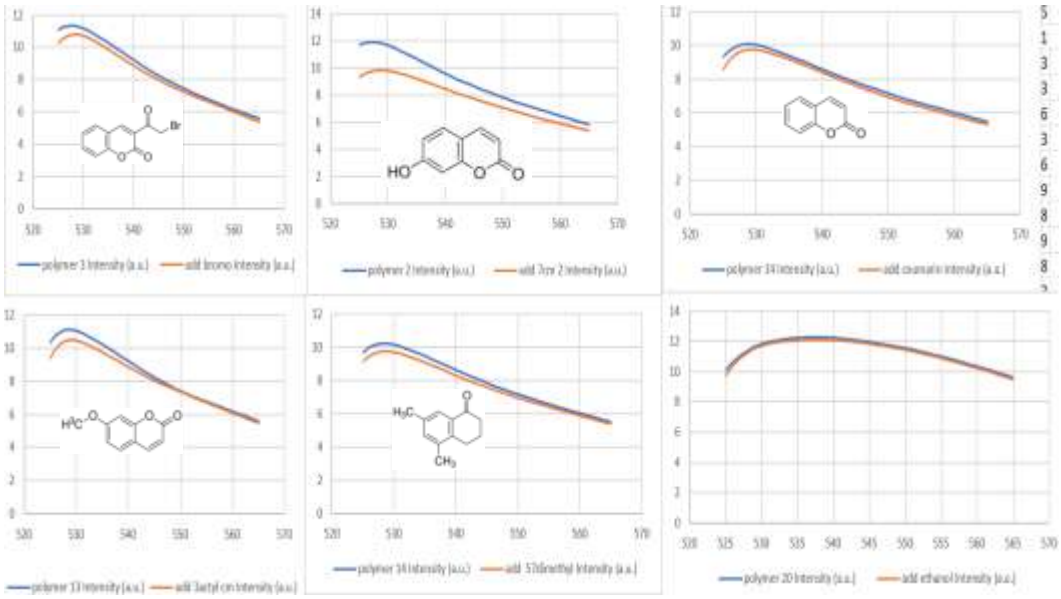

Figure 6.19 Selectivity tests

After subtracting the dilution effect of the addition of solvent ethanol, the fluorescent quenching for each structural analogue was calculated and shown in figure 6.20. Based on the data, the MIP sensor can selectively response to the template molecule with significant signal change while responding weakly to other structural analogues.

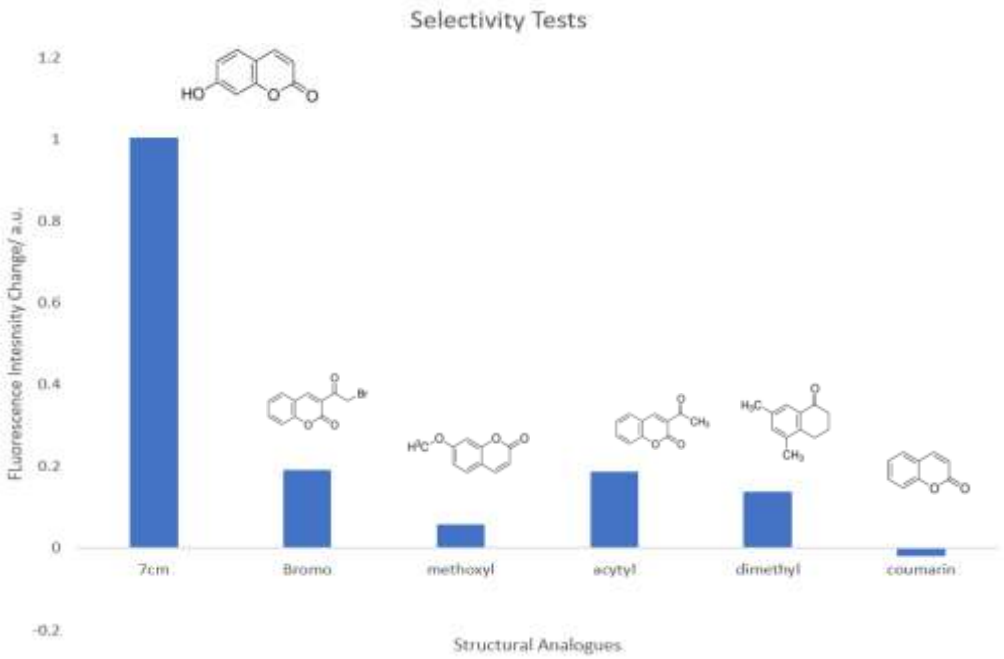

Figure 6.20 Selectivity tests

The fluorescent sensor based on NBD-lysine can selectively detect the template molecules with high affinity. However, the test can only be conducted in ethanol because of the weak fluorescent intensity of NBD-lysine in aqueous solvent.

To solve this problem fluorescein based trifunctional monomer (F-Lysine) was synthesized by reacting fluorescein isothiocyanate (FITC) with α-amino group of lysine. Quantum dots embedded silica nanoparticles were synthesized to support the MIP and acted as internal standard. A ratiometric fluorescent sensor based on fluorescein trifuctional monomer with quantum dots as internal standard was developed.

It was expected the F-lysine can interact strongly with template and can be incorporated into the biding sites. In the event of the binding, the intensity of the F-lysine will be quenched and the intensity of the red quantum dots will stay the same. If the ratio of the quantum dots and

the F-lysine were controlled properly, the composite nanoparticle would emit red light dominated by the red quantum dots. In the event of the binding, the composite nanoparticle would emit green light due to the quenching effect of the template to the F-lysine.

6.8 Synthesis of ratiometric fluorescent sensor based on fluorescein trifuctional monomer with quantum dots as internal standard

6.8.1 Synthesis of the fluorescein based trifunctional monomer (F-lysine)

(0.0037g, 0.01 mmol) FITC was dissolved in 5ml methanol. (0.013g, 0. 1mmol) acryloyl lysine was dissolved in 1ml 0.1 molar sodium bicarbonate buffer. The two solutions were mixed and stirred at room temperature for 48 hour in dark. Thin layer chromatography on silica gel plates of the product mixture with methanol as eluent is shown in figure 6.21. The lower component was purified by flash chromatography with methanol as eluent. The NMR spectrum for the F-lysine is shown in figure 6.22.

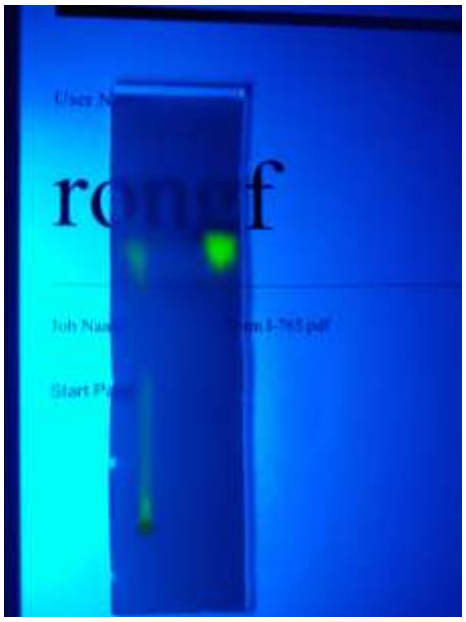

Figure 6.21 Thin layer chromatography for the reaction between FITC and acryloyl lysine (left) and FITC (right)

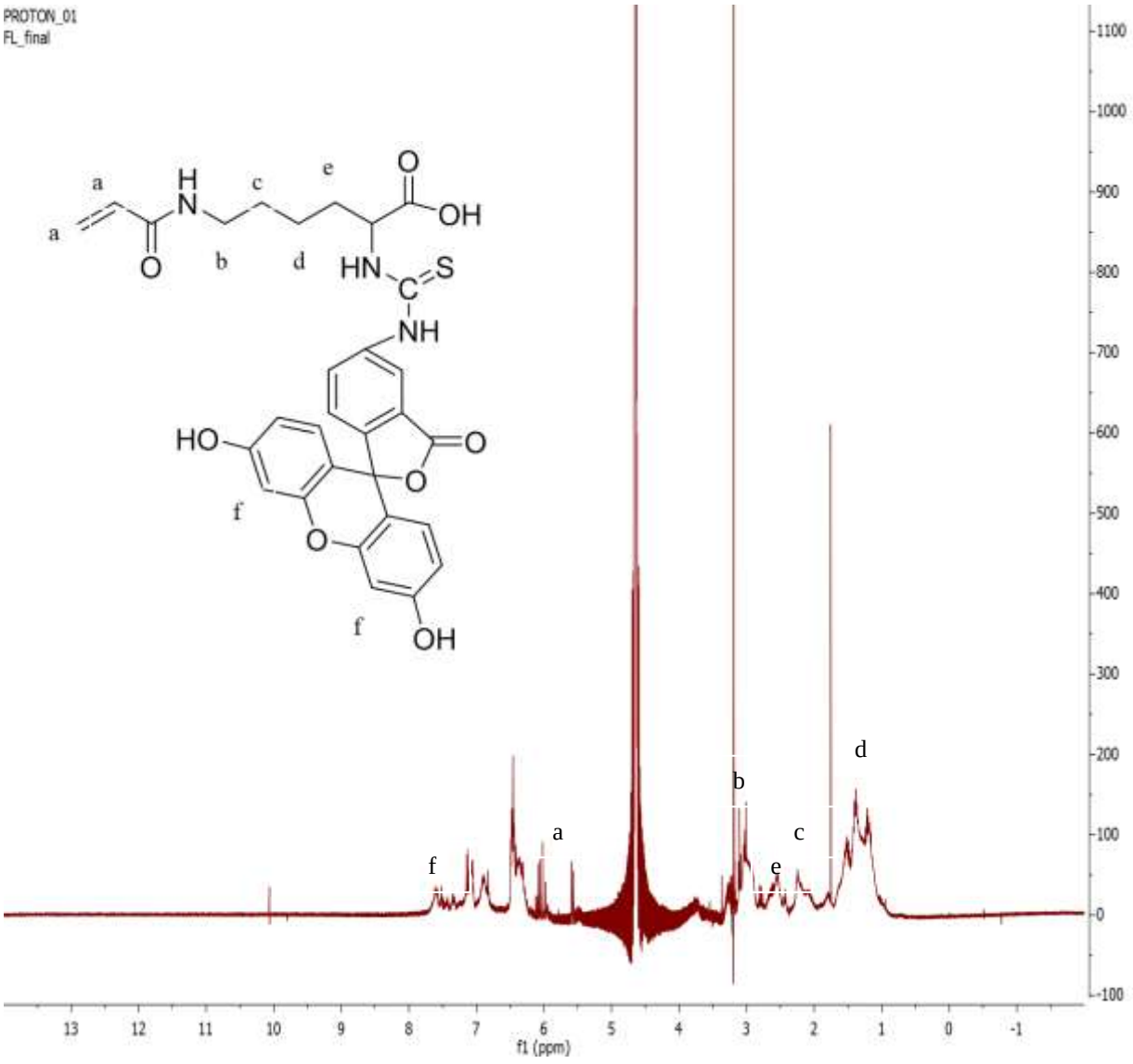

Figure 6.22 ^{1}H NMR spectrum of F-lysine (D_2O, 400 MHz)

6.8.2 Synthesis of quantum dots embedded silica nanoparticles

The red CdTe quantum dots were synthesized by the method developed by Zhang et al. with minor modification.[129] Briefly, 0.0638 g of tellurium powder and 0.1 g of $NaBH_4$ were added to 10 mL of ultrapure water under nitrogen atmosphere. The mixture was stirred for 8 h in an ice bath to form NaHTe. 0.2284 g of $CdCl_2 \cdot 2.5H_2O$ and 210 μL of 3-mercaptopropionic acid (MPA) were dissolved in 125 mL of ultrapure water, and the pH value of the solution was adjusted to 9 with 1.0 M NaOH. After degassing for 30 min, the freshly prepared NaHTe solution was added. The mixture was refluxed 48 hours to produce red CdTe quantum dots. The prepared CdTe QD solution was then illuminated for 10 h with a UV lamp to enhance the fluorescence quantum yield. The photo of red CdTe quantum dots is shown in figure 6.23.

Figure 6.23 Photo of red CdTe quantum dots

The fluorescent emission spectra for F-lysine and the red CdTe quantum dots are shown in figure 6.24. The maximum emission wavelength of F-lysine is 520 nm. The maximum emission spectrum for the quantum dots was at 620 nm.

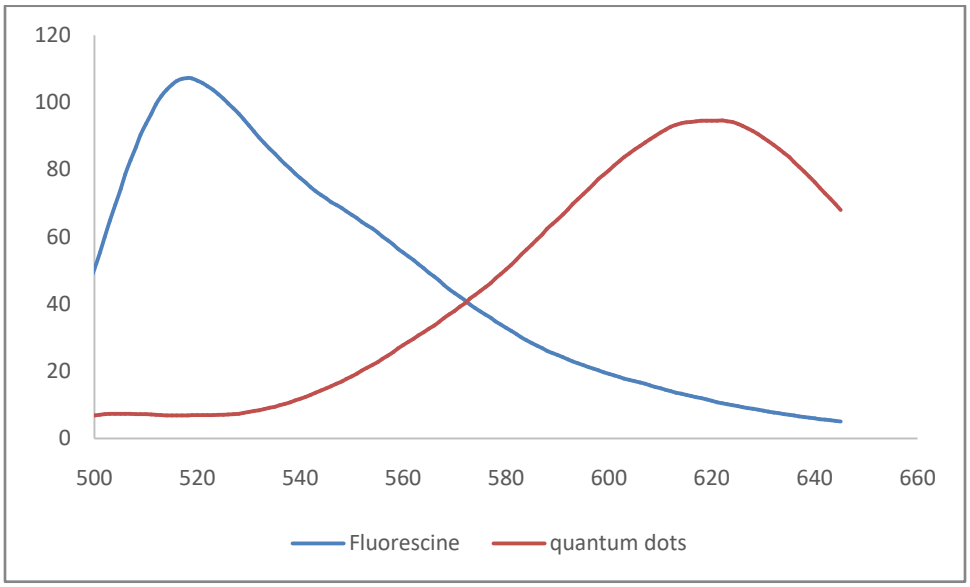

Figure 6.24 The fluorescent emission spectra for F-lysine and the red CdTe quantum dots (excited wavelength was at 480 nm)

The red CdTe quantum dots were embedded inside the silica naoparticles by microemulsion method developed by Wang et at. with minor modification.[130] In this method, cyclohexane was used as a continuous phase, and Triton X-100 and *n*-hexanolwere regarded as surfactant and co-surfactant respectively. Briefly, 7.5mL cyclohexane, 1.77mL Triton X-100, 1.8mL *n*-hexanol, 400uL aqueous solution of as-prepared CdTe QDs and 60ul NH_4OH were mixed to form microemulsion. After addition of 100uL TEOS, the reaction was stirred in dark for 24h. The CdTe/SiO_2 composite nanoparticles were washed with ethanol and anhydrous

dioxane for future modification. The photos of the CdTe/SiO_2 composite nanoparticles without and with UV excitation is shown in figure 6.25

Figure 6.25 The photos of the CdTe/SiO_2 composite nanoparticles without and with UV excitation

6.8.3 Coating MIPs onto nanoparticle surface

The RAFT agent MPTT was attached onto the CdTe/SiO_2 composite with the method described in 5.3.3. The formulation of the MIPs was the same as the MIPs in 6.5 except that F-lysine is the functional monomer. The template was removed by rinsing the composite nanoparticles with THF and acetic acid and water 6v:v, 10:90).

6.8.4 Fluorescent tests

The fluorescent emission spectra of the polymer coated nanoparticle are shown in figure 6.26. Instead of two independent peaks at 520 nm for the F-lysine and 620 for the red quantum dots, there is only one peak at 550nm.

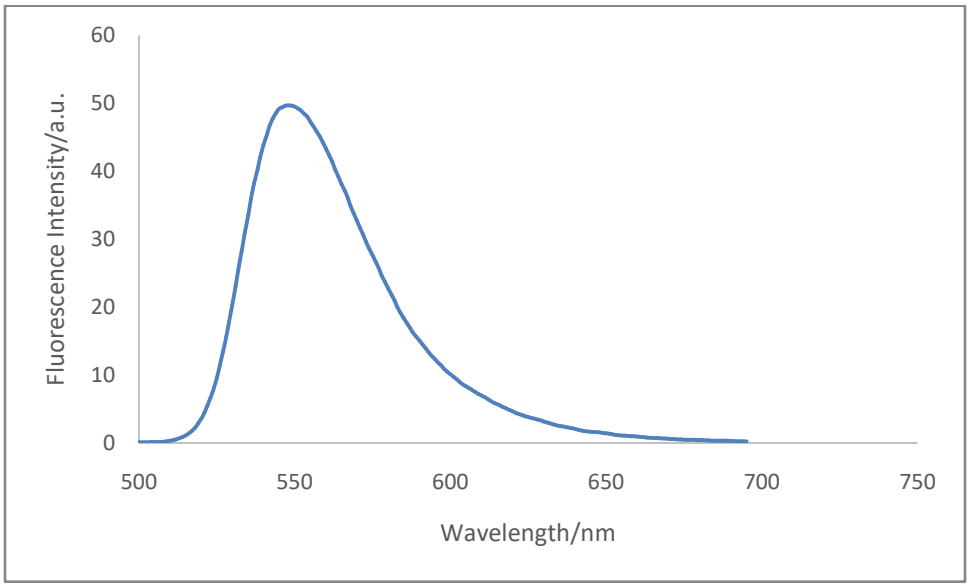

Figure 6.26 Fluorescent emission spectra of the composite nanoparticles (The composite nanoparticles were composed by MIPs shell using F-lysine as functional monomer, and silica nanoparticles core with red CdTe quantum dots embeded)

This result indicated that the amount of the green F-lysine in the MIP layer and amount of the red quantum dots in the silica core need further adjustment so both peak can appear individually.

6.9 Conclusion

In this chapter, two trifunctional monomers NBD-lysine and F-lysine were synthesized. The MIPs with NBD-lysine as functional monomer can detect the template at 1 nano molar concentration, which indicated the high binding affinity. The selectivity of the MIPs was also promising.

However, NBD-lysine can only work in ethanol, the fluorescent intensity of NBD-lysine in water is too low for template detecting.

To solve this problem, F-lysine was synthesized. This fluorescein based fluorophore fluorescence green light strongly in water. A ratiometric sensor was designed by attaching the MIPs with F-lysine as function monomer onto silica nanoparticles embedded by red CdTe quantum dots. It was expected that the green peak would be quenched in the presence of the template while the red peak stayed same as a standard. So the color of the sensor would change with the addition of the template.

The results indicated that it was feasible to synthesize the composite nanoparticle. However, more adjustments need to be done on the amount of each fluorophore.

CHAPTER 7 CONCLUSIONS AND FUTURE WORK

In this dissertation, different fluorescent sensors were developed for sensitive and selective detection of template molecules using the novel biomimetic MIPs as receptors.

The sensor developed in chapter 3 was based on FRET energy transfer for the detection of 4NP. It can detect 4NP at as low as $1x10^{-7}$molar concentration. The sensor can selectively bind to the templates while ignoring the isomers. However, the distance change caused by the binding between the templates with MIPs was not significant enough to change the acceptor to donor fluorescent intensity ratio (A/D ratio). Therefore, sensors based on this design do not produce a ratiometric response.

The free floating biomimetic receptors developed in chapter 4 and 5 have high binding affinity ($K_{binding}=1x10^{8}M$). The binding sites are maintained by 2% mole covalent crosslinking with 5 % percent acid base crosslinking. The backbones of the MIPs are thermally sensitive PNIPAm, which undergoes a phase transition at the LCST. The hydrophobic interactions between the isopropyl groups help to maintain the configuration of the binding sites. The problem for this receptor is the tedious template removal process. Future work needs to focus on the development of more efficient template removal methods.

The sensor developed in chapter 6 used the synthesized trifunctional fluorescent NBD-lysine as functional monomer. This sensor can selectively detect template at 1nM with high selectivity. The problem is that the sensor can only be used in ethanol. The problem can be solved by using a fluorescein based monomer (f-lysine). A ratiometric fluorescent sensor can be developed by using quantum dot embedded silica nanoparticles as core, f-lysine incorporated MIPs as shell. It is feasible to synthesize the quantum dots with the right emission wavelength.

The F-lysine functional monomers have been synthesized successfully. The protocol to grow polymers from silica surface has been established. Future work needs to been done to determine the best ratio for detecting signal from F-lysine and internal standard signal from quantum dots.

LIST OF REFERENCES

1. Emil Alexov, Barry Honig, Handbook of Cell Signaling (Second Edition), **2010**

2. Lockett, M.,Lange, H.,Breiten, B., Heroux,A.,Sherman, W., Rappoport, D., Snyder,P., Whitesides,G., "The Binding of Benzoarylsulfonamide Ligands to Human Carbonic Anhydrase is Insensitive to Formal Fluorination of the Ligand". *Angew. Chem. Int. Ed*. **2003**. 52. 7714–7717.

3. Water Networks Contribute to Enthalpy/Entropy Compensation in Protein–Ligand Binding". *J. Am. Chem. Soc*. 135. 15579–15584.

4. "Macromolecular bioactivity: is it resonant interaction between macromolecules?—theory and applications". *IEEE transactions on bio-medical engineering*. 41. 1101–14.

5. Lettau K., Warsinke A., Katterle M., Danielsson B., Scheller F.W. "A bifunctional molecularly imprinted polymer (MIP): analysis of binding and catalysis by a thermistor." *Angew. Chem. Int. Ed*. **2006**. 45:6986–6990

6. Liao, X., Chen, G., Jiang, M., "Hydrogels locked by molecular recognition aiming at responsiveness and functionality." *Polym. Chem*. **2013**.4, 1733–1745

7. Fischer E "Einfluss der Configuration auf die Wirkung der Enzyme" [Influence of configuration on the action of enzymes]. *Berichte der Deutschen chemischen Gesellschaft zu Berlin* (in German). **1894**.27 (3): 2985–93.

8. Xu, S.; Lu, H.; Zheng, X.; Chen, L., "Stimuli-responsive molecularly imprinted polymers: versatile functional materials." *Journal of Materials Chemistry C,* **2013**, *1*, 4406.

9. Korytkowska-Wałach, A., "Molecularly imprinted hydrogels for application in aqueous environment." *Polymer Bulletin* **2012**, *70* (5), 1647-1657.

10. Xu, Z.; Kuang, D.; Zhang, F.; Tang, S.; Deng, P.; Li, J., "Fluorogenic molecularly imprinted polymers with double recognition abilities synthesized via click chemistry." *Journal of Materials Chemistry B* **2013**, *1* (13), 1852.

11. Xu, L.; Pan, J.; Dai, J.; Li, X.; Hang, H.; Cao, Z.; Yan, Y., "Preparation of thermalresponsive magnetic molecularly imprinted polymers for selective removal of antibiotics from aqueous solution." *Journal of hazardous materials* **2012**, *233-234*, 48-56.

12. Tedford,M.; Stimson, w.; "Molecular recognition in antibodies and its application" *Cellular and Molecular life science* **1991**, Volume 47, Page 1129

13. Xu, H. E.; Lambert, M; Montana, V et. al "Molecular Recognition of Fatty Acids by Peroxisome Proliferator–Activated Receptors." *Molecular Cell*. **1999**.Volume 3, 397–403,

14. Bar-Even A, Noor E, Savir Y, Liebermeister W, Davidi D, Tawfik DS, Milo R. "The moderately efficient enzyme: evolutionary and physicochemical trends shaping enzyme parameters". *Biochemistry*. **2011**.50: 4402–10

15. Mashaghi A, Katan A. "A physicist's view of DNA". De Physicus. 2013 24e (3): 59–61

16. Swanson, M. D.; Winter, H. C.; Goldstein, I. J.; Markovitz, D. M. "A Lectin Isolated from Bananas is a Potent Inhibitor of HIV Replication". *Journal of Biological Chemistry*.2**010**. 285 (12): 8646–55

17. King TH, Liu B, McCully RR, Fournier MJ. "Ribosome structure and activity are altered in cells lacking snoRNPs that form pseudouridines in the peptidyl transferase center". *Molecular Cell*. 11 2**003**.(2): 425–35

*18. Schomburg I, Chang A, Placzek S, Söhngen C, Rother M, Lang M, Munaretto C, Ulas S, Stelzer M, Grote A, Scheer M, Schomburg D "BRENDA in 2013: integrated reactions, kinetic data, enzyme function data, improved disease classification: new options and contents in BRENDA". Nucleic Acids Research. **2013**.41.764–72*

19. Jaeger KE, Eggert T "Enantioselective biocatalysis optimized by directed evolution". *Current Opinion in Biotechnology*. **2004**.15 (4): 305–13.

20. Boyer R (2002). "Chapter 6: Enzymes I, Reactions, Kinetics, and Inhibition". Concepts in Biochemistry (2nd ed.). New York, Chichester, Weinheim, Brisbane, Singapore, Toronto.: John Wiley & Sons, Inc. pp. 137–8.

21. Jacobson, R.H., Zhang, X-J, DuBose, R.F., and Matthews, B.W., "Three-dimensional structure of β-galactosidase from E. coli."Nature, **1994**, 369, 761-766.

22. Garrett, R.H. and Grisham, C.M., Principles of Biochemistry With a Human Focus, Brooks/Cole and Thomson Learning, 2002.

23. Ullmann, A., "Escherichia coli Lactose Operon", Encyclopedia of Life Sciences, Nature Publishing Group, **2001**, www.els.net

24. Jit, Mark; Newall, Anthony T.; Beutels, Philippe "Key issues for estimating the impact and cost-effectiveness of seasonal influenza vaccination strategies". *Human vaccines & immunotherapeutics*. **2013**.9. 834–840.

25. Hardman Reis T "The role of intellectual property in the global challenge for immunization". *J World Intellect Prop*.**2006**. 9. 413–25.

26. Cooper, Max D. "The early history of B cells". *Nature Reviews Immunology*. **2015**. 15: 191–7.

27. Borghesi L, Milcarek C "From B cell to plasma cell: regulation of V(D)J recombination and antibody secretion". *Immunologic Research*. **2006**. 36. 27–32.

28. Woof JM, Burton DR "Human antibody-Fc receptor interactions illuminated by crystal structures". *Nature Reviews. Immunology*. **2004**.4 .89–99.

29. Esteves-Villanueva JO, Trzeciakiewicz H, Martic S. "A protein-based electrochemical biosensor for detection of tau protein, a neurodegenerative disease biomarker." *Analyst.* **2014**.7.2823-31

30. Sorell L, López JA, Valdés I, Alfonso P, Camafeita E, Acevedo B, Chirdo F, Gavilondo J, Méndez E. "An innovative sandwich ELISA system based on an antibody cocktail for gluten analysis" *FEBS Lett.* **1998**.439.46-50.

31. Seyfi Abad Shapouri, Masoud Reza. "Production of a monoclonal antibody against chicken immunoglobulin G:A valuable molecule with research and diagnostic applications" *Veterinary research forum,* **2018**.9.67-72

32. Warren BL, Eid A, Singer P, Pillay SS, Carl P, Novak I, Chalupa P, Atherstone A, Pénzes I, Kübler A, Knaub S, Keinecke HO, Heinrichs H, Schindel F, Juers M, Bone RC, "Caring for the critically ill patient: high-dose antithrombin III in severe sepsis: a randomized controlled trial." *JAMA* **2001**;286.1869-78.

33. Ankan Dutta, ChowdhuryAkhilesh, BabuGanganboina, Yuan-chung, Tsai Hsin-chengChiu, Ruey-anDoong, "Multifunctional GQDs-Concanavalin A@Fe_3O_4nanocomposites for cancer cells detection and targeted drug delivery," *Analytica Chimica Acta* **2018**.1027, 109-120

34. Cieplak, M; Kutner, W; "Artificial Biosensors: How Can Molecular Imprinting Mimic Biorecognition?" *trend in biotechnology*. **2016**. 34,922–941

35. Nelson, D., Cox, M., Lehnenger Principles of Biochemistry, 5th ed., W.H. Freeman and co. **2008**.

36. Lozinsky, V. I., "Approaches to chemical synthsis of protein-like copolymer." *Adv. Polym. Sci.* **2006**,*196*, 87-127

37. Alexander C, Andersson HS, Andersson LI, Ansell RJ, Kirsch N, Nicholls IA, O'Mahony J, Whitcombe MJ J. Mol. "*Molecular imprinting science and technology: a survey of the literature for the years up to and including 2003*" *Recognit*. **2006**; 19: 106–180

38. Lingxin Chen,*ab Xiaoyan Wang,ac Wenhui Lu,a Xiaqing Wua and Jinhua Lia "Molecular imprinting: perspectives and applications" *Chem. Soc. Rev.,* **2016**, 45, 2137

39. MIPs-Molecularly Imprinted Polymers. http://www.biotage.com. (Accessed Aug 2018)

40. Giuseppe Vasapollo *, Roberta Del Sole, Lucia Mergola, Maria Rosaria Lazzoi, Anna Scardino, Sonia Scorrano and Giuseppe Mele. "Molecularly Imprinted Polymers: Present and Future Prospective *." Int. J. Mol. Sci.* **2011**, *12*, 5908-5945;

41. Karsten, H., "Imprinting molecular memory on the surface of polymer nanoparticles creates artificial antibodies that can recognize and neutralize a toxic peptide in vivo." *Nature Materials* **2010**, 9, 612–614

42. Z. Zhang, J. Li, X. Song, J. Ma and L. Chen, "Hg2+ ion-imprinted polymers sorbents based on dithizone–Hg2+ chelation for mercury speciation analysis in environmental and biological samples."RSC Adv., **2014**, 4, 46444–46453.

43. J. Fu, L. Chen, J. Li and Z. Zhang, "Current status and challenges of ion imprinting."*J. Mater. Chem. A,* **2015**, 3, 13598–13627.

44. O.Hayden and F. L. Dickert, "Selective Microorganism Detection with Cell Surface Imprinted Polymers."*Adv. Mater.,* 2**001**, 13, 1480–1483.

45. Y. Zhang, D. Song, L. M. Lanni and K. D. Shimizu, "Importance of Functional Monomer Dimerization in the Molecular Imprinting Process"*Macromolecules*, **2010**, 43, 6284–6294.

46. 42 K. Golker, B. R. C. Karlsson, G. D. Olsson, A. M. Rosengren and I. A. Nicholls, "Influence of Composition and Morphology on Template Recognition in Molecularly Imprinted Polymers."*Macromolecule*s, **2013**, 46, 1408–1414.

47. Komiyama, M., Takeuchi, T., Mukawa, T., Asanuma H., "Molecular Imprinting: From Fundamentals to Applications." *Wiley-VCH Verlag,* Weingheim, **2003**.

48. Piletsky, S., Turner, A., " Molecular Imprinting of Polymers." *Landes Bioscience* **2006**.

49. H. Yan and K. H. Row, "Characteristic and Synthetic Approach of Molecularly Imprinted Polymer"Int. J. Mol. Sci., **2006,** 7, 155–178.

50. Cameron, A., Ha, A., Lars,. I. Andersson, R., Kirsch, N., Nicholls, I, Mahony, J., Whitcombe, M., "Molecular imprinting science and technology: a survey of the literature for the years up to and including 2006." *J. Mol. Recognit*. **2006**; 19: 106–180

51. Lanza, F.; Sellergren, B., "The application of molecular imprinting technology to solid phase extraction." *Chromatographia 53* (11), 599-611.

52. Zhang, H.; Song, T.; Zong, F.; Chen, T.; Pan, C., "Synthesis and characterization of molecularly imprinted polymers for phenoxyacetic acids." *International journal of molecular sciences* **2008**,*9* (1), 98-106.

53. Yusof, N. A.; Zakaria, N. D.; Maamor, N. A. M.; Abdullah, A. H.; Haron, M. J., "Synthesis and characterization of molecularly imprinted polymer membrane for the removal of 2, 4-dinitrophenol." *International journal of molecular sciences* **2013**,*14* (2), 3993-4004.

54. Li B, Xu J, Hall, A.J., Haupt, K. Tse Sum B. "Water-compatible silica sol-gel molecularly imprinted polymer as a potential delivery system for the controlled release of salicylic acid" *J Mol Recognit.* **2014** Sep;27(9):559-65

55. Zhang,W, She, X.,Wang, L., Fan, H.,Zhou,Q., Huang, X.,Tang,J., "Preparation, Characterization and Application of a Molecularly Imprinted Polymer for Selective Recognition of Sulpiride." Materials **2017**, 10, 475

56. Mayes AG, Mosbach K. "Molecularly imprinted polymer beads: suspension polymerization using a liquid perfluorocarbon as the dispersing phase." *Anal Chem.* **1996**, 68(21):3769-74

57. Gizem Ertürk and Bo Mattiasson "Molecular Imprinting Techniques Used for the Preparation of Biosensors" *Sensors* 2**017**, 17, 288

58. Engen, J.; Smith, D., Investigating the higher order structure of proteins. Hydrogen exchange, proteolytic fragmentation, and mass spectrometry. *Methods in molecular biology (Clifton, NJ)* **2000**, *146*, 95.

59. Binkert, T.; Oberreich, J.; Meewes, M.; Nyffenegger, R.; Ricka, J., Coil-globule transition of poly (N-isopropylacrylamide): a study of segment mobility by fluorescence depolarization. *Macromolecules* **1991**, *24* (21), 5806-5810.

60. Wu, C.; Zhou, S., "Laser light scattering study of the phase transition of poly (N-isopropylacrylamide) in water. 1. Single chain." *Macromolecules* **1995**, *28* (24), 8381-8387.

61. Sin, M.Z.,G.;Wu,C., "Effect of comonomer distribution on the coil to globule transition of a single copolymer chain in dilutionsolution." *Macromolecules* 2002, *35*, 2723---2727.

62. Knono, K., H.Morimoto,K., Takagishi,T,"Tempreture dependent permeability of polyeletrolyte complez capsule membranes having N-Isopropylacrylamide Domains."*Journal of Applied Polymer Science* 2000, *77*, 2703---2710

63. Chiefari, J.; Chong, Y.; Ercole, F.; Krstina, J.; Jeffery, J.; Le, T. P.; Mayadunne, R. T.; Meijs, G. F.; Moad, C. L.; Moad, G., "Living free-radical polymerization by reversible addition-fragmentation chain transfer: the RAFT process." *Macromolecules* 1998,*31* (16), 5559-5562.

64. Jian Zhu a , Xiulin Zhu a,, Di Zhou a , Jianying Chen b , Xiaoyan Wang. " a, Study on reversible addition-fragmentation chain transfer (RAFT) polymerization of MMA in the presence of 2-cyanoprop-2-yl 1-dithiophenanthrenate (CPDPA)." European Polymer Journal 40 (2004) 743–749

65. Perrier, S.; P. Takolpuckdee (2005). "Macromolecular Design via Reversible Addition–Fragmentation Chain Transfer (RAFT)/Xanthates (MADIX) Polymerization". *J. Polym. Sci. Part A.* 43 (22): 5347–5393.

66. Perrier, S.; Takolpuckdee, P.; Mars, C.A. (2005). "Reversible addition-fragmentation chain transfer polymerization: end group modification for functionalized polymers and chain transfer agent recovery". *Macromolecules*. 38: 2033–2036.

67. Tajon, Cheryl A.; Yang, Hao; Tian, Bining; Tian, Yue; Ercius, Peter; Schuck, P. James; Chan, Emory M.; Cohen, Bruce E. "Photostable and efficient upconverting nanocrystal based chemical sensors". *Optical materials*. 2018, 84, 345-353

68. Pavase, Tushar Ramesh; Lin, Hong; Shaikh, Qurat-ul-ain; Hussain, Sameer; Li, Zhenxing; Ahmed, Ishfaq; Lv, Liangtao; Sun, Lirui; Shah, Syed Babar Hussain; Kalhoro, Muhammad Talib, "Recent advances of conjugated polymer (CP) nanocomposite-based chemical sensors and their applications in food spoilage detection: A comprehensive review" Sensors and actuators. B, Chemical, 2018, 273, 1113-1138

69. Hazra, Surajit Kumar; Basu, Sukumar Edited by Thakur, Vijay Kumar; Thakur, Manju Kumari. "Chemical modification of graphene and applications for chemical sensors" *Chemical Functionalization of Carbon Nanomaterials*. 2016,915-937

70. Guo, Shirui; Wang, Wei; Ozkan, Cengiz S.; Ozkan, Mihrimah, Edited by Aliofkhazraei, Mahmood. "Graphene-based biological and chemical sensors" *Graphene Science Handbook Mechanical and Chemical Properties*, 2016,127-145

71. Jung, Dong Geon; Jung, Daewoong; Kong, Seong Ho. "A Lab-on-a-Chip-Based Non-Invasive Optical Sensor for Measuring Glucose in Saliva" *sensor*,2017,17,2607

72. Eric Bakker*, and Martin Telting-Diaz, "Electrochemical Sensors" *Anal. Chem.* 74, 12, 2781-2800

73. Jian Zhao, Yongcun Zhang, Renjing Gao, Shutian Liu, "A new sensitivity improving approach for mass sensors through integrated optimization of both cantilever surface profile and cross-section" ,*Sensors and actuators B: chemical*,2015,206,343-350

74. P.J.Hore, "Sensitivity of DNA repair enzymes to weak magnetic fields may have relevance to the mechanism by which birds sense the Earth's magnetic field." *ACS Cent. Sci.* 4, 3, 318-320

75. H. Wang, Y. Wang, J. Jin, R. Yang "Gold nanoparticle-based colorimetric and "turn-on" fluorescent probe for mercury (II) ions in aqueous solution" Anal. Chem., 2008, 80. 9021-9028

76. G. Yang, X. Wan, Y. Su, X. Zeng, J. Tang "Acidophilic S-doped carbon quantum dots derived from cellulose fibers and their fluorescence sensing performance for metal ions in an extremely strong acid environment" J. Mater. Chem. A, 4 (2016), pp. 12841-12849

77. Zhang, Fan, Zhao, Kang, Du, and Peng "Mitochondria-Accessing Ratiometric Fluorescent Probe for Imaging Endogenous Superoxide Anion in Live Cells and *Daphnia magna"* ACS Sensors2018 *3* (3), 735–741

78. Kaur, A., Haghighatbin, M. A., Hogan, C. F. & New, E. J. "*A FRET-based ratiometric redox probe for detecting oxidative stress by confocal microscopy, film and flow cytometry*." *Chem. Commun.* 51, 10510–10513 (2015)

79. Huang, K. *et al. "*Ratiometric and colorimetric detection of hydrogen sulfide with high selectivity and sensitivity using a novel FRET-based fluorescence probe.*" Dyes Pigments* 118, 88–94 (2015).

80. Lubna Rasheed, Muhammad Yousuf, Il Seung Youn, Genggongwo Shi and Kwang S. Kim, "An efficient non-reaction based colorimetric and fluorescent probe for the highly selective discrimination of Pd 0 and Pd 2+ in aqueous media." *RSC Advances*, 2016, 6, 65,60546-60549

81. Seong Youl Lee, Kwon Hee Bok, Jin Ah Kim, So Young Kim and Cheal Kim. "Simultaneous detection of Cu2+ and Cr3+ by a simple Schiff-base colorimetric chemosensor bearing NBD (7-nitrobenzo-2-oxa-1,3-diazolyl) and julolidine moieties." *Tetrahedron*, 10, (5563-5570), (2016).

82. Chen Hou, Yijia Xiong, Na Fu, Caitlin C.Jacquot,Thomas C.Squier, Haishi Cao. "Turn-on ratiometric fluorescent sensor for Pb^{2+}detection". Tetrahedron Letters Volume 52, Issue 21, 25 2011, Pages 2692-2696

83. Joshi BP, Park J, Lee WI, Lee KH. "Ratiometric and turn-on monitoring for heavy and transition metal ions in aqueous solution with a fluorescent peptide sensor" *Talanta* Volume 78, Issue 3, 15 May 2009, Pages 903-909

84. Laurence M. Harwood, Christopher J. Moody (1989*). "Experimental organic chemistry: Principles and Practice." Oxford: Blackwell Scientific Publications*. pp. 127–132

85. Petrucci, Harwood, Herring, Madura. General Chemistry: Principles & Modern Applications, Ninth Ed. Upper Saddle River, NJ: Pearson Education, Inc., 2007.

86. Hsu CY, Lin HY, Thomas JL, Wu BT, Chou TC. "Incorporation of styrene enhances recognition of ribonuclease A by molecularly imprinted polymers." Biosens Bioelectron. 2006 (3):355-63

87. Shriver, D. F., Drezdn, M. A. *The Manipulation of Air Sensitive Compounds.* 2nd ed. Wiley & Sons: New York, NY (1986).

88. "Freeze-Pump-Thaw Degassing of Liquids" (PDF). University of Washington.

89. JoVE Science Education Database. *Organic Chemistry*. Degassing Liquids with Freeze-Pump-Thaw Cycling. JoVE, Cambridge, MA, (2018).

90. "Soxhlet Extraction" [Online] http://community.asdlib.org. (Accessed Aug2018)

91. Li Yang, Yang Tang, Na Liu, Chun-Hua Liu, Yunsheng Ding, and Zong-Quan Wu "Facile Synthesis of Hybrid Silica Nanoparticles Grafted with Helical Poly(phenyl isocyanide)s and Their Enantioselective Crystallization Ability"*Macromolecules* 2016 *49* (20), 7692-7702

92. Thermal fisher scientific. "N-hydroxysuccinimide esters (NHS esters)" [Online] https://www.thermofisher.com (Accessed Aug 2018)

93. Matsui, J.; Akamatsu, K.; Hara, N.; Miyoshi, D.; Nawafune, H.; Tamaki, K.; Sugimoto, N., “SPR sensor chip for detection of small molecules using molecularly imprinted polymer with embedded gold nanoparticles.” *Analytical Chemistry* 2005,*77* (13), 4282-4285.

94. "Fluorescence Spectrophotometry". *Encyclopedia of Life Sciences*. Macmillan Publishers Ltd. 2002.

95. A. Marais, M. Martini, F. Lepoivre, M. Ould-Metidji, A. Collet, and O. Tillement, Université de Lyon; C. Hurtevent, and S. Baraka-Lokmane, Total “Time-Resolved Fluorescence for Real-Time Monitoring of Both Scale and Corrosion Inhibitors: A Game-Changing Technique” SPE-179867-MS,2016

96. Li, Tongcang; Kheifets, Simon; Medellin, David; Raizen, Mark (2010). "Measurement of the instantaneous velocity of a Brownian particle" (PDF). *Science*. 328 (5986): 1673–1675.

97. Morozov, A. N.; Skripkin, A. V. (2011). "Spherical particle Brownian motion in viscous medium as non-Markovian random process". *Physics Letters A*. 375 (46): 4113–4115.

98. Malvern. “Zetasizer Nano User Manual” MAN0485 Issue 1.1 April 2013

99. Chu, B. (1 January 1970). "Laser Light Scattering". *Annual Review of Physical Chemistry*. 21 (1): 145–174.

100. Oppenheimer, J. H.; Squee, R.; Surks, M. I.; Hauer, H., Binding of thyroxine by serum proteins evaluated by equilibrium dialysis and electrophoretic techniques. Alterations in non-thyroidal illness. *Journal of Clinical Investigation* 1963,*42* (11), 1769.

101. Behm, H. L.; Wagner, J. G., Errors in interpretation of data from equilibrium dialysis protein binding experiments. *Research communications in chemical pathology and pharmacology* 1979,*26* (1), 145-160.

102. Teeraporn Suteewong, Hiroaki Sai, Michelle Bradbury, Lara A. Estroff, Sol M. Gruner, and Ulrich Wiesner “Synthesis and Formation Mechanism of Aminated Mesoporous Silica Nanoparticles“*Chem. Mater.*, 2012, *24* (20), pp 3895–3905

103. Sevier, C. S.; Kaiser, C. A. (2002). "Formation and transfer of disulphide bonds in living cells". *Nature Reviews Molecular Cell Biology* . 3 (11): 836–847

104. Gilbert, H. F. (1995). "Thiol/disulfide exchange equilibria and disulfide bond stability". *Methods in Enzymology*. 251: 8–28.

105. Legon, A. C.; Millen, D. J. (1987). "Angular geometries and other properties of hydrogen-bonded dimers: a simple electrostatic interpretation of the success of the electron-pair model". *Chemical Society Reviews*. 16: 467.

106. D. Egan, R. O'Kennedy, E. Moran, D. Cox, E. Prosser and R.D. Thornes, Drug Metab. Rev., 22 (1990) 503.

107. Elizabeth Moran, Richard O'Kennedy, R.Douglas Thornes. “Analysis of coumarin and its urinary metabolites by high-performance liquid chromatography” Chromatogr., 416 (1987) 165.

108. Leal, L. K. A. M.; A. A. G. Ferreira; G. A. Bezerra; F. J. A. Matos; G. S. B. Viana (May 2000). "Antinociceptive, anti-inflammatory and bronchodilator activities of Brazilian medicinal plants containing coumarin: a comparative study". *Journal of Ethnopharmacology*. 70 (2): 151–159.

109. Katja Skrabania, Anna Miasnikova, Achille Mayelle Bivigou-Koumba,bDaniel Zehmb and Andr Laschewsky “Examining the UV-vis absorption of RAFT chain transfer agents and their use for polymer analysis” Polym. Chem., 2011, 2, 2074

110. William Bauer, Jr. "Methacrylic Acid and Derivatives" in Ullmann's Encyclopedia of Industrial Chemistry 2002

111. Yang, W., Zhou, W., Li, H., Huang, W., Jiang, B., Zhou, Z., Yang, Y.,Synthesis and Characterization of a Surface Molecular Imprinted Polymer as a New Adsorbent for the Removal of Dibenzothiophene *J. Chem. Eng. Data*, 2012, *57* (6), pp 1713–1720

112. Zlokarnik G, Negulescu PA, Knapp TE, Mere L, Burres N, Feng L, et al. “Quantitation of transcription and clonal selection of single living cells with beta-lactamase as reporter.” Science. 1998 Jan 2;279(5347):84–8

113. Yimeng Du , Li Li , C.W. Leung , P. T. Lai , and Philip W. T. Pong, “Synthesis and Characterization of Silica-Encapsulated Iron Oxide Nanoparticles” IEEE TRANSACTIONS ON MAGNETICS, VOL. 50, NO. 1, JANUARY 2014

114. Liu, H., Wang, Y., Li, H., Wang, Z., Xu, D., “Luminescent Rhodamine B doped coreeshell silica nanoparticle labels for protein microarray detection” Dyes and Pigments 98 (2013) 119-124

115. Zhao, Y., Perrier, S. “Reversible Addition-Fragmentation Chain Transfer Graft Polymerization Mediated by Fumed Silica Supported Chain TransferAgents” Macromolecules 2007, 40, 9116-9124

116. Batra D, Shea KJ (2003) “Novel trifunctional building blocks for fluorescent polymers.” Org Lett 5:3895–3898

117. Wu Y, Liu Y, Gao X, Gao K, Xia H, Luo M,Wang X, Ye L, Shi Y,Lu B (2015) “Monitoring bisphenol A and its biodegradation in water using a fluorescent molecularly imprinted chemosensor.” Chemosphere 119:515–523

118. Gao L, Li X, Zhang Q, Dai J, Wei X, Song Z, Yan Y, Li C (2014) Molecularly imprinted polymer microspheres for optical measurement of ultra trace nonfluorescent cyhalothrin in honey. Food Chem 156:1–6

119. Wackerlig J, Lieberzeit PA (2015) “Molecularly imprinted polymer nanoparticles in chemical sensing - synthesis, characterisation and application.” Sensors Actuators B 207:144–157

120. Moreno-Bondi MC, Navarro-Villoslada F, Benito-Peña E, Urraca JL (2008) “Molecularly imprinted polymers as selective recognition elements in optical sensing.” Curr Anal Chem 4:316–340

121. Lavignac N, Allender CJ, Brain KR (2004) “4-(3-Aminopropylene)-7-nitrobenzofurazan: a new polymerisable monomer for use in homogeneous molecularly imprinted sorbent fluoroassays.” Tetrahedron Lett 45:3625–3627

122. Wagner R,WanW, Biyikal M, Benito-Peña E, Moreno-Bondi MC, Lazraq I, Rurack K, Sellergren B (2013) “Synthesis, spectroscopic, and analyte-responsive behavior of a polymerizable naphthalimide- based carboxylate probe and molecularly imprinted polymers prepared thereof.” J Org Chem 78:1377–1389

123. Wan W, Biyikal M, Wagner R, Sellergren B, Rurack K (2013) “Fluorescent sensory microparticles that Blight-up^ consisting of a silica core and a molecularly imprinted polymer (MIP) shell.” Angew Chem Int Ed 52:7023–7027

124. Awino JK, Zhao Y (2014) “ Molecularly imprinted nanoparticles as tailor-made sensors for small fluorescent molecules.” Chem Commun 50:5752–5755

125. Means, G. E.; Feeney, R. E. “Chemical modifications of proteins: history and applications.” *Bioconjugate Chem*. 1990, 1, 2−12.

126. Chen, X.; Muthoosamy, K.; Pfisterer, A.; Neumann, B.; Weil, T. “Site-Selective Lysine Modification of Native Proteins and Peptides via Kinetically Controlled Labeling.” Bioconjugate Chem. 2012, 23, 500−508

127. Mariana Amaro, Hugo A. L. Filipe,J. P. Prates Ramalho, Martin Hof and Luı ´s M. S. Loura* “Fluorescence of nitrobenzoxadiazole (NBD)- labeled lipids in model membranes is connected not to lipid mobility but to probe location†” *Phys.Chem.Chem.Phys.,* 2016, 18, 7042

128. Shoji Nagaoka,Atsuomi Shundo, Takao Satoh, Kazuhiko Nagira, Ryoich Kishi,Katsuhiko Ueno, Kokoro Iio,Hirotaka Ihara “Method for a Convenient and Efficient Synthesis of Amino Acid Acrylic Monomers with Zwitterionic Structure.” Synthetic Communications, Volume 35, 2005, 2529-2534

129. Mingyuan Gao, Stefan Kirstein, and Helmuth Mo1hwald, “Strongly Photoluminescent CdTe Nanocrystals by Proper Surface Modification” *J. Phys. Chem. B* 1998, *102*, 8360-8363

130. ChaoWang, Qiang Ma,Wenchao Dou, Shamsa Kanwal, GuannanWang, Pingfan Yuan, Xingguang Su, “Synthesis of aqueous CdTe quantum dots embedded silica nanoparticles and their applications as fluorescence probes” Talanta 77 (2009) 1358–1364